

An Overview of the Unified Transport Approach

A. H. Eraslan
A. J. Witten

Prepared for the
U.S. Nuclear Regulatory Commission
Office of Nuclear Regulatory Research
Washington, D.C. 20555
under Interagency Agreement DOE 40-550-75

NOTICE

This report was prepared as an account of work sponsored by an agency of the United States Government. Neither the United States Government nor any agency thereof, or any of their employees, makes any warranty, expressed or implied, or assumes any legal liability of responsibility for any third party's use, or the results of such use, of any information, apparatus, product or process disclosed in this report, or represents that its use by such third party would not infringe privately owned rights.

NOTICE

Availability of Reference Materials Cited in NRC Publications

Most documents cited in NRC publications will be available from one of the following sources:

1. The NRC Public Document Room, 1717 H Street, N.W.
Washington, DC 20555
2. The NRC/GPO Sales Program, U.S. Nuclear Regulatory Commission,
Washington, DC 20555
3. The National Technical Information Service, Springfield, VA 22161

Although the listing that follows represents the majority of documents cited in NRC publications, it is not intended to be exhaustive.

Referenced documents available for inspection and copying for a fee from the NRC Public Document Room include NRC correspondence and internal NRC memoranda; NRC Office of Inspection and Enforcement bulletins, circulars, information notices, inspection and investigation notices; Licensee Event Reports; vendor reports and correspondence; Commission papers; and applicant and licensee documents and correspondence.

The following documents in the NUREG series are available for purchase from the NRC/GPO Sales Program: formal NRC staff and contractor reports, NRC-sponsored conference proceedings, and NRC booklets and brochures. Also available are Regulatory Guides, NRC regulations in the *Code of Federal Regulations*, and *Nuclear Regulatory Commission Issuances*.

Documents available from the National Technical Information Service include NUREG series reports and technical reports prepared by other federal agencies and reports prepared by the Atomic Energy Commission, forerunner agency to the Nuclear Regulatory Commission.

Documents available from public and special technical libraries include all open literature items, such as books, journal and periodical articles, and transactions. *Federal Register* notices, federal and state legislation, and congressional reports can usually be obtained from these libraries.

Documents such as theses, dissertations, foreign reports and translations, and non-NRC conference proceedings are available for purchase from the organization sponsoring the publication cited.

Single copies of NRC draft reports are available free, to the extent of supply, upon written request to the Division of Technical Information and Document Control, U.S. Nuclear Regulatory Commission, Washington, DC 20555.

Copies of industry codes and standards used in a substantive manner in the NRC regulatory process are maintained at the NRC Library, 7920 Norfolk Avenue, Bethesda, Maryland, and are available there for reference use by the public. Codes and standards are usually copyrighted and may be purchased from the originating organization or, if they are American National Standards, from the American National Standards Institute, 1430 Broadway, New York, NY 10018.

Energy Division

**AN OVERVIEW OF THE
UNIFIED TRANSPORT APPROACH**

A. H. Eraslan*
A. J. Witten

*ERAS, Inc.

Manuscript Completed: June 1984
Date Published: August 1984

Prepared for the
Division of Radiation Programs and Earth Sciences
Office of Nuclear Regulatory Research
U.S. Nuclear Regulatory Commission
Washington, D.C. 20555

NRC FIN No. B0168-9

Prepared by the
OAK RIDGE NATIONAL LABORATORY
Oak Ridge, Tennessee 37831
operated by
MARTIN MARIETTA ENERGY SYSTEMS, Inc.
for the
U.S. DEPARTMENT OF ENERGY
under
Contract No. DE-AC05-84OR21400

ABSTRACT

The Unified Transport Approach (UTA) consists of a set of nine complementary models developed for assessing the environmental impacts associated with nuclear power plant discharges to receiving water bodies. This set of models has the capability to simulate natural and plant-induced flow, temperature, salinity, sediment transport, radio-nuclide transport, and chemical species concentrations. While these UTA models were developed for predicting impacts associated with the operation of nuclear power plants, they are quite general and can be applied to a variety of situations. The UTA models have been used to simulate the impacts associated with the operation of many industrial and energy production technologies, as well as to simulate laboratory and naturally occurring conditions. In all cases where data have been available for validation, the UTA model results have compared favorably. The purpose of this report is to provide an overview of the UTA as whole, highlighting the important features and unique capabilities of this approach.

TABLE OF CONTENTS

	<u>Page</u>
ABSTRACT	iii
LIST OF FIGURES	vii
LIST OF TABLES	xi
SUMMARY	xiii
1. INTRODUCTION	1
2. OVERVIEW AND SUMMARY OF THE UNIFIED TRANSPORT APPROACH . . .	6
2.1 Overview of the Unified Transport Approach	6
2.2 Summary of the Unified Transport Approach Codes	16
2.2.1 Computer Code: ESTONE	16
2.2.2 Computer Code: FLOWER	18
2.2.3 Computer Code: CHMONE	21
2.2.4 Computer Code: SEDONE	23
2.2.5 Computer Code: RADONE	26
2.2.6 Computer Code: RADTWO	28
3. MODEL FORMULATION	31
3.1 Three-Dimensional Equations	32
3.2 One-Dimensional Equations	36
3.3 Model Closure	41
3.4 Formation of Discrete Model Equations	43
4. TREATMENT OF BOUNDARIES	47
4.1 Shoreline Boundaries	47
4.2 Open Boundaries	50
5. ZONE-MATCHING METHODOLOGIES	52
5.1 Uniformly Valid Singular Perturbation Theory	55
5.1.1 Horizontal Jets	56
5.1.2 Vertical Jets	61
5.2 ORSMAC	66
6. RESULTS	69
6.1 The Hudson River Study	69
6.2 San Onofre	90
6.3 The Green River Case	97
REFERENCES	106

LIST OF FIGURES

	<u>Page</u>
Fig. 2.1. A schematic representation of the sequential application of all UTA models. Numbers refer to list of model inputs and outputs in Sect. 2.1	8
Fig. 2.2. An example of an actual channel cross section as digitized from a navigational chart and as input to ESTONE	10
Fig. 2.3(a). An example of the variable computational grid and represent a shoreline tion as input to two- and three-dimensional UTA models	12
Fig. 2.3(b). An example of bathymetry as input to two- and three-dimensional UTA models	13
Fig. 2.4. An example of the assumed power-law vertical velocity profile used in the one- and two-dimensional UTA models	15
Fig. 3.1. (a) Representation of the vertical variation of the x-component (horizontal) of velocity over the vertical extent of the discrete element and (b) the three-term decomposition of this velocity	34
Fig. 3.2. A schematic representation of the type of lateral and vertical variations in (a) downstream flow, shown as constant velocity contours, (b) temperature, shown as isotherms, and (c) salinity shown as isohalines, accounted for in the one-dimensional ESTONE model	38
Fig. 3.3. A schematic representation of the vertical profiles and three-term decomposition for (a) velocity, (b) temperature, and (c) salinity, as assumed in the one-dimensional ESTONE model	39
Fig. 4.1. An example of (a) a stepped shoreline boundary typical of many computational schemes and (b) the more accurate shoreline representation used in the two- and three-dimensional UTA models	47
Fig. 4.2. A schematic representation of the treatment of a shoreline element in the UTA models	48
Fig. 5.1. Wall jet solution based upon classical jet theory	53
Fig. 5.2. A schematic representation of a jet-induced flow field under commonly encountered conditions. Note the reentrainment resulting from the limited depth and variable bathymetry	54

	<u>Page</u>
Fig. 5.3. A schematic representation of a typical situation which can be modeled by the horizontal jet zone-matching methodology	57
Fig. 5.4. A schematic representation of the flow induced behind an off-shore horizontal discharge	57
Fig. 5.5. A schematic representation of straight shoreline boundary correction using the method of images showing (a) the actual configuration and (b) the configuration with the image source	58
Fig. 5.6. An example of a shoreline and grid system used for the numerical correction for arbitrary shorelines used in the horizontal jet zone-matching methodology	59
Fig. 5.7. A schematic representation of the treatment of shoreline boundary conditions in the numerical horizontal jet shoreline boundary correction	60
Fig. 5.8. An example of the full off-shore horizontal jet induced flow field predicted by the horizontal jet zone-matching methodology, including the numerical shoreline boundary correction	61
Fig. 5.9. An example of the vertical jet zone-matching methodology applied to a bottom discharge in water of finite depth for (a) quiescent conditions	62
Fig. 5.9. An example of the vertical jet zone-matching methodology applied to a bottom discharge in water of finite depth for (b) ambient cross-flow and (c) ambient cross-flow and an adjacent bottom discharge and (d) ambient cross-flow and an adjacent bottom intake	63
Fig. 5.10. Comparison of the variations of (1) the entrainment ratio for the bottom vertical discharge of a single, turbulent slot jet in a bounded, constant-depth flow region and (2) the entrainment ratio of a turbulent slot jet in an unbounded flow region with the dimensionless depth factor	65
Fig. 5.11. ORSMAC results for a hot, turbulent, vertically-discharging bottom jet shows predicted (a) streamlines and (b) isotherms	67
Fig. 6.1. Comparisons of detailed actual profiles and approximated input data to ESTONE model for two typical cross sections along the Hudson River. Actual profiles from U.S. Department of Commerce, National Oceanic and Atmospheric Administration, National Ocean Survey, C&GS Charts Nos. 282, 283, 284, 745, and 746	70

	<u>Page</u>
Fig. 6.2. Freshwater flow rate and temperature conditions at the Troy Dam as input data to the ESTONE code for April 1974	72
Fig. 6.3. Comparisons of six-harmonic functional predictions and field-measured tidal data at the Battery during April 1 - September 30, 1974, simulation period	73
Fig. 6.4. Daily water temperatures and salinity conditions at the Battery during April 1 - September 30, 1973, simulation period	74
Fig. 6.5. Collective freshwater flow rate for two tributaries entering a discrete element as input data to the ESTONE code: April and May 1974	75
Fig. 6.6. (a) Maximum normal solar radiation flux and (b) daily-averaged cloud cover factor and daily-maximum cloud cover factor variations, during the simulation period April 1 - September 30, 1974	76
Fig. 6.6. (c) Daily-averaged air temperature and (d) daily-averaged wind speed and daily-maximum wind speed variations during the simulation period April 1 - September 30, 1974	77
Fig. 6.6. (e) Daily-averaged rainfall rate and (f) daily-averaged relative humidity and daily-maximum relative humidity variations during the simulation period April 1 - September 30, 1974 .	78
Fig. 6.7. Indian Point plant cooling water flow rate and plant cooling water temperature rise as input to ESTONE for July 1974 . .	79
Fig. 6.8. Comparisons of computer simulation results by ESTONE for cross-section-averaged temperature and salinity variations and continuous daily measurements and field-measured data for temperature and salinity conditions in the vicinity of Indian Point area during May 1974. Measurements from Texas Instruments Incorporated Ecological Services, Hudson River Ecological Study in the Area of Indian Point. Thermal Effects Report , prepared for Consolidated Edison Company of New York, Inc., September 1976	80
Fig. 6.9. ESTONE simulation results for the variations of daily-averaged and cross-sectional-averaged water temperature conditions in the vicinity of Indian Point Power Plant for three cases during June and July	81
Fig. 6.10. Computer simulation results for the longitudinal distribution of Monochloramine (top figure) and hypochlorous acid (bottom figure) concentrations in the Hudson River for hypothetical power plant chlorination conditions	83

	<u>Page</u>
Fig. 6.11. Computer simulation results for the longitudinal distributions of the sediment size classes in the Hudson River for (a) the suspended sediment layer and (b) the bed slurry sediment layer	84
Fig. 6.12. Comparison computer simulation results and field-measured data for the total sediment discharge in the Mississippi River	85
Fig. 6.13. Computer simulation results for the longitudinal distribution of radionuclide concentrations in the Hudson River for hypothetical prompt release conditions from Indian Point power plant as predicted in (a) the sediment layer and (b) the suspended sediment layer	86
Fig. 6.14. Computer-generated discrete-element grid system for the section of the Hudson River in the vicinity of Indian Point and Lovett power plants	87
Fig. 6.15. Computer-generated constant-depth contours and depth values for the grid system shown in Fig. 6.14	88
Fig. 6.16. Results of the horizontal jet zone-matching methodology applied to the Indian Point discharge using the grid system shown in Fig. 6.14	90
Fig. 6.17. Computer simulation results for the two-dimensional natural and plant-induced flow field in the region of Indian Point and Lovett power plants at 9:00 a.m. on August 23, 1974 . .	91
Fig. 6.18. Computer simulation results for the full two-dimensional (depth-averaged) temperature distribution in the region of Indian Point and Lovett power plants at 9:00 a.m. on August 23, 1974	92
Fig. 6.19. Configuration of the San Onofre circulating water systems .	93
Fig. 6.20. Plot of actual shoreline and grid system used for the San Onofre application	94
Fig. 6.21. Plant-induced flow field resulting from the operation of all three San Onofre units as predicted by the horizontal jet zone-matching methodology	95
Fig. 6.22. Predicted, depth-averaged, full flow field in the San Onofre region at 2:00 a.m. on the fifth day of the simulation . .	96
Fig. 6.23. Predicted, depth-averaged, full flow field in the San Onofre region at 8:00 a.m. on the fifth day of the simulation . .	97

Fig. 6.24. Predicted, depth-averaged, excess temperatures in the San Onofre region at 2:00 a.m. on the fifth day of the simulation	98
Fig. 6.25. Predicted, depth-averaged, excess temperatures in the San Onofre region at 8:00 a.m. on the fifth day of the simulation	99
Fig. 6.26. Computer simulation results for the radionuclide concentration conditions for (a) the water layer and (b) the sediment layer in the San Onofre coastal region, 24 hrs after the start of the hypothetical accidental release scenario . . .	100
Fig. 6.27. Discrete-element, variable-size, rectangular grid system and shoreline representation used for the Green River power plant simulation	101
Fig. 6.28. Depth contours for the flow region of the Green River power plant simulation. Gradations of constant depth contours are from 3 to 10 m, respectively	101
Fig. 6.29. Predicted horizontal velocity vectors in (a) the bottom layer and (b) layer 2 after 20 and 40 min of the simulation . . .	102
Fig. 6.29. Predicted horizontal velocity vectors in (c) layer 3 and (d) the surface layer after 20 and 40 min of the simulation . .	103
Fig. 6.30. Predicted total temperature shown as isotherms for (a) the bottom layer and (b) layer 2 after 20 and 40 of the simulation. Isotherms are drawn in 1°C increments between 19°C and 22°C	104
Fig. 6.30. Predicted total temperature shown as isotherms for (c) layer 3 and (d) the surface layer after 20 and 40 min of the simulation. Isotherms are drawn in 1°C increments between 19°C and 22°C	105

LIST OF TABLES

Tbl. 1.1. UTA model name and reference	4
--	---

EXECUTIVE SUMMARY

The Unified Transport Approach (UTA) consists of a set of nine complementary models for assessing the environmental impacts associated with nuclear power plant discharges to receiving water bodies. Model development was sponsored by the U.S. Nuclear Regulatory Commission Office of Nuclear Regulatory Research and was motivated by an existing need for improved predictive capabilities. This need arises, in part, as a result of limitations in the predictive capabilities of existing techniques as well as limitations associated with the level of effort required to implement sophisticated, state-of-the-art methodologies.

The set of nine UTA models consists of six hydrodynamic and transport codes and three zone-matching methodologies. The ESTONE code predicts transient, one-dimensional (cross-sectionally averaged) hydrodynamic, temperature and salinity conditions. The FLOWER code is the three-dimensional counterpart to ESTONE. The CHMONE code is similar to ESTONE but predicts chemical species concentrations in place of salinity conditions. The SEDONE and RADONE codes are both one-dimensional and both predict hydrodynamic conditions. Additionally, SEDONE predicts the longitudinal distribution of sediment size classes, and RADONE predicts the longitudinal distribution of radionuclides in the water column and bottom sediment. RADTWO is the two-dimensional (horizontal) counterpart to RADONE.

The three zone-matching methodologies are intended to provide enhanced near-field resolution of power plant-induced discharge and intake flow fields. These methodologies were developed to be used

either alone for assessing near-field impacts or to be matched to the far-field UTA codes. Two of these methodologies, the horizontal jet and the vertical jet, are analytic, based on the uniformly valid singular perturbation theory. The horizontal jet methodology is used to simulate jet-induced flows resulting from off-shore discharges and to account rigorously for entrained flow parallel to the discharge direction. There is also an optional numerical component to this methodology to allow for arbitrary shoreline geometries. The vertical jet methodology is used for vertically oriented bottom discharges and rigorously accounts for multiple jet, jet/intake, and jet/cross-flow interactions. The third zone-matching methodology, ORSMAC, is fully numerical using a simplified marker-and-cell technique applied to a two-dimensional, vertical plane. The ORSMAC code is used to simulate near-field flow and temperature, allows for arbitrary discharge angle and bathymetry, and accounts for free-surface and densimetric effects.

While these UTA models were developed for predicting impacts associated with the operation of nuclear power plants, they are quite general and can be applied to a variety of situations. The UTA models have been used to simulate the impacts associated with the operation of many industrial and energy production technologies, as well as to simulate laboratory and naturally occurring conditions. In all cases where data have been available for validation, the UTA model results have compared favorably.

The UTA is, as the name implies, a set of transport and ancillary models based upon a unified conceptual, mathematical, and numerical formulation specifically developed for ease of application. The UTA

models have input requirements at least as prodigious as those of any sophisticated numerical model; input requirements may be even greater because of the realism the UTA models can accommodate. This, however, is more than offset by the ease with which multiple UTA models can be implemented. Once the effort has been expended to develop input data sets for one UTA model, all other models can be applied with only minor modifications or additions to the original input data. While this consistency and economy of effort in applying UTA models was an important objective, other equally important objectives included, the realistic representation of modeled setting, the enhanced treatment of physical phenomena, the lack of any externally specified empirical parameters, model versatility, and computational accuracy and efficiency.

One important feature of the UTA model system is that all the one-dimensional codes use identical channel geometry, bathymetry, and hydrodynamic boundary condition input data. Once this input information is prepared for one model, (e.g., ESTONE), the identical data set can be directly input to all other one-dimensional codes (RADONE, CHMONE, SEDONE). It should also be noted that all channel geometry input to the one-dimensional models is three dimensional, in the form of channel cross sections. This provides an accurate representation in the simulations and allows the three-dimensional character of the dependent variables to be incorporated into the models.

Any of the one-dimensional codes can be used as a stand-alone model since each has the capability of hydrodynamic calculations. Each one-dimensional code has the option to by-pass the hydrodynamic computations and instead use externally specified flow conditions. Thus if any one of these codes is applied, the resulting flow field can be input

directly to the other codes, by-passing the hydrodynamic calculations. This is an important feature of the UTA since it offers greatly enhanced computational efficiency.

The two- and three-dimensional UTA codes (FLOWER and RADTWO) are designed for shorter time and smaller spatial extent simulations than the one-dimensional models. FLOWER and RADTWO can use the same channel geometry data as the one-dimensional models; however, they are typically used to provide simulations with greater spatial resolution than the one-dimensional models provide. In this case, supplemental data is required. The two- and three-dimensional models utilize a discrete element grid superimposed on a selected shoreline and bathymetry.

FLOWER and RADTWO can be applied independently of the one-dimensional model applications. In some cases, however, it is desirable to have the one-dimensional model results to establish boundary conditions for models of higher dimensionality. FLOWER and RADTWO are computationally more demanding than one-dimensional codes and consequently can only be applied to a limited study region. This frequently results in open water boundaries which are far removed from locations where data is available. In such situations, simulated ESTONE transient values for cross-sectional flow, surface elevation, temperature, and salinity can be used as FLOWER boundary conditions. Similarly, if sources of radio-nuclides exist outside the RADTWO study region, these source contributions can be incorporated into the RADTWO simulations by using radio-nuclide concentration predicted by a RADONE application, which includes all sources, as boundary conditions.

The zone-matching methodologies were developed to provide high resolution detail of the shearing flows near intakes and discharges. Although, in principle, FLOWER can provide high resolution near field detail, in practice this is computationally cost prohibitive. After selecting the appropriate zone-matching methodology, a near-field, plant-induced flow field is generated using geometric, ambient flow and power plant information. This flow field is input to FLOWER and superimposed on the internally calculated far-field conditions.

Along with the features of the UTA highlighted above, there are other important features inherent in the UTA models. These include accurate shoreline representation, variable grid size, the convective defect formulation, turbulent closure, and a discrete element system.

The two- and three-dimensional UTA models allow accurate shoreline representation, in contrast with many computer codes which require the shoreline boundary to coincide with sides of the computation grid and produce a stepped boundary. A major advantage of the smooth boundary representation of the UTA is that it avoids the numerical (computational) artifacts which occur in the presence of stepped boundaries.

The variable or telescoping grid feature allows high resolution in regions of interest without producing an unmanageable number of computational elements.

The convective defect formulation introduces three-dimensional features into the one- and two-dimensional models. This is accomplished by assuming a similarity profile for the vertical variations in the dependent variables (flow, temperature, etc.). These profiles may vary during the course of model simulations as a result of changing

conditions. These similarity profiles are an inherent, fundamental feature of the basic one- and two-dimensional model formulation.

Turbulent closure is a problem encountered in the modeling of all large Reynolds number flows. The most common means of treating turbulence is the eddy viscosity approach in which turbulent stresses are represented as viscous stresses but with an eddy viscosity many orders of magnitude larger than molecular viscosity. The value of eddy viscosity is commonly taken as constant, but realistically it should vary as a function of local conditions. The appropriate value for the eddy viscosity for large-scale flow situations, such as wind-driven currents, is considerably different from that for turbulent jets. The UTA formulation incorporates a variable eddy viscosity formulation which allows the eddy viscosity to vary (from zero for laminar flows) according to the local velocity. This allows the UTA codes to be applied to a wide range of conditions including laboratory-scale simulations.

The discrete element system considers the integral form of the governing equations applied to individual discrete elements (control volumes). This system offers computational advantages and at the same time allows the incorporation of other previously described features such as arbitrary shorelines and the convective defect formulation.

1. INTRODUCTION

The Unified Transport Approach (UTA) consists of a set of nine complementary models for assessing the environmental impacts associated with nuclear power plant discharges to receiving water bodies. This work was sponsored by the U.S. Nuclear Regulatory Commission Office of Nuclear Regulatory Research and was motivated by an existing need for improved predictive capabilities. This need arises, in part, as a result of limitations in the predictive capabilities of existing techniques as well as limitations associated with the level of effort required to implement sophisticated, state-of-the-art methodologies.

The UTA is, as the name implies, a set of transport and ancillary models based upon a unified conceptual, mathematical, and numerical formulation specifically developed for ease of application. The UTA models have input requirements as prodigious as those of any sophisticated numerical model; input requirements may be even greater because of the realism that the UTA models can accommodate. This, however, is more than offset by the ease with which multiple UTA models can be implemented. Once the effort has been expended to develop input data sets for one UTA model, all other models can be applied with only minor modifications or additions to the original input data. While this consistency and economy of effort in applying UTA models was an important objective, other equally important objectives included, the realistic representation of modeled setting, the enhanced treatment of physical phenomena, the lack of any externally specified empirical parameters, model versatility, and computational accuracy and efficiency.

The set of nine UTA models consists of six hydrodynamic and transport codes and three zone-matching methodologies directed toward predicting the fate of pollutants discharged to the water. The ESTONE code predicts transient, one-dimensional (cross-sectionally averaged) hydrodynamic, temperature and salinity conditions. The FLOWER code is the three-dimensional counterpart to ESTONE. The CHMONE code is similar to ESTONE but predicts chemical species concentrations in place of salinity conditions. The SEDONE and RADONE codes are both one dimensional and both predict hydrodynamic conditions. Additionally, SEDONE predicts the longitudinal distribution of sediment size classes, and RADONE predicts the longitudinal distribution of radionuclides in the water column and bottom sediment. RADTWO is a two-dimensional version of RADONE. RADTWO requires the flow field to be externally specified.

The three zone-matching methodologies are intended to provide enhanced near-field resolution of power plant-induced discharge and intake flow fields. These methodologies were developed to be used either alone for assessing near-field impacts or to be matched to the far-field UTA codes. Two of these methodologies, the horizontal jet and the vertical jet, are analytic, based on the uniformly valid singular perturbation theory (Eraslan and Benek, 1971). The horizontal jet methodology is used to simulate jet-induced flows resulting from offshore discharges and to account rigorously for entrained flow parallel to the discharge direction. There is also an optional numerical component to this methodology to allow for arbitrary shoreline geometries. The vertical jet methodology is used for vertically oriented bottom discharges and rigorously accounts for multiple jet, jet/intake, and

jet/cross-flow interactions. The third zone-matching methodology, ORSMAC, is fully numerical using a simplified marker-and-cell technique applied to a two-dimensional, vertical plane. The ORSMAC code is used to simulate near-field flow and temperature, allows for arbitrary discharge angle and bathymetry, and accounts for free-surface and densimetric effects.

While these UTA models were developed for predicting impacts associated with the operation of nuclear power plants, they are quite general and can be applied to a variety of situations. The UTA models have been used to simulate the impacts associated with the operation of many industrial and energy production technologies, as well as to simulate laboratory and naturally occurring conditions. In all cases where data have been available for validation, the UTA model results have compared favorably.

The purpose of this report is not to provide an exhaustive description of the individual UTA models, but rather to provide an overview of the UTA as a whole, highlighting the important features and unique capabilities of this approach. While considerable detail and technical derivation is presented in some parts of this document, this is restricted to aspects common to all, or many, of the individual UTA models. Section 2 presents an overview of the UTA and a summary of the individual UTA models. It is intended for a reader who wishes to obtain an understanding of the UTA without wading through the technical development presented in Sect. 3, 4, and 5. Section 3 presents a simplified derivation of the basic UTA model formulation and Sect. 4 presents the associated treatment of boundaries. Section 5 provides a

detailed discussion of the three zone-matching methodologies. Section 6 provides sample results of the UTA models. These results were selected specifically to demonstrate the systematic application of multiple UTA models.

In this report, individual UTA models are cited by model or descriptive name (ESTONE, horizontal jet, etc.). The complete reference associated with each model name is given in Table 1.1.

Table 1.1. UTA model name and reference

Model Name	Reference
ESTONE	Eraslan, A. H. Nov. 1983. <u>ESTONE: A Computer Code for Simulating Fast-Transient, One-Dimensional Hydrodynamic, Thermal, and Salinity Conditions, in Controlled Rivers and Tidal Estuaries for the Assessment of the Aggregated Impact of Multiple Power Plant Operation.</u> NUREG/CR-2621. U.S. Nuclear Regulatory Commission, Washington, D.C.
FLOWER	Eraslan, A. H., W. L. Lin, and R. D. Sharp. Dec. 1983. <u>FLOWER: A Computer Code for Simulating Three-Dimensional Flow, Temperature, and Salinity Conditions in Rivers, Estuaries, and Coastal Regions.</u> NUREG/CR-3172. U.S. Nuclear Regulatory Commission, Washington, D.C.
CHMONE	Fischer, S. K. et al. Apr. 1984. <u>CHMONE: A One-Dimensional Computer Code for Simulating Temperature, Flow and Chemical Concentrations in Water Bodies.</u> NUREG/CR-3410. U.S. Nuclear Regulatory Commission, Washington, D.C.
SEDONE	Hetrick, D. M. et al. Feb. 1979. <u>SEDONE: A Computer Code for Simulating Tidal-Transient, One-Dimensional Hydrodynamic Conditions and Three-Layer, Variable-Size, Sediment Concentrations in Controlled Rivers and Estuaries.</u> NUREG/CR-0430. U.S. Nuclear Regulatory Commission, Washington, D.C.

Table 1.1 (Continued)

Model Name	Reference
RADONE	Eraslan, A. H. et al. <u>RADONE: A Computer Code for Simulating Fast-Transient, One-Dimensional Hydrodynamic Conditions and Radionuclide Concentrations Including the Effect of Bed-Deposition in Controlled Rivers and Tidal Estuaries.</u> NUREG/CR-3441. U.S. Nuclear Regulatory Commission, Washington, D.C.
RADTWO	Eraslan, A. H., H. Diament, and R. D. Codell. <u>RADTWO: A Computer Code for Simulating Fast-Transient, Two-Dimensional, Two-Layer Radionuclide Concentration Conditions in Lakes, Reservoirs, Rivers, Estuaries, and Coastal Regions.</u> NUREG/CR-3442. In press.
HORIZONTAL JET	Eraslan, A. H., and A. J. Witten. Oct. 1983. <u>Application of Zone-Matching Methodology to Interacting Submerged Multiport Diffusers.</u> NUREG/CR-3095. U.S. Nuclear Regulatory Commission, Washington, D.C.
VERTICAL JET Matching ZONE MATCHING	Eraslan, A. H., and W. L. Lin. Oct. 1983. <u>Zone Methodology for Slot Jets in Water Bodies.</u> NUREG/CR-2596. U.S. Nuclear Regulatory Commission, Washington, D.C.
ORSMAC	Park, J. E., and K. E. Cross. Dec. 1983. <u>Calculation of Fluid Circulation Patterns in the Vicinity of Submerged Jets Using ORSMAC.</u> NUREG/CR-3153. U.S. Nuclear Regulatory Commission, Washington, D.C.

2. OVERVIEW AND SUMMARY OF THE UNIFIED TRANSPORT APPROACH

2.1 Overview of the Unified Transport Approach

The fundamental objective of the UTA is the development of a comprehensive set of models for assessing power plant impacts to receiving water bodies. The UTA models include one-dimensional sediment transport and chemical species concentration computer codes; one- and two-dimensional radionuclide transport computer codes; one-, two-, and three-dimensional hydrodynamic, thermal, and salinity codes; and three zone-matching methodologies for simulating near field jet dynamics.

A problem common to all sophisticated numerical models is the extreme effort required to develop model input data sets. In most of these situations, the level of effort required discourages the application of multiple models and creates a significant practical limitation in environmental impact assessments. Thus, a primary driving force in the UTA concept was the requirement that any number of UTA models could be applied with minimal incremental effort. One of the most powerful features of the UTA is that once a single UTA code is applied, additional UTA codes may be applied with only minor supplemental input data. The following list describes the sets of model inputs and outputs:

Model Inputs

1. Three-dimensional channel geometry and bathymetry; hydrodynamic boundary conditions; power plant locations, intake and discharge flow rates.

2. Thermal boundary conditions, power plant discharge temperatures, meteorological parameters for surface heat transfer and wind stress calculations.
3. Salinity boundary conditions.
4. Ambient and plant-discharge chemical species concentrations.
5. Plant-discharge radionuclide concentrations.
6. Ambient sediment distribution; upstream, downstream, and tributary sediment loading.
7. Supplemental geometry and bathymetry data for higher resolution simulations.
8. Power plant intake and discharge configuration.

Model Output

1. Transient, longitudinal flow rates and free-surface displacement.
2. Transient, longitudinal water temperatures.
3. Transient, longitudinal salinities.
4. Transient, longitudinal chemical species concentrations.
5. Transient, longitudinal, two-layer radionuclide concentrations.
6. Transient, longitudinal sediment-size class distribution.
7. Transient, three-dimensional velocity vectors, temperatures, and salinities.
8. Transient, two-dimensional (horizontal), two-layer radionuclide concentrations.

Figure 2.1 schematically outlines the procedure for sequential model applications. Input and output numbers shown in this figure correspond to the input and output numbers on the list given above. Inspection of

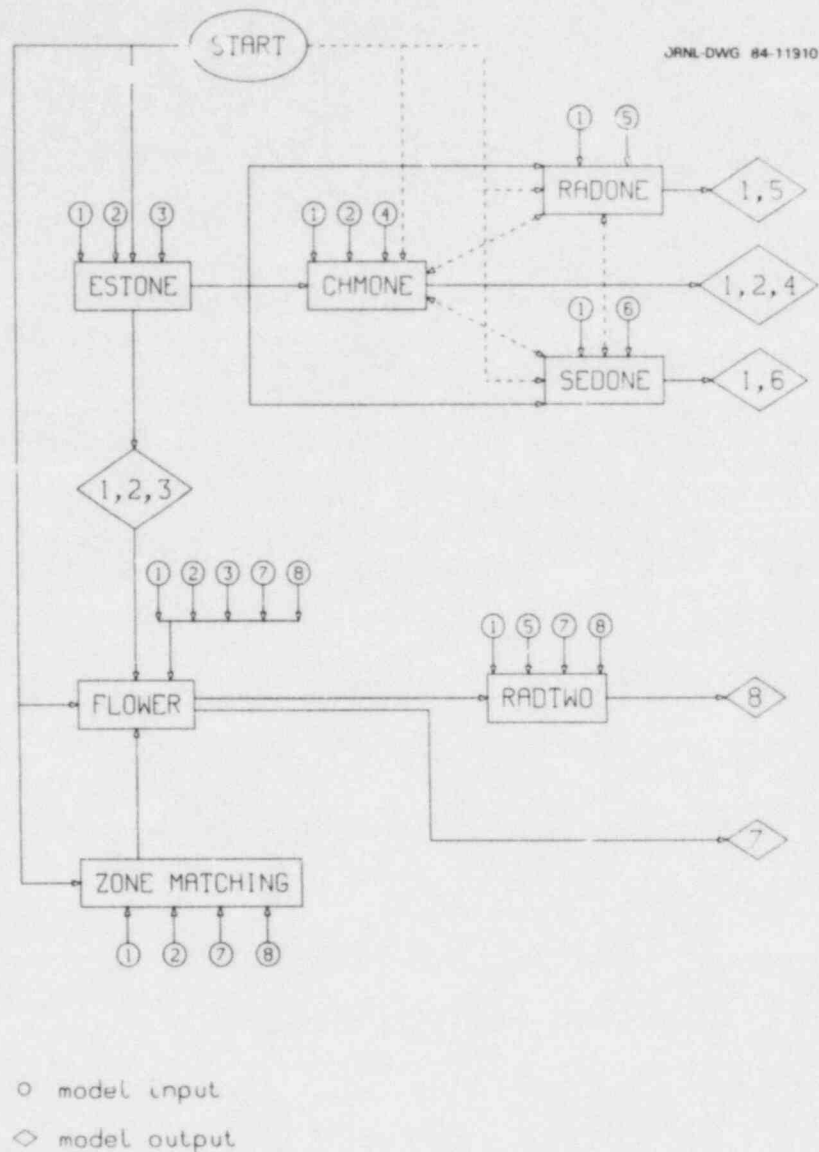


Fig. 2.1. A schematic representation of the sequential application of all UTA models. Numbers refer to list of model inputs and outputs in Sect. 2.1.

the model inputs indicated in Figure 2.1 clearly shows that once a full input data set is developed for one UTA code, all other UTA codes can be applied with minor additional input data.

Figure 2.1 illustrates the sequential application of all the UTA models. The one-dimensional codes are applied first, beginning with ESTONE, for transient, long duration (months) simulations over long

reaches (or the entire length) of a river or estuary. The first important feature of this sequential implementation is that all the one-dimensional codes use identical channel geometry, bathymetry, and hydrodynamic boundary condition input data. Once this input information is prepared for the ESTONE application, the identical data set can be directly input to all other one-dimensional codes. It should also be noted that all channel geometry input to the one-dimensional models is three dimensional, in the form of channel cross sections, as shown in Fig. 2.2. This provides a more accurate representation in the simulations than would be provided by cross-sectional areas and allows the three-dimensional character of the dependent variables to be incorporated into the models. This second aspect will be discussed in greater detail later.

Any one of the other one-dimensional codes (RADONE, CHMONE, and SEDONE) can be used as stand-alone models since all have the capability of hydrodynamic calculations. Each one-dimensional code has the option to by-pass the hydrodynamic computations and instead use externally specified flow conditions. Thus if any one of these codes is applied, the resulting flow field can be input directly to the other codes, by-passing the hydrodynamic calculations. This is an important feature of the UTA since it offers greatly enhanced computational efficiency.

The two- and three-dimensional UTA codes (FLOWER and RADTWO) are designed for more limited duration and spatial extent simulations than the one-dimensional models. These models can use the same channel geometry data as the one-dimensional models; however, two- and three-dimensional models are typically used to provide simulations with

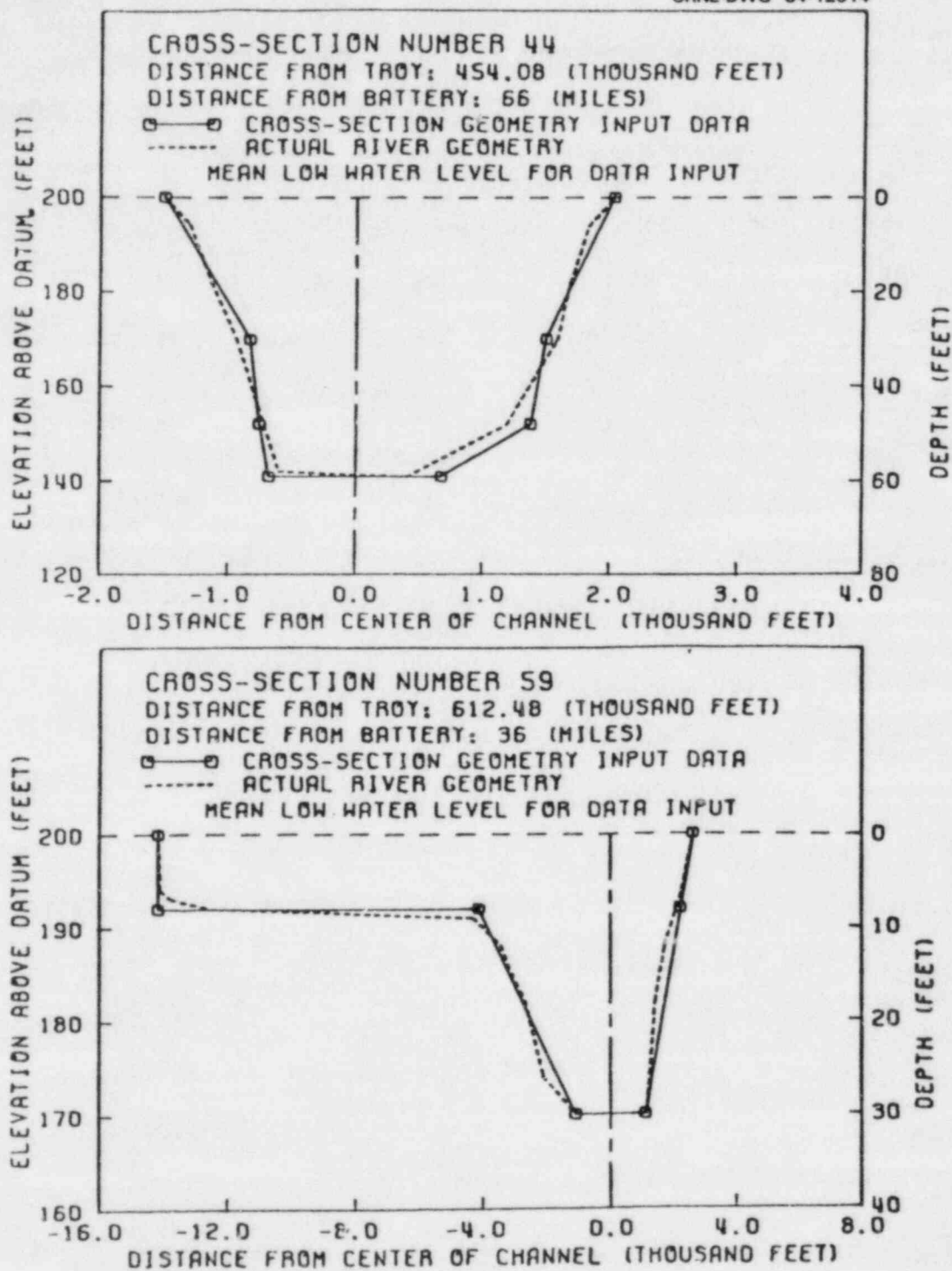


Fig. 2.2. An example of an actual channel cross section as digitized from a navigational chart and as input to ESTONE.

greater spatial resolution. In this case, supplemental data is required. The two- and three-dimensional models use a discrete element grid superimposed on a selected shoreline and bathymetry, as shown in Fig. 2.3.

FLOWER and RADTWO can be applied independently of the one-dimensional model applications. In some cases, however, it is desirable to have the one-dimensional model results to establish boundary conditions for models of higher dimensionality. FLOWER and RADTWO are computationally more demanding than one-dimensional codes and consequently can only be applied to a limited study region. This frequently results in open water boundaries which are far removed from locations where data is available. In such situations, simulated ESTONE transient values for cross-sectional flow, surface elevation, temperature, and salinity can be used as FLOWER boundary conditions. Similarly, if sources of radionuclides exist outside the RADTWO study region, these source contributions can be incorporated into the RADTWO simulations by using radionuclide concentration predicted by a RADONE application, which includes all sources, as boundary conditions.

As illustrated in Fig. 2.1, FLOWER uses the same meteorological input parameters as ESTONE. Because of the higher dimensionality of the model, FLOWER does require power plant intake discharge configuration information beyond that required by ESTONE. This power plant information can be incorporated into the model either directly, by the specification of appropriate intake and discharge boundary conditions, or indirectly, by first applying a zone-matching methodology. The zone-matching methodologies were developed to provide high resolution detail

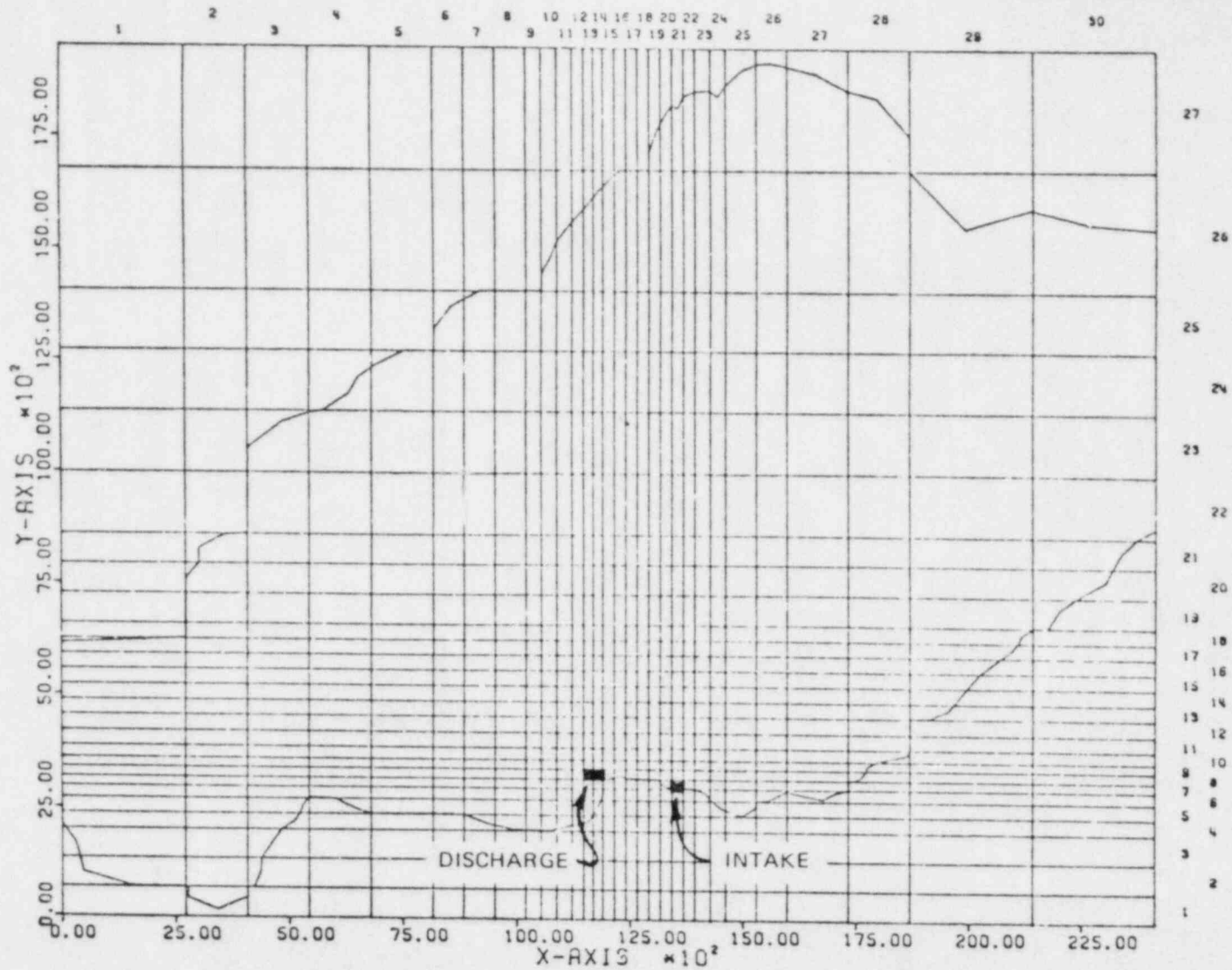


Fig. 2.3(a). An example of the variable computational grid and shoreline representation as input to two- and three-dimensional UTA models.

ORNL-DWG 84-12016

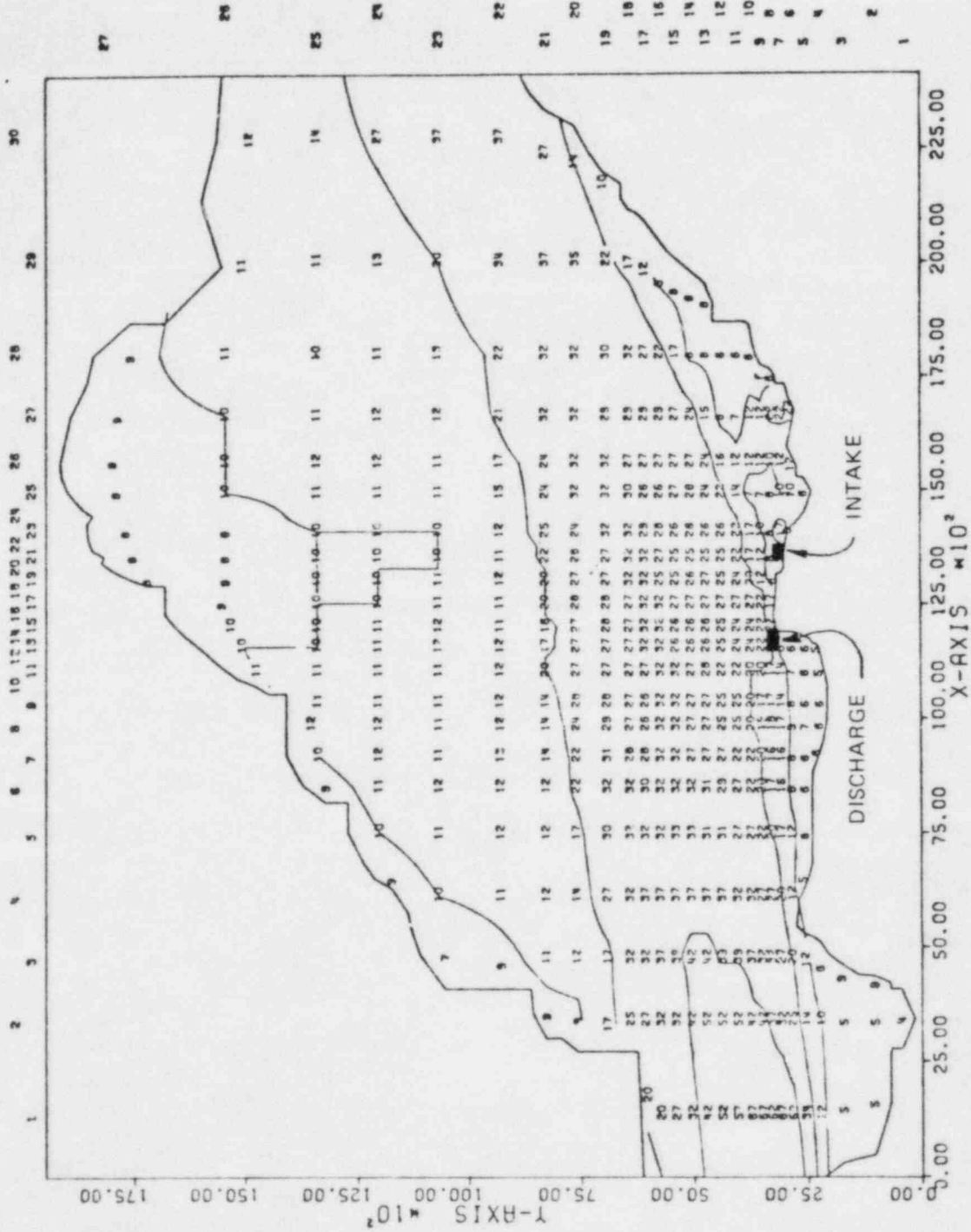


Fig. 2.3(b). An example of bathymetry as input to two- and three-dimensional UTA models.

of the shearing flows near intakes and discharges. Although, in principle, FLOWER can provide high-resolution near-field detail, in practice this is computationally cost prohibitive. After selecting the appropriate zone-matching methodology, a near-field, plant-induced flow field is generated using geometric, ambient flow, and power plant information. This flow field is input to FLOWER and superimposed on the internally calculated far-field conditions.

RADTWO uses identical geometric and bathymetric input as FLOWER. RADTWO, however, does not have the capacity to generate internally the flow field, which must be externally specified. The most convenient way to input this is to use directly the depth-averaged FLOWER output.

Along with the features of the UTA highlighted above, there are other important features inherent in the UTA models. These include accurate shoreline representation, variable grid size, convective defect formulation, turbulent closure, and the discrete element system.

The two- and three-dimensional UTA models allow accurate shoreline representation as shown in Fig. 2.3. In contrast, many computer codes require the shoreline boundary to coincide with sides of the computation grid, producing a stepped boundary. A major advantage of the smooth boundary representation of the UTA is that it avoids the numerical (computational) artifacts which occur in the presence of stepped boundaries.

The variable or telescoping grid feature (also shown in Fig. 2.3) allows high resolution in regions of interest without producing an unmanageable number of computational elements.

The convective defect formulation introduces three-dimensional features into the one- and two-dimensional models. This is accomplished

by assuming a similarity profile for the vertical variations in the dependent variables (flow, temperature, etc.). An example of such a profile is shown in Fig. 2.4. These profiles may vary during the course of model simulations as a result of changing conditions. These similarity profiles are an inherent, fundamental feature of the basic one- and two-dimensional model formulation.

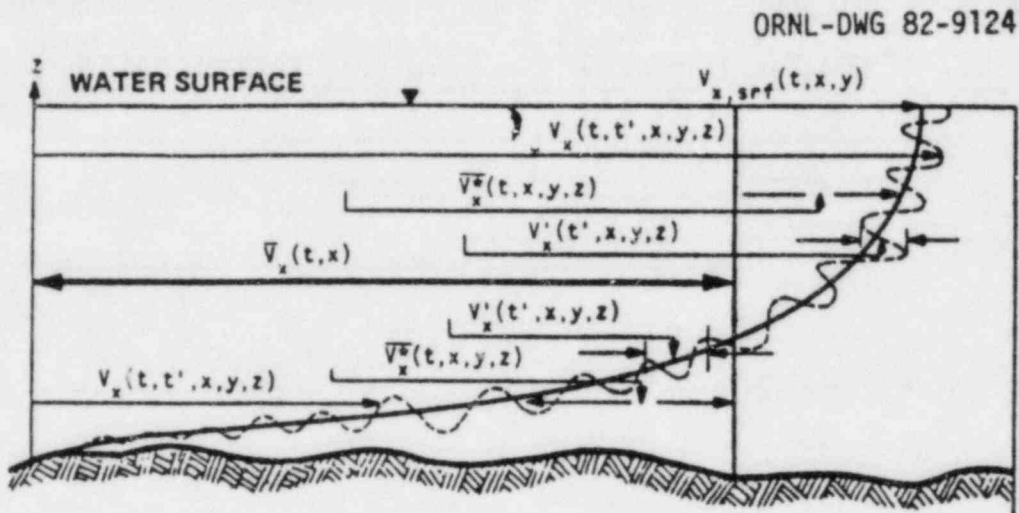


Fig. 2.4. An example of the assumed power-law vertical velocity profile used in the one- and two-dimensional UTA models.

Turbulent closure is a problem encountered in the modeling of all large Reynolds number flows. The most common means of treating turbulence is the eddy viscosity approach in which turbulent stresses are represented as viscous stresses but with an eddy viscosity many orders of magnitude larger than molecular viscosity. The value of eddy viscosity is commonly taken as constant, but realistically it should vary as a function of local conditions. The appropriate value for the eddy viscosity for large-scale flow situations, such as wind-driven currents, is considerably different from that for turbulent jets. The UTA formulation incorporates a variable eddy viscosity formulation which allows the eddy

viscosity to vary (from zero for laminar flows) according to the local velocity. This allows the UTA codes to be applied to a wide range of conditions including laboratory-scale simulations.

The discrete element system considers the integral form of the governing equations applied to individual discrete elements (control volumes). This system offers computational advantages and at the same time allows the incorporation of other previously described features such as arbitrary shorelines and the convective defect formulation.

2.2 Summary of Unified Transport Approach Codes

The UTA consists of six discrete-element fast-transient computer codes (ESTONE, FLOWER, RADONE, RADTWO, CHMONE, and SEDONE) and three zone-matching methodologies. The zone-matching methodologies involve analytic and semi-analytic jet solutions based on the uniformly valid singular perturbation theory and a fully numerical solution using a simplified marker and cell technique. The zone-matching methodologies are presented in detail in Sect. 5. A summary description of the six UTA discrete element codes is given below.

2.2.1 Computer Code: ESTONE

Classification: Fast-transient (tidal-transient), one-dimensional code for simulating hydrodynamic, thermal, and saline conditions in controlled rivers and tidal estuaries, with geometrically complex (or simple) cross sections.

Mathematical Model: Transient, longitudinally one-dimensional, discrete-element formulation. Internally determined nonconvective

transport model which includes the effects of the vertical and lateral variations of flow conditions on the longitudinal, one-dimensional transport.

Computational Algorithm: Explicit, multi-time-step (time-splitting) numerical integration. Second-upwind-differencing interpolation. For the simulation of hydrodynamic conditions, the stability of numerical solutions according to CFL (Courant, Friedrichs and Lewy) criterion, based on maximum speed of surface gravity wave. For simulation of temperature and salinity conditions, the stability of numerical solutions according to the Courant criterion, based on maximum channel flow velocity. Options to exclude hydrodynamic calculations with specified input data for flow conditions (for saving computer time in repetitive simulations of temperature and salinity conditions for the same flow conditions).

Special Features: Longitudinal diffusion and dispersion internally calculated based on convective-defect and eddy-turbulent transport rates. Applicable to all rivers and estuaries without requiring any site-specific dispersion coefficients.

Input Data Capabilities: Includes options for using input data with wide ranges of accuracy and detail, either as simple data sets for approximate simulations or as extensive data sets for detailed and accurate simulations for validation and for the assessment of power plant impact. Specified input data sets can include (1) cross-section

contour profiles; (2) conditions which vary with time or are uniform for all flow variables at the controlled-flow dams, tributaries, discharges, and intakes of power plants, pump storage facilities, and ocean ends; (3) complete meteorological information in the climatological region; (4) rainfall-runoff drainage, and (5) bottom seepage in the geophysical region.

Simulation Capabilities: Predicts longitudinal distributions of the flow conditions (with option to include vertical stratification effects) at specified time intervals (hourly or less) in the specified elements, as (1) water-surface elevation (stage), (2) channel-flow rate, (3) channel-flow velocity, (4) water-temperature, and (5) salinity.

2.2.2 Computer Code: FLOWER

Classification: Fast-transient (tidal-transient) three-dimensional, densimetrically coupled code for simulating stratified (or unstratified) natural and plant-induced hydrodynamic, thermal, and saline conditions in general meso-scale geophysical flow regions (e.g., lakes, rivers, reservoirs, estuaries, and coastal zones), with geometrically complex shoreline boundaries and variable depth conditions.

Mathematical Model: Transient, three-dimensional, discrete-element formulation. Complete formulation of densimetric effects in the form of compressible fluid (without Boussinesq Approximation) in terms of variations of water temperature and salinity. Complete formulation of the

vertical momentum equation (without requiring hydrostatic pressure assumption). Complete formulation of the Coriolis acceleration (force) effects. Complete formulation of free-surface conditions (without requiring rigid lid approximation). Internally determined turbulent transport model, based on local element Reynolds number, universally applicable to flows with different geometrical scale flow regions, including meso-scale geophysical flow regions and laboratory-model-scale flow regions. Application of the model does not require specification of any site-specific coefficient or parameter for the formulation of the turbulent transport model.

Computational Algorithm: Explicit, multi-time-step, composite time-splitting, numerical integration method. Transportative-upwind-differencing interpolation (second-order accuracy for minimizing numerical dispersion). Separate, explicit single-time-step numerical integration of the convective transport terms for minimizing numerical dispersion. Separate, explicit, two-time-step numerical integration of the nonconvective (dispersive) transport terms to guarantee numerical stability. Stability of numerical solutions according to CFL criterion based on maximum speed of surface gravity wave. Could include special option for approximate, computationally efficient simulations with the stability criterion depending on the surface gravity wave associated only with the surface-layer depth rather than the maximum depth of the flow region.

Special Features: Complete nonconvective transport model (laminar and/or eddy-turbulent) is internally determined without requiring any specified coefficient or parameter. Applicable to all geometrical scales of flow regions. Can simulate vortex formations caused by thermally stratifying flows and sinking plumes in lakes, rivers, and reservoirs. Can simulate complete near-field zone (and/or far-field zone), stratified flow conditions in the vicinities and heated water discharges. Can simulate selective intake flow conditions under skimmer walls.

Input Data Capabilities: Includes options for using input data with wide ranges of accuracy and detail, either as simple data sets for approximate simulations, as extensive data sets for detailed and accurate simulations for validations or for predicting the complete physical impact of power plant operations on actual meso-scale flow regions. Specified input data sets can include (1) detailed shoreline boundary geometry; (2) detailed depth variations; and (3) flow conditions which vary with time or are uniform for (a) water surface elevation, temperature and salinity at the open-region boundaries, (b) flow rate, velocity, temperature, and saline conditions at the discharges and intakes of power plants, and (c) complete meteorological data in the climatological region.

Simulation Capabilities: Predicts three-dimensional distributions of flow conditions at specified time intervals (hours, minutes or less) for (1) water surface elevation, (2) three components of velocity, (3) water

temperature, (4) salinity, and (5) pressure (optional) in the elements of the flow region. Can include option to simulate approximate flow conditions by using computationally efficient (less computer time) solution algorithm which restricts the effect of the surface gravity wave to the surface layer.

2.2.3 Computer Code: CHMONE

Classification: Fast-transient (tidal-transient), one-dimensional code for simulating hydrodynamic, thermal, and chemical-species-concentration conditions in controlled rivers and tidal estuaries, with geometrically complex (or simple) cross sections.

Mathematical Model: Transient, longitudinally one-dimensional, discrete-element formulation. Internally determined nonconvective transport model which can include the effects of the vertical and lateral variation of the hydrodynamic, thermal, and chemical-species-concentration conditions on the longitudinal one-dimensional transport. Includes a complete nonequilibrium chemical kinetics model (CHMKIN subroutine) for calculating local time rates of generation of chemical species concentrations.

Computational Algorithm: Explicit, fourth-order Runge-Kutta-Gill numerical integration method. Second upwind-differencing interpolation. For the simulation of hydrodynamic conditions, the stability of numerical solutions according to the CFL criterion, based on maximum speed of

surface gravity wave. For simulations of temperature and chemical species concentrations, the stability of the numerical solutions is according to the Courant criterion, based on maximum channel flow velocity, provided the time rates of chemical reactions are sufficiently slower than the rates of longitudinal transport through the elements. For fast chemical reaction rates, the stability of numerical solutions of the chemical species concentration must be based on the time step of the fourth-order, Runge-Kutta-Gill numerical integration method. Includes option to exclude hydrodynamic calculations with specified input data for flow conditions (for saving computer time in repetitive simulations of chemical species concentration for the same flow conditions).

Special Features: Longitudinal diffusion and dispersion internally calculated based on convective and eddy-turbulent transport rates. Applicable to all rivers and estuaries without requiring any site-specific dispersion coefficients for the transport of dissolved chemical species.

Input Data Capabilities: Includes options for using input data with wide ranges of accuracy and detail, either as simple data sets for approximate simulations or as extensive data sets for detailed and accurate simulations for validation and for the assessment of the chemical impact of discharges on water quality. Specified input data sets can include (1) cross-section contour profiles; (2) conditions which vary across time or are uniform for all flow variables and for the

chemical species concentrations at the controlled-flow dams, tributaries, discharges and intakes of power plants, pump storage facilities, and ocean ends; (3) complete meteorological information in the climatological region, (4) rainfall-runoff drainage and (5) bottom seepage in the geophysical region. Complete nonequilibrium chemical kinetics data can be included for determining the local rates of generation of the chemical species.

Simulation Capabilities: Predicts (1) longitudinal distributions of flow conditions and chemical species concentrations in the element at specified time intervals (hourly or less), (2) water surface elevation (stage), (3) channel-flow rate, (4) channel-flow velocity, and (5) water temperature.

2.2.4 Computer Code: SEDONE

Classification: Fast-transient (tidal-transient), one-dimensional, multi-layer code for simulating hydrodynamic conditions and concentration of multi-class (size, weight, etc.) sediment concentrations in three layers (resident sediment layer, slurry sediment layer, and suspended sediment layer) in controlled rivers and tidal estuaries, with geometrically complex or simple cross sections.

Mathematical Model: Transient, longitudinally one-dimensional, discrete-element formulation, with three layers in vertical direction.

Internally determined, nonconvective longitudinal transport model which incorporates the effect of the vertical variations of the concentrations of each sediment in the slurry sediment layer and suspended sediment layer. Internally determined vertical transport model which includes the effects of local, bottom shear stress and fall velocities of the different sediment classes.

Computational Algorithm: Explicit, multi-time-step (time-splitting) numerical integration. Second-upwind-differencing interpolation. For the simulation of hydrodynamic conditions, the stability of numerical solutions according to the CFL criterion, based on maximum speed of surface gravity wave. For the simulations of the concentrations of sediment classes, the stability of numerical solutions according to the Courant criterion, based on maximum channel-flow velocity or maximum fall velocity of a particular sediment class. Includes option to exclude hydrodynamic calculations with specified input data for flow conditions (for saving computer time in repetitive simulation of sediment concentrations for the same flow conditions).

Special Feature: Longitudinal diffusion and dispersion internally calculated based on convection-defect and eddy-turbulent transport rates which include the vertical distribution of the different sediment classes. Applicable to all rivers and estuaries without requiring any site-specific dispersion coefficients. The specified input data associated with the vertical transport of sediment classes automatically

modifies the longitudinal transport, based on the variations of the concentrations of sediment classes in three layers (resident sediment layer, slurry sediment layer and suspended sediment layer).

Input Data Capabilities: Includes options for using input data with wide ranges of accuracy and detail, either as simple data sets for approximate simulations or as extensive data sets for detailed and accurate simulations for validation and for the assessment of impact on sedimentation. Specified input data sets can include (1) cross-section contour profiles; (2) conditions which vary with time or are uniform for all flow variables and for the concentrations of sediment classes at the controlled-flow dams, tributaries, discharges and intakes of power plants, pump storage facilities, and ocean ends; (3) rainfall conditions in the climatological region; (4) rainfall-runoff drainage; and (5) bottom seepage in the geophysical region.

Simulation Capabilities: Predicts (1) longitudinal distributions of flow conditions at time intervals of an hour or less in the specified elements, as (a) water surface elevation (stage), (b) channel-flow rate, and (c) channel-flow velocity; and (2) distributions of the concentrations of sediment classes in three layers (resident sediment layer, slurry sediment layer and suspended sediment layer) in the elements at specified time intervals (hourly or less). Can accurately simulate the deposition of heavy sediment classes during low flow conditions and resuspension of light sediment classes during high flow conditions. Includes additional capability to simulate tagged sediment concentrations associated with contaminant transport problems.

2.2.5 Computer Code: RADONE

Classification: Fast-transient (tidal-transient), one-dimensional code for simulating hydrodynamic conditions and dissolved-adsorbed two-layer radionuclide concentrations in the bottom sediment layer and in the main flow channel in controlled rivers and tidal estuaries, with geometrically complex (or simple) cross sections.

Mathematical Model: Transient, longitudinally one-dimensional, discrete-element formulation. Internally determined nonconvective longitudinal transport model which incorporates the effect of the vertical variations of the radionuclide concentrations in the main flow channel. Vertical transport model which approximately simulates the bottom deposition and resuspension of adsorbed radionuclides (as concentrations) based on the effects of local bottom shear stress and approximate values for full velocities representing the overall sediment settling effect in the main flow channel. Includes radiological decay rate.

Computational Algorithm: Explicit, fourth-order, Runge-Kutta-Gill numerical integration method. Second-upwind-differencing interpolation. For the simulation of hydrodynamic conditions, the stability of numerical solutions according to the CFL criterion based on maximum speed of surface gravity wave. For simulation of the radionuclide concentrations, the stability of numerical solutions according to the Courant

criterion, based on maximum channel-flow velocity. Includes option to exclude hydrodynamic calculations with specified input data for flow conditions (saving computer time for repetitive flow simulations).

Special Features: Longitudinal diffusion and dispersion internally calculated based on convective-defect and eddy-turbulent transport rates. Applicable to most rivers and estuaries without requiring any site-specific dispersion coefficients for simulating sediment transport conditions. Approximately incorporates the bottom deposition and resuspension effects on the longitudinal and dispersion transport of radionuclides in the main flow channel.

Input Data Capabilities: Includes option for using input data with wide ranges of accuracy and detail, either as simple data sets for approximate simulations or as extensive data sets for detailed and accurate simulations for validation and for determining the distribution of radionuclide concentration resulting from actual releases. Specified input data sets can include cross-section contour profiles; conditions which vary with time or are uniform for the flow variables and radionuclide concentrations at the controlled-flow dams, tributaries, intakes and discharges of power plants, and ocean ends, rainfall and fallout conditions in the climatological region; and rainfall runoff, drainage, and bottom seepage in the geophysical region.

Simulation Capabilities: Predicts longitudinal distributions of the flow conditions at specified time intervals of an hour or less in (1) water surface elevation (stage), (2) channel flow rate, and (3) channel flow velocity. Predicts distribution of the radionuclide concentration in the bottom sediment layer and in the main flow channel in the specified elements and at specified time intervals (hourly or less).

2.2.6 Computer Code: RADTWO

Classification: Transient (tidal-transient), horizontally two-dimensional code for simulating dissolved-adsorbed two-layer radionuclide concentrations in the bottom sediment layer and in the main flow region and in lakes, rivers, reservoirs, estuaries and coastal zones with geometrically complex or simple shoreline boundaries and variable depth conditions.

Mathematical Model: Transient, two-dimensional (in the horizontal geophysical surface plane) discrete-element formulation. Internally determined nonconvective transport model which includes the vertical variations of the velocity conditions and the radionuclide concentrations in the main flow region. Internally determined vertical transport model which approximately simulates the bottom deposition and resuspension of radionuclides as concentrations based on the effects of local bottom shear stress and approximate values for fall velocities representing the overall sediment settling effect in the main flow region. Includes radiological decay rate.

Computational Algorithm: Explicit, multi-time-step (time-splitting) numerical integration method with the option for using fourth-order, Runge-Kutta-Gill method. Second-upwind-differencing interpolation. Stability of numerical solutions is according to the Courant criterion based on maximum velocity component of flow conditions.

Special Features: Horizontally two-dimensional diffusion and dispersion internally calculated based on convective-defect and eddy-turbulent transport rates. Approximately incorporates bottom deposition and resuspension effects on the horizontal transport of radionuclides in the main flow region.

Input Data Capabilities: Includes options for using input data with wide ranges of accuracy and detail, either as simple data sets for approximate simulations or as extensive data sets for detailed and accurate simulations for validation or for predicting the outcome of an actual accidental release. Specified input data sets for flow conditions can include (1) conditions which vary with time or remain constant, (2) multi-harmonic tidal-flow conditions, (3) wind-induced flow conditions, and (4) plant-induced flow conditions. All non-harmonic (non-periodic) flow conditions must be mass conservative. Specified input data for flow conditions can be generated by the output of the computer codes for simulating hydrodynamic conditions. Specified input data sets can include (1) varying depth in the flow region; (2) temporally varying (or uniform) radionuclide concentration conditions at the controlled-flow dams, tributaries, discharges and intakes of power

plants, pump storage facilities, and open region boundaries in coastal zones, and (3) rainfall and fallout conditions in the climatological region.

Simulation Capabilities: Predicts horizontally two-dimensional radio-nuclide concentration conditions in the bottom resident layer and in the main flow region at specified time intervals of an hour or less in the specified elements of the flow region, under general, periodically reversing, and/or uniform drift flow conditions. Can approximately simulate the gradual movement of contaminated bottom deposits by the tidal conditions in a coastal zone, or by the reversing flow conditions in a controlled reservoir.

3. MODEL FORMULATION

A unique and powerful feature of the UTA approach is the inherent three-dimensional aspects of all models. The starting point of the models is a set of three-dimensional governing equations. For models of reduced dimensionality, these governing equations are integrated down, maintaining as much of the more realistic three-dimensional character of the problem as is feasible. This section presents a simplified derivation of the basic equations used in the UTA approach. For specific model details, refer to individual code documentation reports.

All UTA codes begin with the integral form of the appropriate three-dimensional governing equations. The discrete form is achieved by considering small control volumes (discrete elements). To illustrate the basic formulation while avoiding extensive mathematics, derivations will be limited to only the continuity and momentum equations (Batchelor, 1970),

$$\frac{\partial}{\partial t} \iiint_V \rho \, dV + \iint_A \rho \bar{v} \cdot \hat{n} \, dA = 0, \quad (3.1)$$

$$\frac{\partial}{\partial t} \iiint_V (\rho \bar{v}) \, dV + \iint_A (\rho \bar{v}) \bar{v} \cdot \hat{n} \, dA = \iiint_V \bar{f}_b \, dV + \iint_A \bar{f}_s \, dA, \quad (3.2)$$

where

t = time,

V = volume,

ρ = density,

A = area,

\bar{v} = velocity vector,

\hat{n} = unit normal to enclosure surface,

\bar{f}_b = body forces, and

\bar{f}_s = surface forces.

For simplicity, constant density is assumed here. Note, however, that the UTA codes include full densimetric effects. With this assumption, the governing equations become

$$\frac{\partial}{\partial t} \iiint_V \bar{v} \, dv + \iint_A \bar{v} \cdot \hat{n} \, d\alpha = 0 \quad (3.3)$$

and

$$\frac{\partial}{\partial t} \iiint_V \bar{v} \, dv + \iint_A \bar{v} \cdot \bar{v} \cdot \hat{n} \, d\alpha = \frac{1}{\rho} \iiint_V \bar{f}_b \, dv + \frac{1}{\rho} \iint_A \bar{f}_s \, d\alpha . \quad (3.4)$$

3.1 Three-Dimensional Equations

The UTA assumes that all dependent variables are represented by a three-component decomposition. This element of model formulation is conceptually identical for all models; however, there are differences in implementation between three-dimensional models and models of lower dimensionality. Consequently, a separate treatment of model formulation is provided for the three-dimensional case.

Making a continuum discrete requires averaging in both space and time of all dependent variables. In order to maintain maximum representation of subgrid-scale phenomena, all variables are decomposed into a spatial- and temporal-averaged primary scale, a subgrid-scale primary component (the convective defect), and a secondary subgrid fluctuating (turbulent) component. For the continuity and momentum equations, these three components are denoted by $\langle \bar{v} \rangle$, \bar{v}^* , \bar{v}' , respectively.

The brackets represent the averaging process. To better illustrate the

function of these three components, consider the vertical (z) variation of the x -component of velocity as shown in Fig. 3.1. Here it is assumed that

$$v_x(z,t) = \langle v_x(t) \rangle + v_x^*(z,t) + v_x^i(z,t), \quad (3.5)$$

where $\langle v_x \rangle$ is the velocity component averaged over the vertical extent of the control volume $\Delta z = z_2 - z$ and time step Δt , v_x^* is the convective defect which represents velocity variations in the vertical direction on the order of Δz , and v_x^i are the high-frequency small-vertical-scale fluctuations. The definition of the averaging operation implies that integration and averaging are interchangeable operations, $\langle \bar{v}^i \rangle = 0$, and that integrals of $\langle \bar{v}^* \rangle$ are zero.

Substitution of Eq. (3.5) into Eq. (3.3) and the x -component of Eq. (3.4), and averaging yields

$$\frac{\partial}{\partial t} \iiint_V dv + \iint_A \langle \bar{v} \rangle \cdot \hat{n} \, da = 0 \quad (3.6)$$

and

$$\begin{aligned} \frac{\partial}{\partial t} \iiint_V \langle v_x \rangle \, dv + \iint_A \langle v_x \rangle \langle \bar{v} \rangle \cdot \hat{n} \, da + \iint_A [\langle v_x^* v_x^* \rangle + \langle v_x^i v_x^i \rangle] \cdot \hat{n} \, da \\ = \frac{1}{\rho} \iiint_V \langle f_{bx} \rangle \, dv + \frac{1}{\rho} \iint_A \langle f_{sx} \rangle \, da. \end{aligned} \quad (3.7)$$

It is clear from inspection of Eq. (3.7) that the last two terms on the right side of Eq. (3.5) are manifested in the momentum equation as Reynold's stresses. In fact, these terms will be treated collectively (discussed under Model Closure, Sect. 3.3). The reason for considering these components separately is formulation consistency. It will be shown that for models of lower dimensionality the convective defect and turbulent fluctuations produce significantly different effects in the momentum equation.

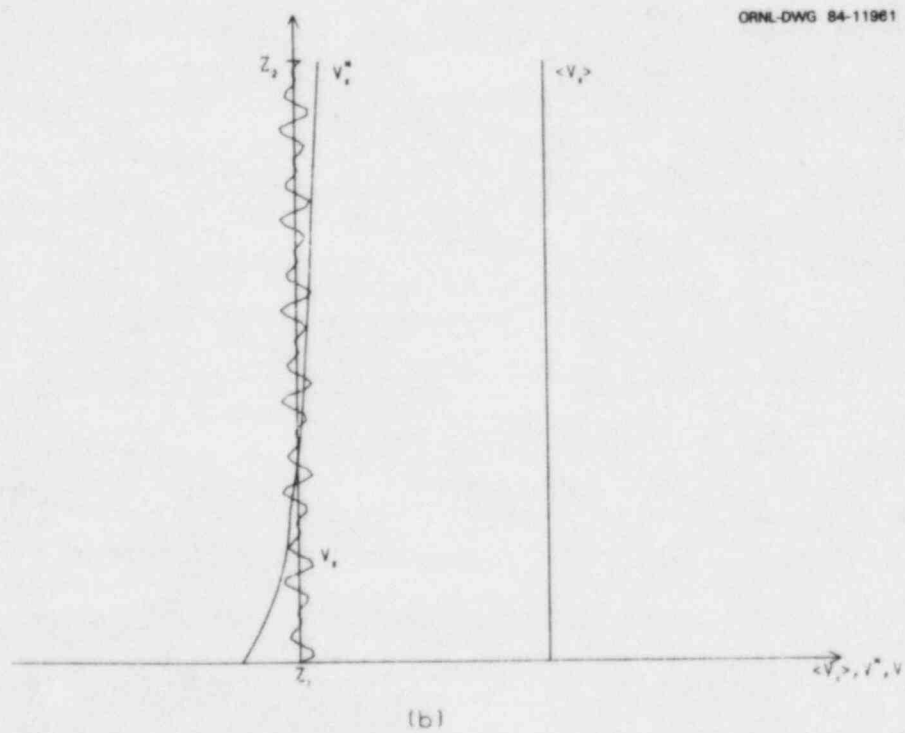
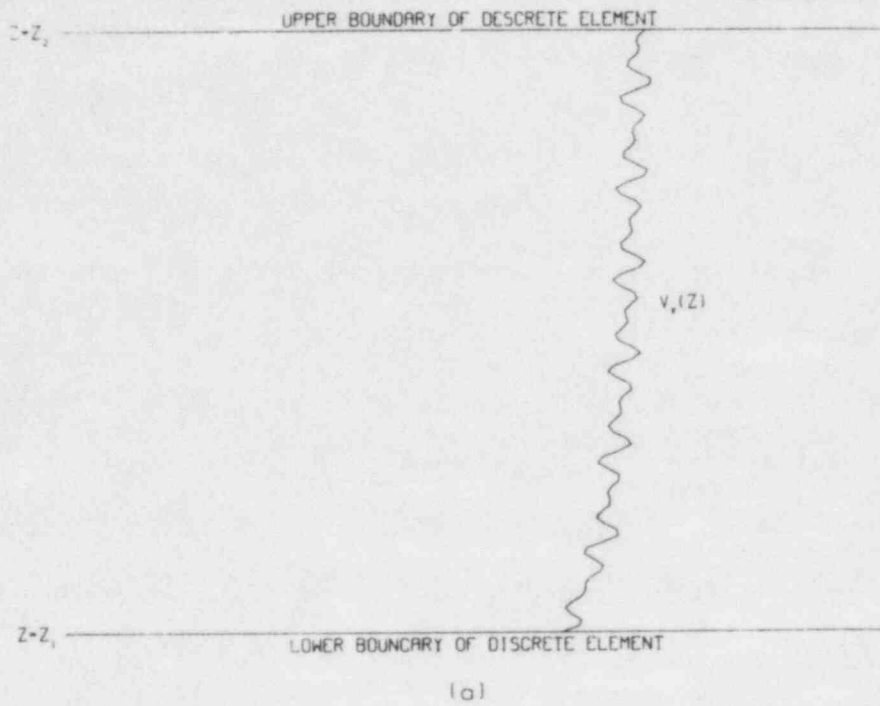


Fig. 3.1. (a) Representation of the vertical variation of the x-component (horizontal) of velocity over the vertical extent of the discrete element and (b) the three-term decomposition of this velocity.

It can now be assumed that the integrands are constant within the small enclosure volumes so that Eqs. (3.6) and (3.7) become

$$\frac{\partial V}{\partial t} + \sum_{\mathbf{i}} \langle v_{\mathbf{i}} \rangle n_{\mathbf{i}} A_{\mathbf{i}} = 0 \quad (3.8)$$

and

$$\begin{aligned} \frac{\partial}{\partial t} (\langle v_x \rangle V) + \sum_{\mathbf{i}} \left[\langle v_x \rangle \langle v_{\mathbf{i}} \rangle - \sigma_{x,\mathbf{i}}^{*'} \right] n_{\mathbf{i}} A_{\mathbf{i}} \\ = \frac{\langle f_{bx} \rangle}{\rho} V + \frac{1}{\rho} \sum_{\mathbf{i}} \langle f_{sx,\mathbf{i}} \rangle n_{\mathbf{i}} A_{\mathbf{i}}, \end{aligned} \quad (3.9)$$

where the summation in these equations indicates summation over enclosure faces, the $n_{\mathbf{i}}$ reflects the sign of the unit normal vector, and the stress term $\sigma_{x,\mathbf{i}}^{*}$ in Eq. (3.9) represents the $\langle v_x^* v^* \rangle + \langle v_x' v' \rangle$ term.

The body force term involves gravity and rotational forces. The inclusion of this term is straightforward and for simplicity will be omitted from the remainder of the derivation. Surface forces include pressure and viscous stresses and can be represented by

$$\langle f_{sx,\mathbf{i}} \rangle = -(p-p_a) i_x + \rho \sigma_{sx,\mathbf{i}} \quad (3.10)$$

where p is pressure, p_a is atmospheric pressure, and $\sigma_{sx,\mathbf{i}}$ are the viscous stress components. The i_x subscript indicates summation over enclosure faces normal to the x -axis. Substituting Eq. (3.10) into Eq. (3.9) and using the definition of volume flux $G_{\mathbf{i}} = \langle v_{\mathbf{i}} \rangle n_{\mathbf{i}} A_{\mathbf{i}}$ in both Eqs. (3.8) and (3.9) yields the final form of the governing equations:

$$\frac{\partial V}{\partial t} + G_{\mathbf{i}} = 0 \quad (3.11)$$

and

$$\frac{\partial}{\partial t} (\langle v_x \rangle V) + \langle v_x \rangle G_{\mathbf{i}} - \sigma_{x,\mathbf{i}}^{*'} n_{\mathbf{i}} A_{\mathbf{i}} = -\frac{1}{\rho} (p-p_a) i_x n_{\mathbf{i}} A_{\mathbf{i}} + \sigma_{sx,\mathbf{i}} n_{\mathbf{i}} A_{\mathbf{i}} \quad (3.12)$$

where for convenience the summation symbol has been omitted but is implied.

Equations (3.11) and (3.12) are a simplified representation of three-dimensional model equations. For illustration purposes, constant density has been assumed, body forces have been neglected, and externally specified sources and sinks have been omitted. All of these are included in the UTA codes, and for more information regarding the inclusion of these terms in the derivation, the reader is referred to FLOWER (Eraslan, Lin, Sharp, 1983). The treatment of stress terms will be addressed in Sect. 3.3.

3.2 One-Dimensional Equations

To illustrate the development of the lower-dimensioned models, to demonstrate the consistency with the three-dimensional formulation, and to highlight the three-dimensional character of UTA models of lesser dimensions, a derivation of the one-dimensional (cross-section-averaged) form of the continuity and momentum equations is presented. The derivation can start with the three-dimensional formulation using Eqs. (3.6) and (3.7), once again ignoring body forces and noting that in the one-dimensional case, $\bar{v} = v_x$. Thus the one-dimensional continuity and momentum equations can be written

$$\frac{\partial}{\partial t} \iiint_V dv + \iint_{A_x} \langle v_x \rangle da \quad (3.13)$$

and

$$\begin{aligned} \frac{\partial}{\partial t} \iiint_V \langle v_x \rangle dv + \iint_{A_x} \langle v_x \rangle \langle v_x \rangle da + \iint_{A_x} \langle v_x^* v_x^* \rangle da + \iint_{A_x} \langle v_x' v_x' \rangle da \\ = \frac{1}{\rho} f_{sx} da, \end{aligned} \quad (3.14)$$

where A_x represents enclosure areas normal to the x-direction. The control volume of an element can be represented by the product of the length Δx , width B , and height to the free surface. With this, Eq. (3.13) can be written

$$\Delta x B \frac{\partial H}{\partial t} + \sum_{i_x} G_{x,i_x} n_{i_x}, \quad (3.15)$$

where the index i_x indicates enclosure faces normal to the x-axis. The first two terms of Eq. (3.14) can similarly be expressed as

$$\begin{aligned} \frac{\partial}{\partial t} \iiint_V \langle v_x \rangle dv &= \Delta x \frac{\partial G_x}{\partial t}, \\ \iint_{A_x} \langle v_x \rangle \langle v_x \rangle da &= \sum_{i_x} \langle v_{x,i_x} \rangle G_{x,i_x}. \end{aligned} \quad (3.16)$$

The third term in Eq. (3.14) involves the convective defect. The inclusion of this term and its treatment in the model formulation is unique to UTA, allowing the explicit inclusion of three-dimensional geometry and flow structure. The convective defect formulation explicitly admits laterally variable vertical gradients of all dependent variables as represented in Fig. 3.2. This is accomplished by assuming laterally varying vertical similarity profiles such as those shown in Fig. 3.3. This is an important deviation from the three-dimensional model formulation where variations over the limited vertical extent of an element are small compared with those over the entire channel depth.

For the momentum convective defect, v_x^* is assumed to exhibit a Blasius power law profile with local channel depth of the form

$$v_x^* = \langle v_x \rangle \left[\frac{(n+1) \langle D \rangle}{n \langle D^2 \rangle} D(y) (1-\eta)^{1/n} - 1 \right], \quad (3.17)$$

where $D(y)$ is the laterally variable local channel depth, $\eta = 1-z/D(y)$, and

$$\langle D^m \rangle = \frac{1}{B(x)} \int_{B(x)} D^m(y) dy, \quad (3.18)$$

ORNL-DWG 82-9125

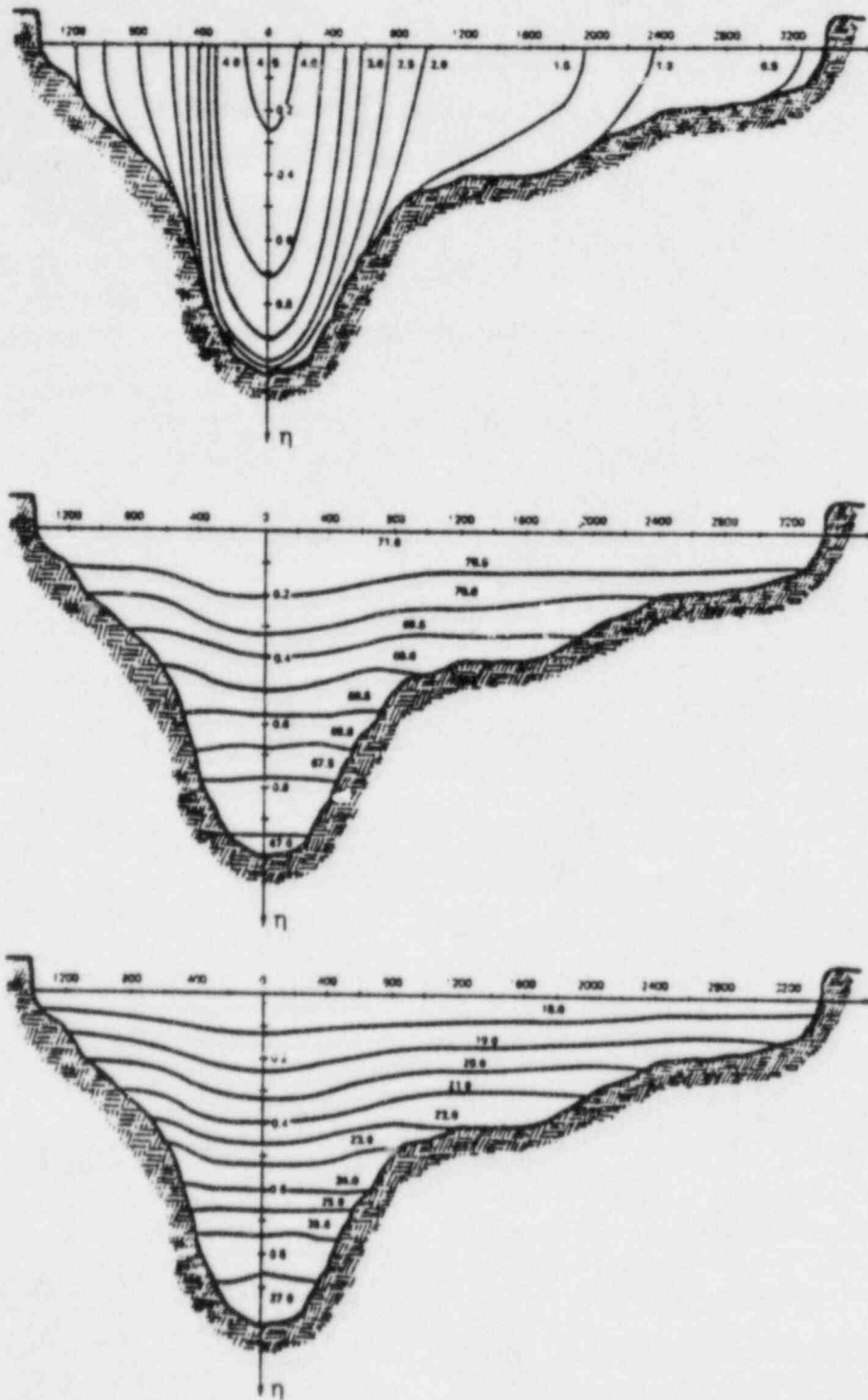


Fig. 3.2. A schematic representation of the type of lateral and vertical variations in (a) downstream flow, shown as constant velocity contours, (b) temperature, shown as isotherms, and (c) salinity shown as isohalines, accounted for in the one-dimensional ESTONE model.

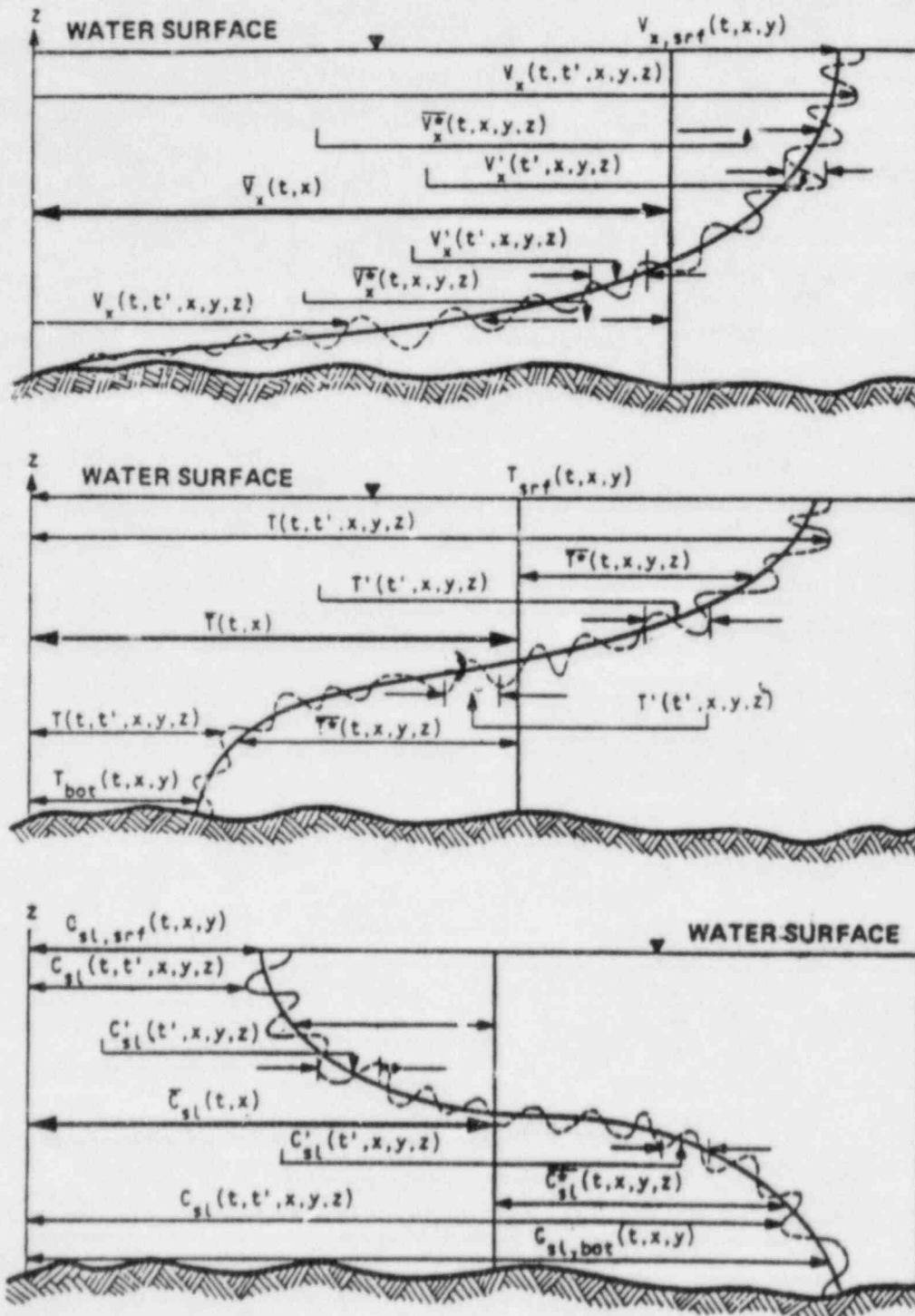


Fig. 3.3. A schematic representation of the vertical profiles and three-term decomposition for (a) velocity, (b) temperature, and (c) salinity, as assumed in the one-dimensional ESTONE model.

where $B(x)$ is the surface channel width. Substituting Eq. (3.17) into the third term of Eq. (3.14) gives

$$G_x^* = \iint_{A_x} \langle v_x^* v_x^* \rangle da = \int_{B(x)} \int_0^1 \langle v_x^* v_x^* \rangle dn dy \quad (3.19)$$

$$= - \left\{ 1 - \left[\frac{n+1}{n} \right]^2 \frac{n}{n+2} \left[\frac{\langle D \rangle \langle D^3 \rangle}{\langle D^2 \rangle^2} \right] \right\} G_x |\langle v_x \rangle|.$$

The convective defect formulation for temperature and salinity uses cubic vertical profiles. The parameters defining these profiles are allowed to vary with time and position as a function of local Froude number to reflect hydrodynamic stability considerations. For more information on the one-dimensional convective defect formulation, the reader is referred to ESTONE (Eraslan, 1983). Note that for the computationally one-dimensional UTA codes, it is possible to generate approximate three-dimensional results, such as shown in Fig. 3.2, by using the computed vertical profiles.

The fourth term of Eq. (3.14) represents turbulent stresses. This term can be combined with the viscous stress component of the surface force term [the last term of Eq. (3.14)], which after integration results in a stress-matching condition at the free surface and channel bottom. These terms then become a wind stress term, $\langle f_{x,srf} \rangle \Delta x B(x)$, and a bottom drag term $\langle F_{x,bot} \rangle \Delta x$. The precise form of these terms will be discussed in Sect. 3.3.

The remaining part of the surface force term accounts for pressure effects. These are represented in terms of the free surface displacement using substitution from the hydrostatic pressure relationship implied by the vertical component of the momentum equation.

The final form of the continuity equation is given by Eq. (3.15), and the final form of the momentum equation can be written

$$\frac{\partial G_x}{\partial t} + \frac{1}{\Delta x} \sum_{i_x} \langle v_{x,i_x} \rangle G_{x,i_x} + \frac{1}{\Delta x} \sum_{i_x} G_{x,i_x}^* = \frac{g}{\Delta x} \sum_{i_x} H_{i_x} A_{i_x} + \langle F_{x,bot} \rangle + B(x) \langle f_{x,srf} \rangle, \quad (3.20)$$

where g is the gravitational acceleration.

All the lateral and vertical integration indicated in this derivation is automatically performed by the computer codes. Thus, one- and two-dimensional models use the same geometric input data as the three-dimensional models. Once a data set is generated for one UTA model, it can be used for all UTA models, independent of dimensionality.

3.3 Model Closure

Closure of the one- and three-dimensional governing equation previously derived requires a representation of viscous and turbulent stress terms. The treatment of the stress term in the three-dimensional model utilizes a eddy viscosity formulation. The deficiency of constant eddy viscosity schemes is that a single value for the eddy viscosity cannot adequately represent the turbulent stresses associated with a variety of flow phenomena. For example, an eddy viscosity value for far-field ambient flows would be inappropriate for near-field, high shear jet regions. In order to achieve a turbulence formulation valid over a broad range of flow conditions while avoiding the computational costs of a higher order closure scheme, the UTA approach uses a variable eddy viscosity formulation in which the turbulent eddy coefficient can vary, in both space and time, as a function of the local large-scale

features of the flow field. In this formulation, the stress term [see Eq. (3.12)] is represented by

$$\sigma_{sx, \hat{i}} = -(1 + \delta_{x, \hat{i}}) \epsilon_x \frac{\partial}{\partial x} \langle v_{\hat{i}} \rangle, \quad (3.21)$$

where $\delta_{x, \hat{i}}$ is the Kronecker delta and ϵ_x is the eddy coefficient.

The eddy coefficient is expressed in terms of the molecular viscosity ν , a Blasius power law, and a locally variable Reynolds number Re_x by

$$\epsilon_x = \nu + \begin{cases} \nu Re_x \left[\left(\frac{n+1}{n} \right)^{2/n+1} \beta^{2n/n+1} \right]^{n-1/n+1} & \text{for } Re_x > 4000 \\ 0 & \text{for } Re_x \leq 4000 \end{cases} \quad (3.22)$$

The Reynolds number is defined as the product of Δx and the absolute value of the local variations of the transverse velocity components ($\langle v_y \rangle$, $\langle v_z \rangle$ in this case) divided by ν .

In the one-dimensional model, shear stress is evaluated at the channel bottom and free surface. The stress at the channel bottom is a drag force per unit channel width. This bottom stress can be calculated based upon the molecular viscosity, ν , and the shear associated with the assumed Blasius power-law vertical velocity profile [Eq. (3.17)] to give

$$\langle F_{x, \text{bot}} \rangle = - \left(\frac{n+1}{n} \right)^{-2n/n+1} \beta^{2n/n+1} \nu^{2/n+1} \frac{\langle D^{2(n-1)/n+1} \rangle}{B(x)^{(n-1)/n+1} \langle D^2 \rangle^{2n/n+1}} G_x^{2n/n+1} \quad (3.23)$$

By rearranging terms, it can be shown that the bottom drag force is proportional to the local Reynolds number in a manner similar to the eddy coefficient in the three-dimensional formulation.

The stress at the free surface is treated by the requirement that stress be continuous across the air/water interface. Thus, the stress at the free surface must be equal to the wind stress at the free surface which is computed using externally specified meteorological parameters.

3.4 Formation of Discrete Model Equations

The previously derived model equations must be cast in a discrete form in order to allow numerical computation. Forming discrete three-dimensional model equations is quite complex because of the many enclosure faces which must be considered for each discrete element. A detailed discussion of the three-dimensional discrete form is beyond the scope of this report. Consequently, the UTA discrete formulation will be illustrated using the one-dimensional model equations. For a complete discussion of three-dimensional discrete equations, the reader is referred to FLOWER (Eraslan, Lin, and Sharp, 1983).

The one-dimensional continuum governing equations is given by Eq. (3.15) and (3.20). The first term of the continuity equation, Eq. (3.15), represents the time-rate-of-change of water volume in a discrete element. This then implies that this term be evaluated at the center of the element. For the i^{th} element, this computational point is denoted by a subscript i , and the first term of Eq. (3.15) is represented in discrete form as $\partial H_i / \partial t$. The second term of the continuity equation is a sum of volume fluxes over the enclosure faces of the discrete element. For the i^{th} discrete element, the locations of the upstream and downstream enclosure faces are denoted by the subscripts $i-1/2$ and $i+1/2$, respectively. The discrete form of the second term of the continuity equation is written as $(G_{x,i-1/2} - G_{x,i+1/2}) / \Delta x_i B_i$, and the discrete form of the continuity equation becomes

$$\frac{\partial H_i}{\partial t} = \frac{1}{\Delta x_i B_i} (G_{x,i-1/2} - G_{x,i+1/2}) \quad , \quad (3.24)$$

where Δx_i is the length of the i^{th} discrete element, and B_i is the surface channel width evaluated at the center of the discrete element.

The discrete form of the momentum equations [Eq. (3.20)] is somewhat different from the continuity equation as a result of the consideration of pressure effects. In order to avoid the misrepresentation of pressure effects, it is necessary to compute momentum at different points than the free surface displacement. This is commonly accomplished by a staggered system where momentum is computed at points midway between free surface displacement computational points. Thus, for the i^{th} element, the momentum could be calculated at the $i+1/2$ location. This is an acceptable approach, however, the UTA formulation considers the momentum at two points between adjacent free surface displacement computation points. The motivation for this is accuracy. Small errors in momentum, when used in the continuity equation, yield small errors in computed free surface displacement. A small error in free surface displacement can produce an amplified error in the pressure term of the momentum equation. This occurs because in the pressure term the free surface displacement is multiplied by the gravitation acceleration. This then results in a magnified momentum error. To minimize such errors, the accuracy of the momentum computation is increased by increasing the number of momentum computation points.

In the UTA formulation, the double momentum computation points are defined by dividing each discrete element i into two half-elements. The upstream half-element is centered at $i-1/4$, and the upstream and downstream enclosure faces for this half-element are at positions $i-1/2$ and

i , respectively. Similarly, the downstream half-element of the i^{th} discrete element has a center point at $i+1/4$, and upstream and downstream enclosure faces are at i and $i+1/2$, respectively.

In the discrete form of the momentum equation for the upstream half-element, the first term of Eq. (3.20) is the time rate of change of momentum in the half element and, therefore, is evaluated at the center of the half-element $i-1/4$. The second and third terms of Eq. (3.20) represent momentum flux into or out of the half-element and are evaluated at the enclosure faces $i-1/2$ and i . The fourth term of Eq. (3.20) is the pressure gradient evaluated at the half-element upstream and downstream enclosure faces. The bottom drag and free surface stress, the last two terms of Eq. (3.20), are evaluated at the surface and bottom enclosure faces using the previously described closure formulation and are specified at the half-element center $i-1/4$. Thus the discrete form of the momentum equation becomes

$$\begin{aligned} \frac{\partial G_{x;i-1/4}}{\partial t} = & \frac{2}{\Delta x_i} \left(G_{x;i-1/2} \langle v_{x;i-1/2} \rangle - G_{x;i} \langle v_{x;i} \rangle \right) \\ & + \frac{2}{\Delta x_i} \left(G_{x;i-1/2}^* - G_{x;i}^* \right) + \frac{2g}{\Delta x_i} \left[A_{i-1/2} \left(H_{i-1/2} - H_{i-1/4} \right) \right. \\ & \left. - A_i \left(H_i - H_{i-1/4} \right) \right] + \langle F_{x,\text{bot};i-1/4} \rangle + B_{i-1/4} \langle f_{x,\text{srf};i-1/4} \rangle \end{aligned} \quad (3.25)$$

The discrete form of the momentum equation for the downstream half-element $i+1/4$ is similar to Eq. (3.25).

Inspection of equations (3.24) and (3.25) reveals that while the free surface displacement is calculated at element centers i , it must also be evaluated at the half-element centers and enclosure faces. A similar situation exists for the volume flux. Consequently, in order to

close the discrete formulation, interpolation formulas must be established. The formulas used for the discrete model equations are

$$H_{\underline{i+1/2}} = (\Delta x_i H_{\underline{i+1}} + \Delta x_{\underline{i+1}} H_i) / (\Delta x_i + \Delta x_{\underline{i+1}}), \quad (3.26a)$$

$$H_{\underline{i+1/4}} = (H_{\underline{i+1/2}} + H_i) / 2, \quad (3.26b)$$

$$G_{x;\underline{i}} = (G_{x;\underline{i-1/4}} + G_{x;\underline{i+1/4}}) / 2, \quad (3.26c)$$

and

$$G_{x;\underline{i+1/2}} = (\Delta x_i G_{x;(\underline{i+1})\underline{-1/4}} + \Delta x_{\underline{i+1}} G_{x;\underline{i+1/4}}) / (\Delta x_i + \Delta x_{\underline{i+1}}). \quad (3.26d)$$

Geometric input data A and B are provided at the $\underline{i+1/2}$ discrete element enclosure faces but must be evaluated at other locations. The interpolation formulas for these variables are

$$B_{\underline{i}} = (B_{\underline{i-1/2}} + B_{\underline{i+1/2}}) / 2, \quad (3.27a)$$

$$B_{\underline{i+1/4}} = (B_{\underline{i+1/2}} + B_{\underline{i}}) / 2, \quad (3.27b)$$

$$A_{\underline{i}} = (A_{\underline{i-1/2}} + A_{\underline{i+1/2}}) / 2, \quad (3.27c)$$

and

$$A_{\underline{i+1/4}} = (A_{\underline{i+1/2}} + A_{\underline{i}}) / 2. \quad (3.27d)$$

4. TREATMENT OF BOUNDARIES

The UTA codes are designed to accommodate solid impermeable boundaries and open boundaries. The impermeable boundaries represent shorelines, while the open boundaries represent water-to-water interfaces. In the one-dimensional codes, the channel geometry is input and used in the cross-sectional averaging operation (Sect. 3.2), and the impermeable boundary condition is only applied in these codes if one end of the channel is closed.

4.1 Shoreline Boundaries

For two- and three-dimensional codes, shoreline boundaries are quite accurately represented. Unlike most finite difference formulations which require shoreline boundaries to coincide with the edge of a rectangular grid cell [Fig. 4.1(a)], the UTA discrete element formula-

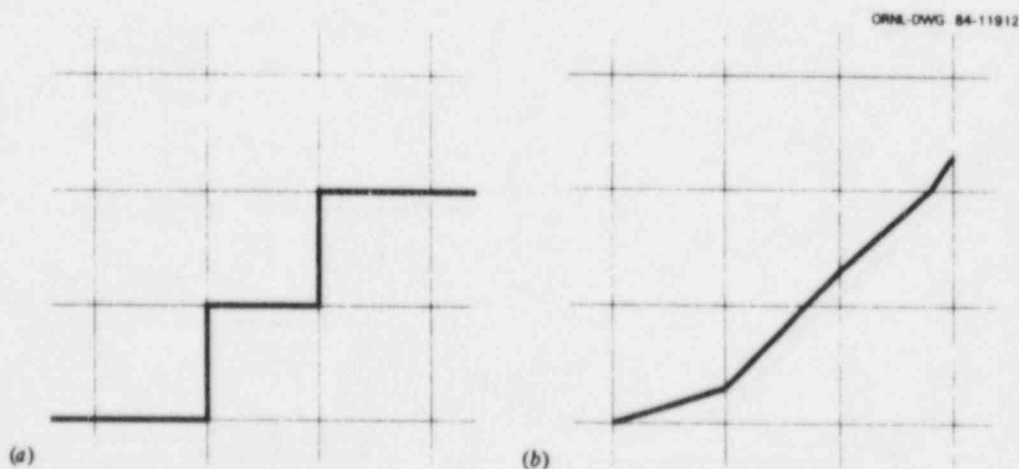


Fig. 4.1. An example of (a) a stepped shoreline boundary typical of many computational schemes and (b) the more accurate shoreline representation used in the two- and three-dimensional UTA models.

tion allows an arbitrary shoreline with respect to each rectangular grid element as shown in Fig. 4.1(b). This is accomplished by specifying as input data shoreline intercept points for each shoreline boundary element as shown in Fig. 4.2. The computer code automatically uses this

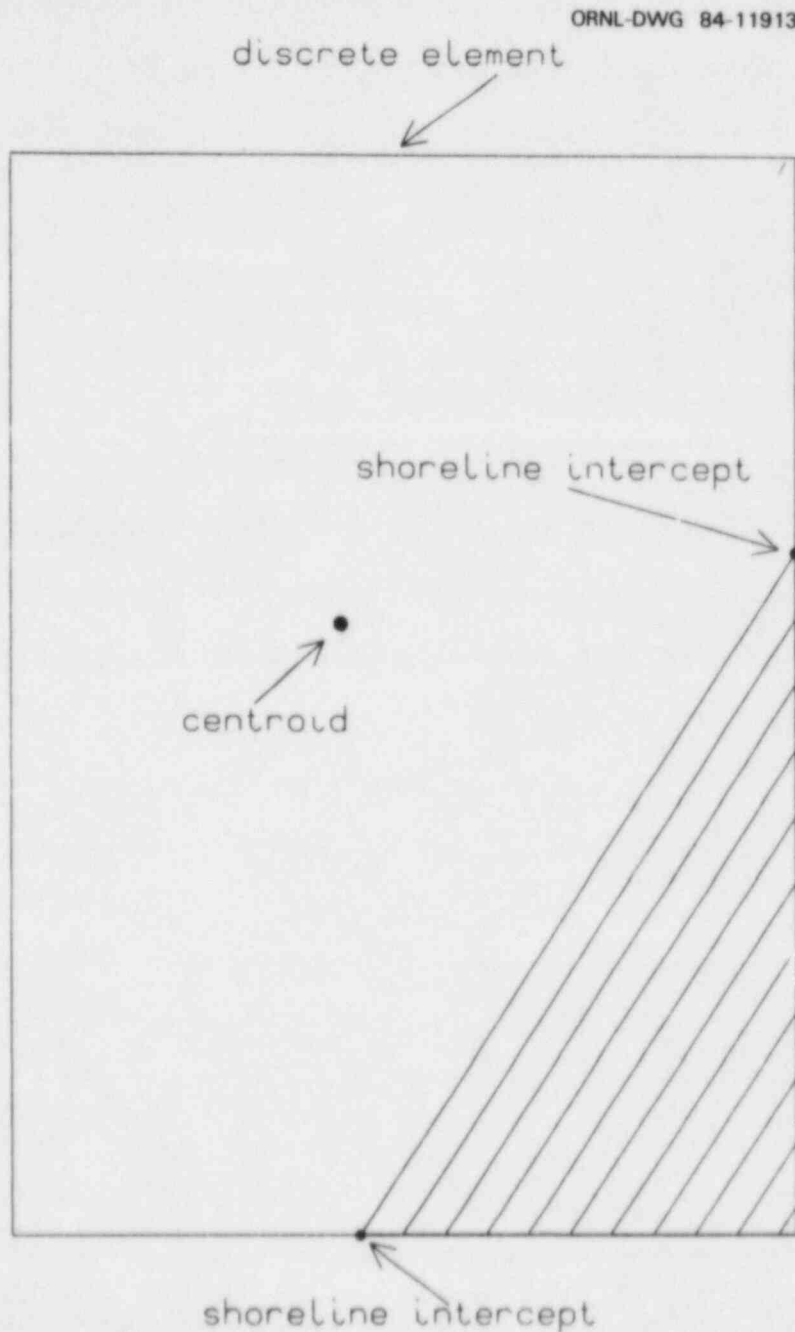


Fig. 4.2. A schematic representation of the treatment of a shoreline element in the UTA models

information to modify enclosure faces and element volume to reflect partially wetted elements and to compute the centroid of water volume, moving the computational point to the element centroid for increased computational accuracy.

The shoreline boundary is assumed to be impermeable, i.e., a no flow boundary. One of the important features of the discrete element formulation is that it does not calculate the velocity component normal to a shoreline boundary in the half-element adjacent to the boundary. Thus this formulation completely eliminates the possibility of numerical instabilities associated with near-shore velocity discontinuities.

While the flow is specified as no flow at shoreline boundaries, the free-surface displacement must be allowed to vary in both space and time at the shoreline elements. The free-surface displacement at shoreline enclosure faces is calculated via an extrapolation formula based upon free-surface displacements computed at nearby internal elements. For simplicity, these formulas will be provided only for the one-dimensional formulation. For comparable information regarding models of higher dimensionality, the reader is referred to the relevant model reports. A shoreline boundary in the one-dimensional formulation implies that one end of the channel is closed and that forcing is provided by an open boundary at the other end and perhaps by tributaries or other intermediate sources or sinks. For an upstream closed boundary, the boundary element is $i=1$, and the impermeable boundary is defined by the enclosure face at $1-1/2$. The free-surface displacement is calculated at this location by

$$H_{1-1/2} = H_1 + \frac{(H_1 - H_2)}{(\Delta x_1 + \Delta x_2)} \quad (4.1)$$

Similarly, if the impermeable boundary occurs at the most downstream element $i=N$, the free-surface displacement is calculated at the $N+1/2$ enclosure face using a comparable extrapolation formula.

For advected (transported) dependent variables such as temperature T (or salinity, passive additives, etc.), shoreline boundaries imply an insulated or zero gradient condition. In discrete form for an upstream closed boundary, the boundary condition is expressed as

$$T_{1-1/2} = T_1 \quad (4.2)$$

4.2 Open Boundaries

Open boundary conditions may occur along three sides of a rectangular modeled region in coastal situations, two sides (upstream and downstream) of a modeled region for rivers or channels, or a part of one or more sides for situations involving embayment regions or tributary inflows. At such boundary elements, it is necessary to specify either a free-surface displacement or a volume flux. For two- and three-dimensional UTA codes, the component of volume flux normal to the open boundary enclosure face is externally specified. For simplicity, the discussion of the formulation of open boundary conditions presented here will be limited to one-dimensional models. A specified volume flux implies that the free surface at the boundary element is allowed to vary. The free surface displacement at the boundary enclosure face is calculated using the same extrapolation formula, Eq. (4.1), used for the shoreline boundary elements. Volume flux is the appropriate variable to specify for tributary inflows, however, for coastal regions or tidal

rivers, free-surface elevation data is more readily available. The UTA codes allow the external specification of free-surface elevations at open boundaries. In this case, the volume flux at the open boundary enclosure face is free to vary and must be internally calculated. For a one-dimensional open boundary condition applied at the upstream $i=1$ discrete element, the volume flux at the open boundary enclosure face $1-1/2$ is calculated based upon the computed volume fluxes at adjacent half-elements using the extrapolation formula

$$G_{x;1-1/2} = G_{x;1-1/4} + \frac{G_{x;1-1/4} - G_{x;1+1/4}}{2} \quad (4.3)$$

A similar extrapolation formula is used for a downstream element $i=N$ open boundary.

The UTA codes can accommodate multiple harmonic tidal forcing. This is achieved by externally specifying tidal free-surface amplitude, frequency, and lag time for each tidal harmonic. Open boundary conditions for tide-driven advected variables (temperature, etc.) can be input for each tidal harmonic in a manner similar to that for tidal free-surface forcing.

When information is available which bounds the volume flux at tidal-driven open boundaries, this information can be used in the UTA codes through the input of externally specified lower and upper bounds for the volume flux. The volume flux at the open boundary is calculated from Eq. (4.3), and, if this provides a value which falls outside the range defined by the specified limits, the computed value is replaced by the appropriate bounding value.

5. ZONE-MATCHING METHODOLOGIES

A problem encountered when numerically modeling a complex hydrodynamic situation is the resolution of the range of length-scales of interest. For example, in considering a jet discharge to a flowing ambient water, the far-field length scales are sufficiently large to allow the use of a coarse computation grid. In the near-field, however, the flow is dominated by large shearing flows with relatively small length scales requiring a very fine grid. One way of dealing with this is a variable grid, such as that used in the UTA codes, with a fine grid in the near-field region expanding to a coarse grid in the far-field region. There is, however, a practical limit to the extent of grid cell size variation which can be achieved. This limit is based upon considerations of numerical stability and numerical dispersion. Stability of numerical computation requires a time step to be selected on the basis of the size of the smallest grid cell with the maximum time step decreasing with grid cell size. Numerical dispersion is an artifact of the discrete form of the continuum governing equations which produces inaccuracies in the computed solution. Numerical dispersion may be minimized or eliminated by a well-conceived computational system; however, this can only be accomplished uniformly for a uniform computational grid. Thus with a variable grid, minimizing numerical dispersion in the near-field will produce large numerical dispersion in the far-field. It is clear that a computationally accurate, high resolution treatment of the near-field zone will be costly to use and will require a limited expansion of the grid size, which in turn limits the size of the modeled region.

The near-field flow region can be analyzed separately using existing empirical or analytic near-field models. All such models have many simplifying assumptions limiting their range of applicability. Many situations exist where no simple near-field model can reliably be applied. Such situations are commonly encountered when dealing with a jet near irregular boundaries, a jet in shallow water, or a jet adjacent to another source or sink. For example, consider the case of a simple wall jet as shown in Fig. 5.1. Analytic solutions exist for this situa-

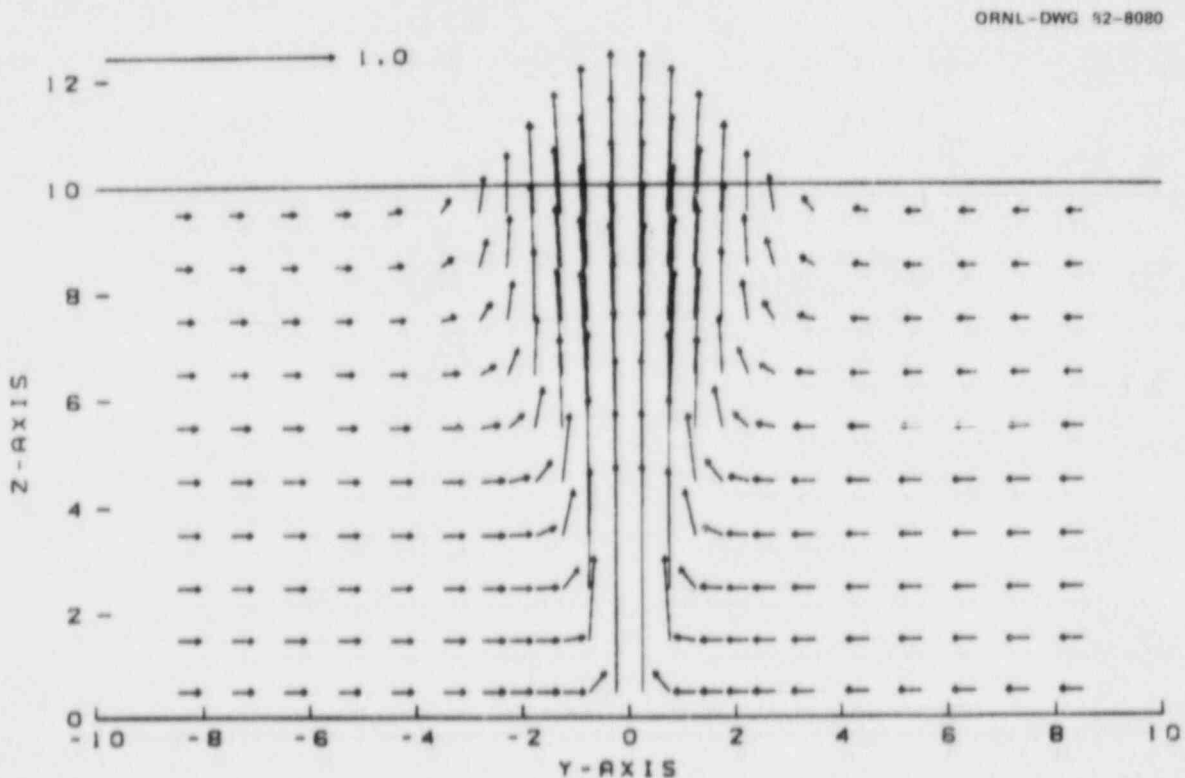


Fig. 5.1. Wall jet solution based upon classical jet theory.

tion (Schlichting, 1968). These solutions only admit entrained flows normal to the direction of jet discharge and consequently will tend to overestimate near-field dilution under conditions where reentrainment is known to exist. Such a situation is illustrated in Fig. 5.2.

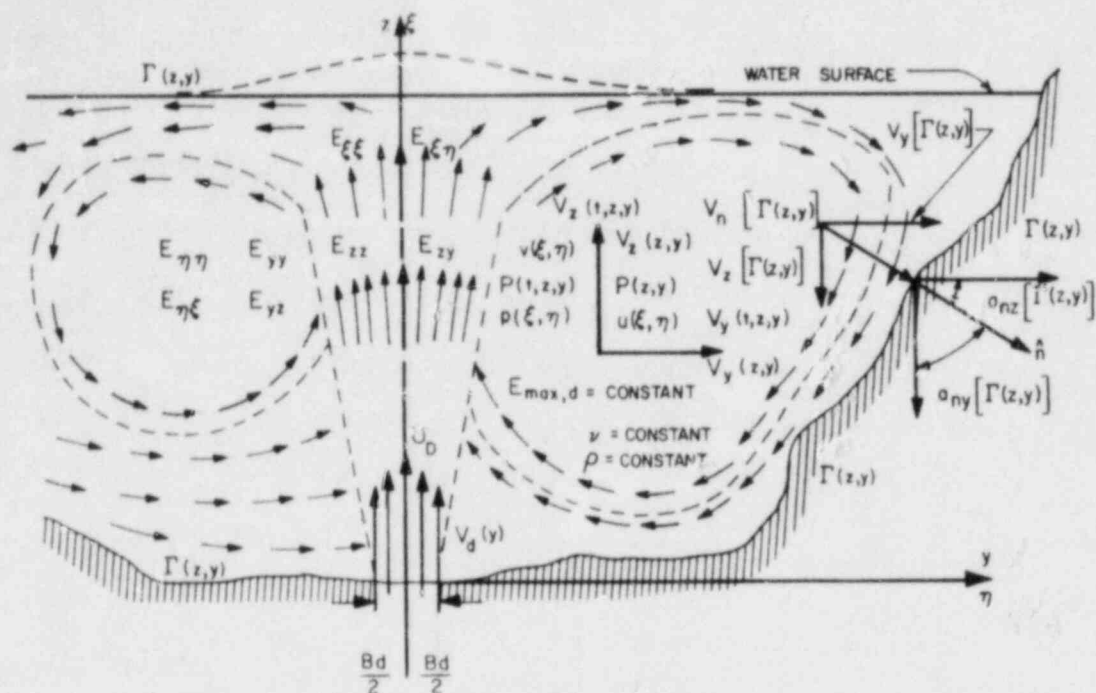


Fig. 5.2. A schematic representation of a jet-induced flow field under commonly encountered conditions. Note the reentrainment resulting from the limited depth and variable bathymetry.

In order to deal with the near-field problems described above, a subtask of the UTA program was the development of zone-matching methodologies. These methodologies are designed to be either stand-alone tools for assessing near-field impacts or used in conjunction with a full flow field modeling effort using one or more of the UTA computer codes. Three zone-matching methodologies have been developed as part of the UTA effort. All of these are two-dimensional, considering either a horizontal plane or a vertical plane, and they range in approach from fully analytic to fully numerical. Two of these methodologies are based upon a uniformly valid singular perturbation theory (Eraslan and Benek, 1971). The vertical jet formulation is fully analytic, while the hori-

zonal jet formulation is semi-analytic. The third methodology, ORSMAC, is fully numerical and uses a simplified marker-and-cell technique to address near-field problems involving jets at arbitrary discharge angles, densimetric effects, and dynamic free-surface effects.

5.1 Uniformly Valid Singular Perturbation Theory

Two of the zone-matching methodologies use an analytic perturbation technique to model the near-field and intermediate-field flows for horizontal and vertical jets. These methodologies are based on the uniformly valid singular perturbation theory which provides a single approximate solution to the boundary layer equations. This approach differs from conventional asymptotic methods in that these methods require multiple solutions, with each solution valid only for a limited range of the study region. In contrast, the uniformly valid theory provides a single solution which is valid for the entire study region.

The uniformly valid singular perturbation theory assumes that the full solution of the boundary layer equations can be represented by a superposition of an inner solution and an outer solution, where both solutions satisfy the boundary layer equations but neither solution alone can satisfy all boundary conditions. The inner solution satisfies the near-field boundary condition; the outer solution satisfies the far-field boundary condition, and the system is closed by appropriate solution-matching conditions. The inner and outer solution dependent variables are expressed as a series expansion in powers of the small

parameter $\lambda = (R_e)^{-1/2}$, where R_e is the Reynolds number. Thus each dependent variable is written in the form

$$u = \sum_{n=0}^{\infty} \lambda^n (U_n + u_n), \quad (5.1)$$

where U_0 is the zero-order outer solution, u_0 is the zero-order inner solution, U_1 , is the first order outer solution correction, u_1 , is the first order inner solution correction, etc.

Assumed solutions of the form given by Eq. (5.1) are used in the boundary layer equations. Terms of each power of λ are collected. This yields a set of partial differential equations for each power of λ . The procedure is terminated after the first power of λ (the first order correction). This is done for convenience. The error introduced by the omission of higher order terms is of the order R_e^{-1} or less, which is quite small for highly turbulent environmental flows.

5.1.1 Horizontal Jets

The horizontal jet zone-matching methodology was developed to address problems involving off-shore jets discharging at or near a horizontal plane. An example of such a situation is depicted in Fig. 5.3. The motivation for this development is the inability of classical jet theory or empirical models to represent properly jet entrainment of water from the back side (upstream) of the jet discharge point as illustrated in Fig. 5.4.

The two-dimensional uniformly valid singular perturbation theory, as described above, is applied to a horizontal plane in polar coordi-

ORNL-DWG 84-19114

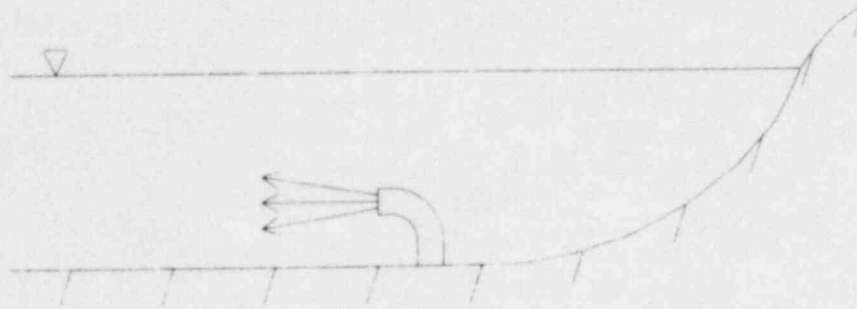


Fig. 5.3. A schematic representation of a typical situation which can be modeled by the horizontal jet zone-matching methodology.

nates. Matching conditions are invoked along the jet center line. The zero-order inner solution represents the classical wall jet solution such as that shown in Fig. 5.1. The zero-order outer solution and first-order corrective solutions provide the necessary correction for

ORNL-DWG 84-19115

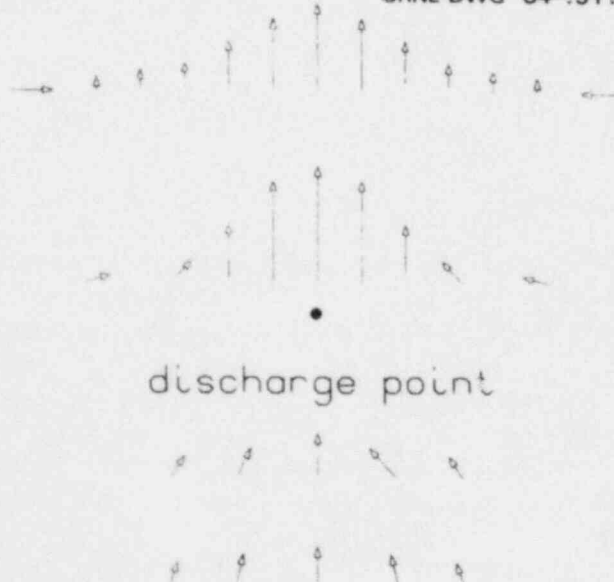


Fig. 5.4. A schematic representation of the flow induced behind an off-shore horizontal discharge.

the upstream entrained flow. Thus the sum of inner and outer solutions provides a full off-shore jet flow field as shown in Fig. 5.4.

At this point, the solution is fully analytic but does not account for the presence of a shoreline. For the case of a straight shoreline normal to the direction of jet discharge [as shown in Fig. 5.5(a)],

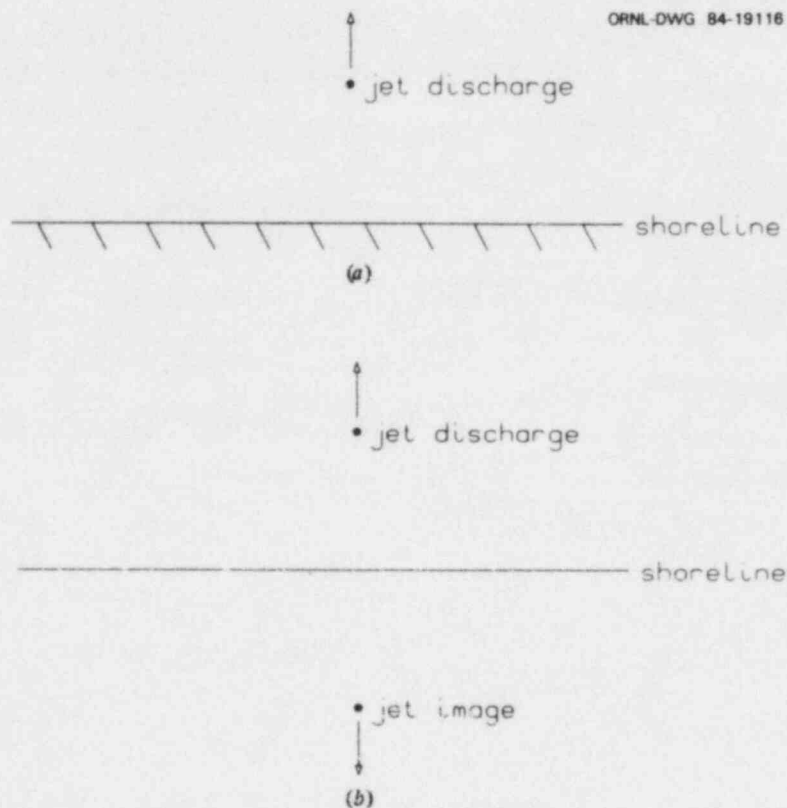


Fig. 5.5. A schematic representation of straight shoreline boundary correction using the method of images showing (a) the actual configuration and (b) the configuration with the image source.

shoreline effects can be incorporated analytically by the application of the method of images. This is accomplished by adding an additional source (jet) of equal strength but opposite direction an equal distance from the shoreline on the opposite side, as shown in Fig. 5.5(b). The sum of the two jet solutions satisfies the governing perturbation

equations and boundary conditions, including the no normal flow condition at the impermeable shoreline.

This zone-matching methodology can also account for irregular shoreline geometries by applying a numerical extension of the method of images (Eraslan and Witten, 1981). To implement this technique, a computational grid is established over the region of interest as shown in Fig. 5.6. The analytic jet solution obtained from the uniformly

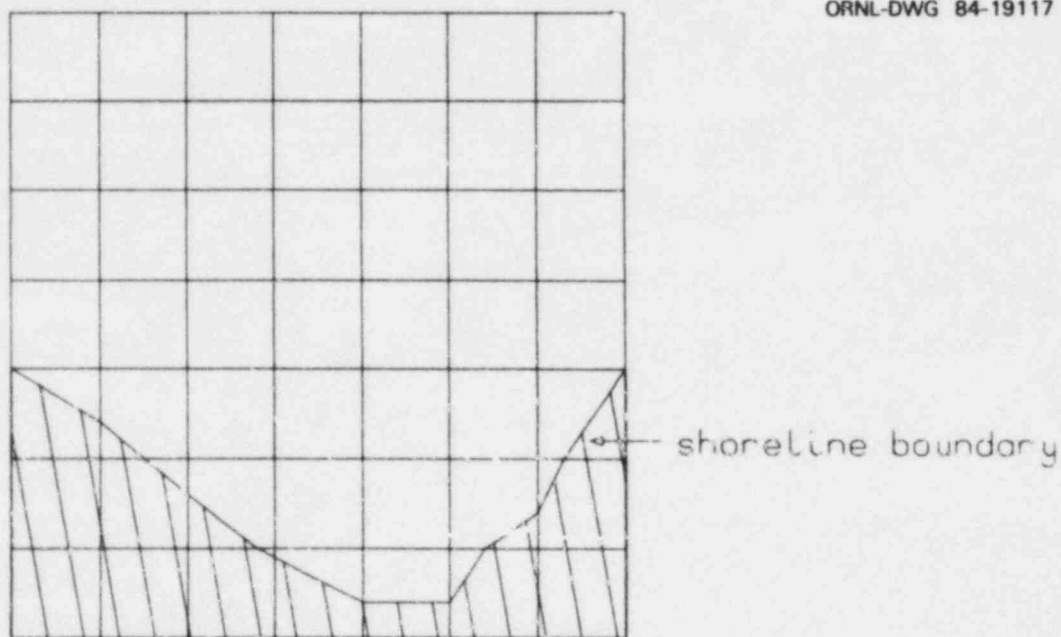


Fig. 5.6. An example of a shoreline and grid system used for the numerical correction for arbitrary shorelines used in the horizontal jet zone-matching methodology.

valid singular perturbation theory is used to calculate the velocity component normal to the shoreline at each shoreline discrete element. A UTA hydrodynamic code (Sect. 3.1) is applied to the computational grid system with accurate shoreline geometry (Sect. 4.1). For this application, the appropriate shoreline condition at each shoreline element is a specified velocity component normal to the shoreline equal in magnitude

but opposite in direction to that obtained from an analytic solution as shown in Fig. 5.7. The resulting numerical shoreline boundary corrective flow field is added to the analytic inner and outer solutions to yield a full flow field which exhibits the proper characteristics of the off-shore jet, while at the same time satisfying the required

shoreline element

ORNL-DWG 84-19118

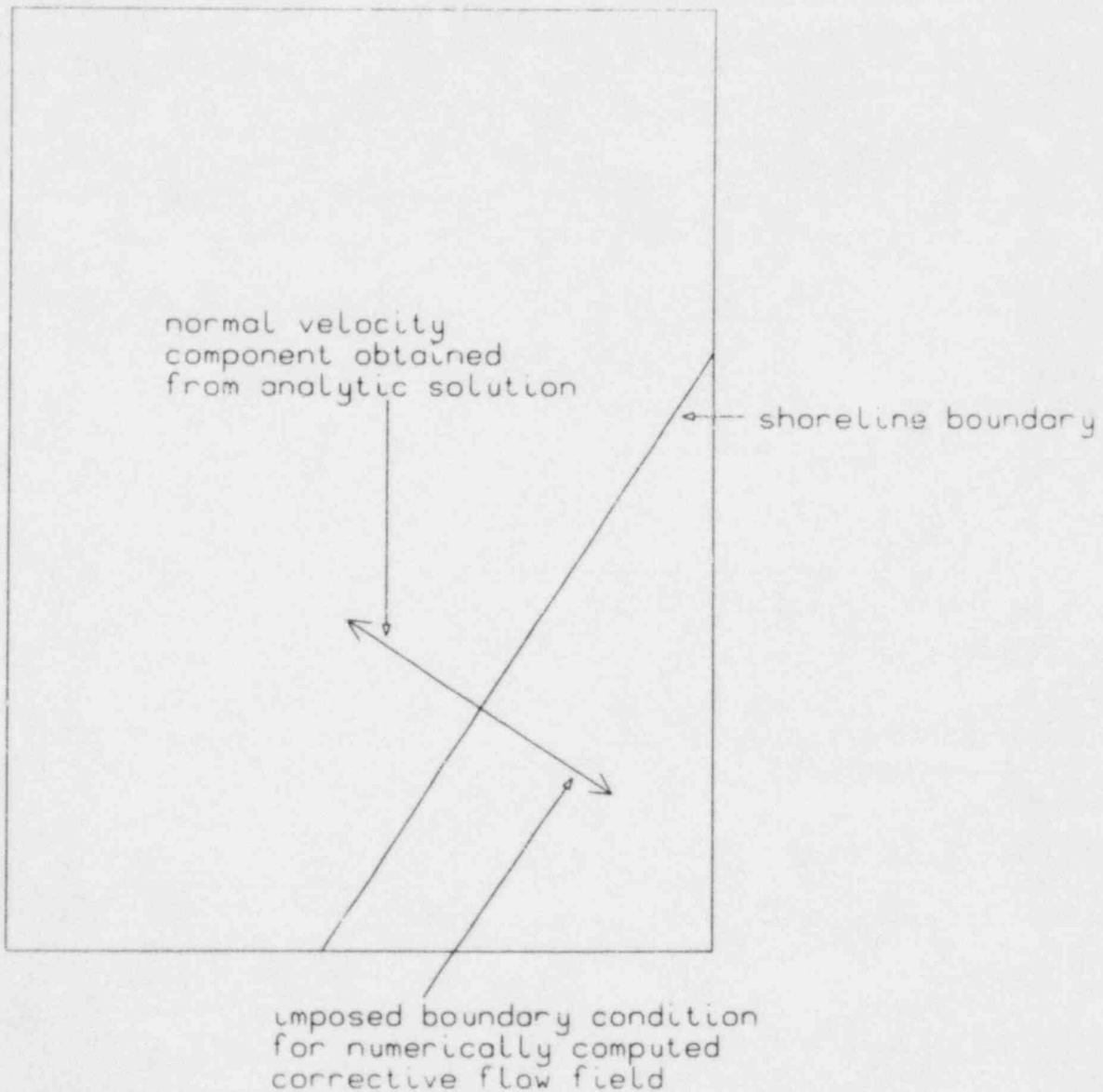


Fig. 5.7. A schematic representation of the treatment of shoreline boundary conditions in the numerical horizontal jet shoreline boundary correction.

boundary conditions at an arbitrary shoreline. An example of the results of horizontal jet solution for an irregular shoreline is given in Fig. 5.8.

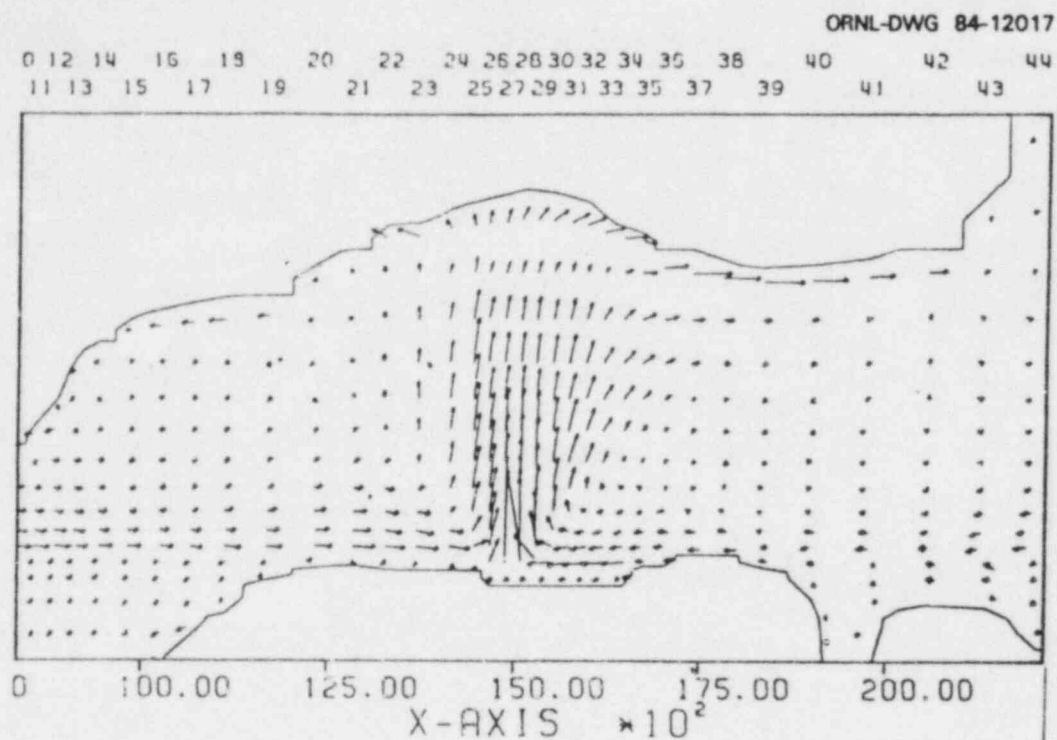


Fig. 5.8. An example of the full off-shore horizontal jet induced flow field predicted by the horizontal jet zone-matching methodology, including the numerical shoreline boundary correction.

5.1.2 Vertical Jets

The uniformly valid singular perturbation theory is applied to the vertical jet problem to provide a more accurate representation of vertical jets, including the effects of finite water depth, multiple jet interactions; discharge and intake interactions, and jet and cross-flow interactions. The uniformly valid singular perturbation theory is applied to a two-dimensional vertical plane in rectangular coordinates

with a jet discharging upward from the channel bottom. As in the horizontal jet, the zero-order inner solution is the classical wall jet (Fig. 5.1), while the zero-order outer solution and the first-order corrective solutions incorporate the effects listed above. For the vertical jet methodology, the complete solution is fully analytic and capable of supporting reentraining eddies as shown in Fig. 5.2.

Figure 5.9 shows examples of the vertical jet uniformly valid singular perturbation theory solution applied to a vertical jet interacting with the free-surface [Fig. 5.9(a)]; the free-surface and ambient cross-flow [Fig. 5.9(b)]; the free-surface, ambient cross-flow and a second jet [Fig. 5.9(c)]; and the free-surface, ambient cross-flow, and an intake [Fig. 5.9(d)]. These results were selected to demonstrate significant flow field features, such as reentrainment and recirculation, which can be resolved by the vertical jet methodology. Figure

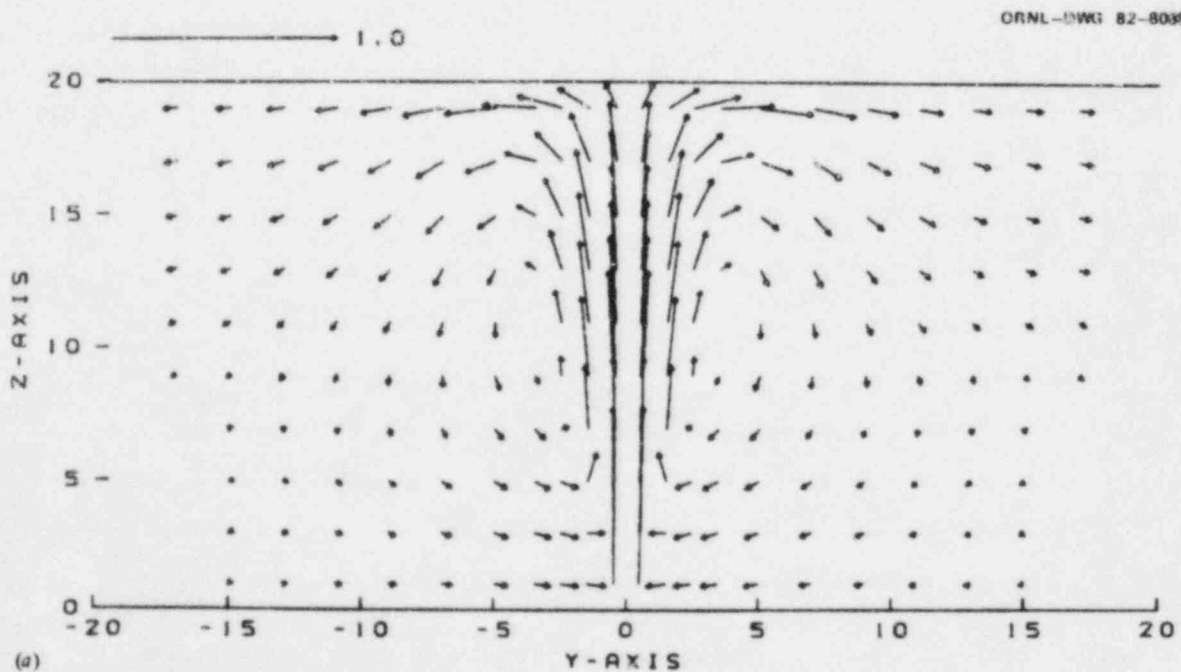


Fig. 5.9. An example of the vertical jet zone-matching methodology applied to a bottom discharge in water of finite depth for (a) quiescent conditions.

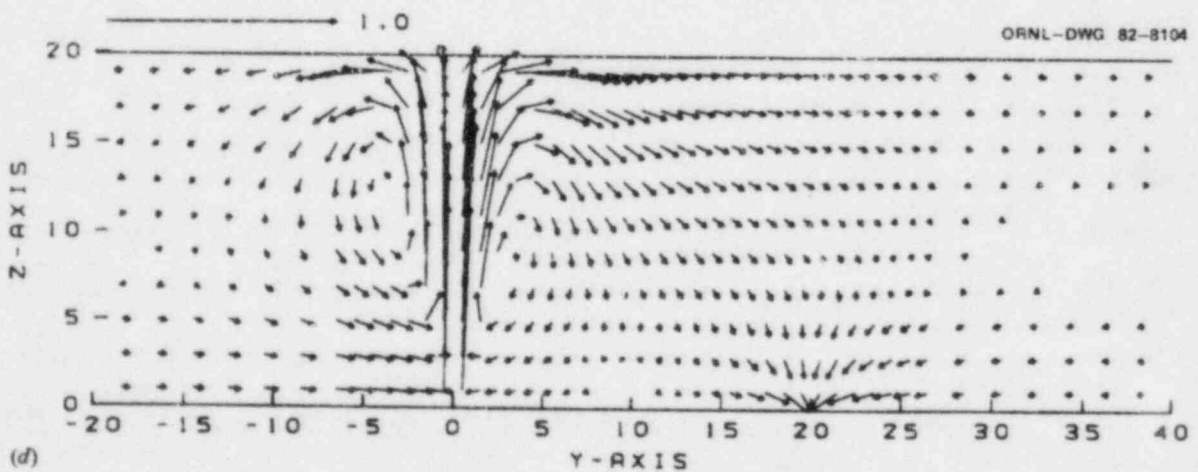
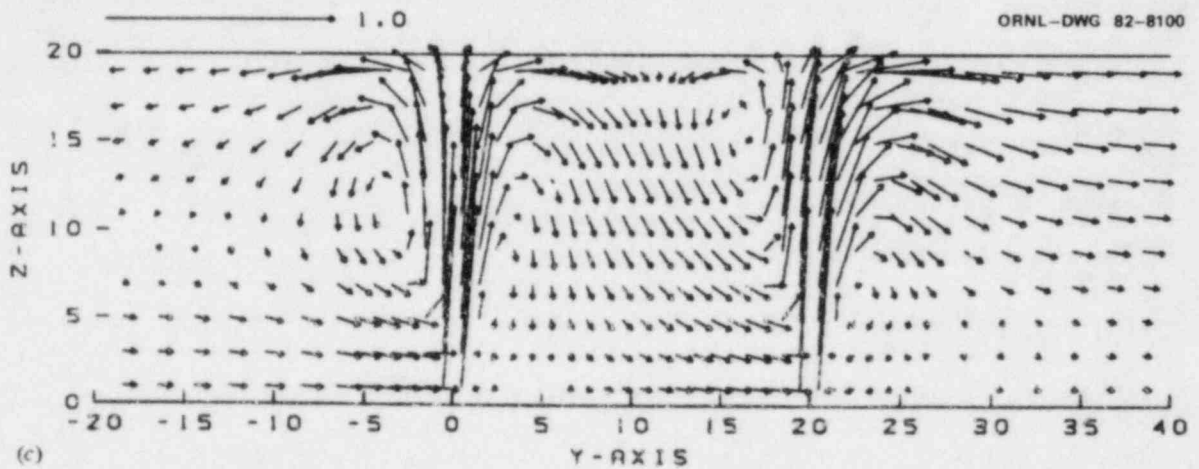
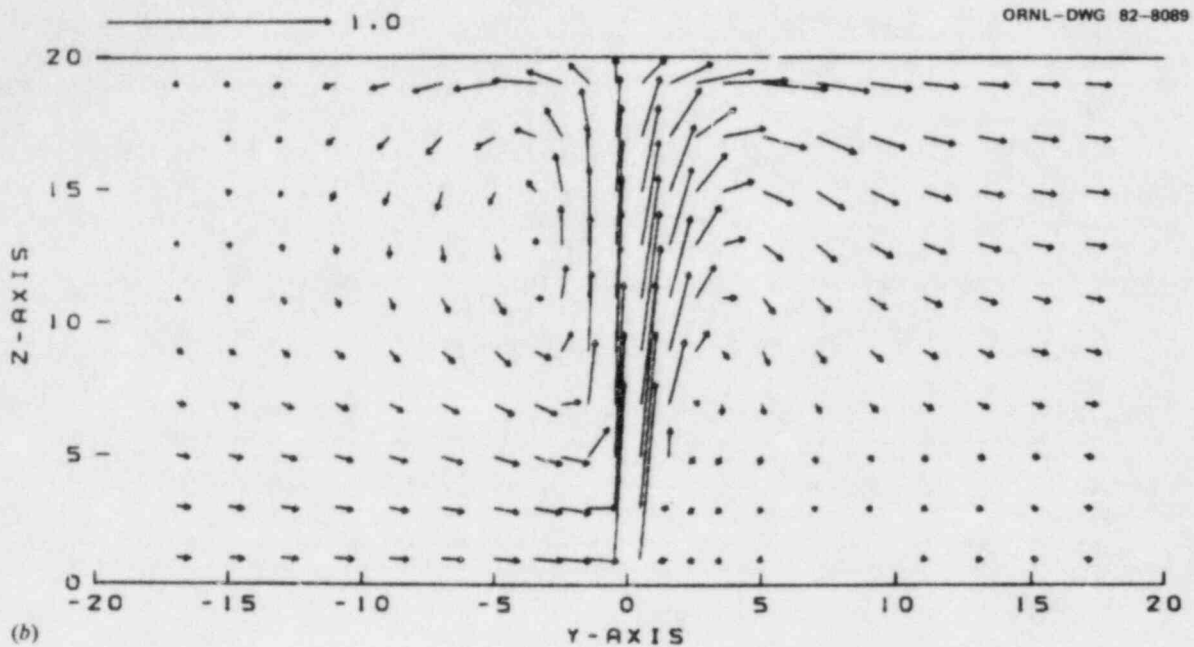


Fig. 5.9. An example of the vertical jet zone-matching methodology applied to a bottom discharge in water of finite depth for (b) ambient cross-flow and (c) ambient cross-flow and an adjacent bottom discharge and (d) ambient cross-flow and an adjacent bottom intake.

5.9(a) demonstrates that significant reentrainment can occur as a result of a bounded water depth. This appears as vertical cells on either side of the jet. In the presence of cross-flow [Fig. 5.9(b)], reentrainment may be reduced but could still occur as small circulatory flows near the surface immediately upstream of jet and near the bottom immediately downstream of the jet. For two adjacent jets [Fig. 5.9(c)], each jet can reentrain its own discharge water, and the downstream jet can entrain water from the upstream jet. Figure 5.9(d) shows that both reentrainment and recirculation can be represented when a bottom intake is adjacent to a jet discharge.

The reentrainment evident in these examples is an important feature because its presence will reduce the dilution factor associated with the jet discharge and could, therefore, limit the ability of a given discharge system to meet design performance objectives. Most simple classical jet or empirical solutions do not adequately account for finite water depth but implicitly assume that all jet discharge outflow occurs at infinity, as would occur in the case of an unbounded jet. They allow the entire finite water depth to be an inflow region providing entrained diluting ambient water. This results in an overestimate of the dilution factor since the entire water depth is not available for entrainment. In reality, a jet outflow region exists in the upper portion of the water column, and an inflow region exists below. Diluting water is only available from the inflow region. As can be seen in Fig. 5.9(a), the inflow region only occupies approximately the lower 25% of the water column. In general, the greater the water depth, the larger the relative vertical extent of the inflow region.

The analytic vertical jet uniformly valid singular perturbation theory solution can be integrated to yield predicted dilution factors for both finite and infinite water depth. The results are shown in Fig. 5.10 as a plot of dilution factor (entrainment ratio), which is a function the ratio of water depth to the width of the discharge, R_D .

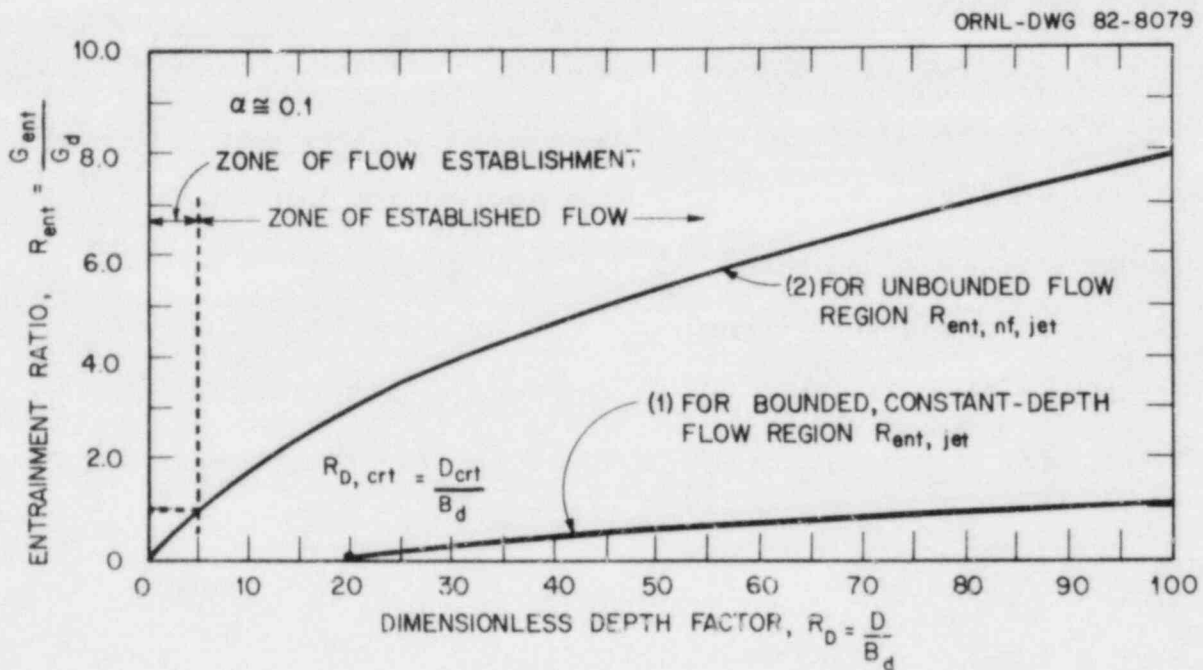


Fig. 5.10. Comparison of the variations of (1) the entrainment ratio for the bottom vertical discharge of a single, turbulent slot jet in a bounded, constant-depth flow region and (2) the entrainment ratio of a turbulent slot jet in an unbounded flow region with the dimensionless depth factor.

This figure has some interesting and important features. In the bounded depth case, no dilution will occur until the water depth exceeds 20 discharge widths. The less realistic unbounded assumption provides an overly optimistic dilution factor of about 3 at $R_D=20$. For large depths ($R_D=100$), using the unbounded approach yields a dilution factor of 8, while more rigorously accounting for finite depth produces a

dilution factor of only 1. Thus, an important application of this zone-matching methodology is as a tool to more accurately estimate vertical jet dilution factors.

5.2 ORSMAC

The computer code ORSMAC was developed to predict the near-field flow and thermal structure resulting from the discharge of heated water to receiving water bodies. This technique is fully numerical and complements the analytic and semi-analytic jet solutions (Sect. 5.1) in that it can accommodate certain physical mechanisms which cannot be rigorously treated in the analytic approach. These include the densimetric effects associated with temperature differences between ambient and discharged water, discharge-induced free-surface displacements, and arbitrary jet discharge orientation.

The ORSMAC code numerically solves the two-dimensional continuity, momentum, and energy equations over a vertical plane, subject to the Boussinesq approximation using a simplified marker and cell method. The model can accommodate either static or cross-flowing ambient conditions.

Examples of ORSMAC results are presented in Fig. 5.11 as printer plots for a turbulent jet that is hot relative to the ambient water and is discharging vertically into a cross-flowing ambient. Figure 5.11(a) shows predicted streamlines. Note the reentrainment cell near the free surface immediately upstream of the jet and near the bottom immediately


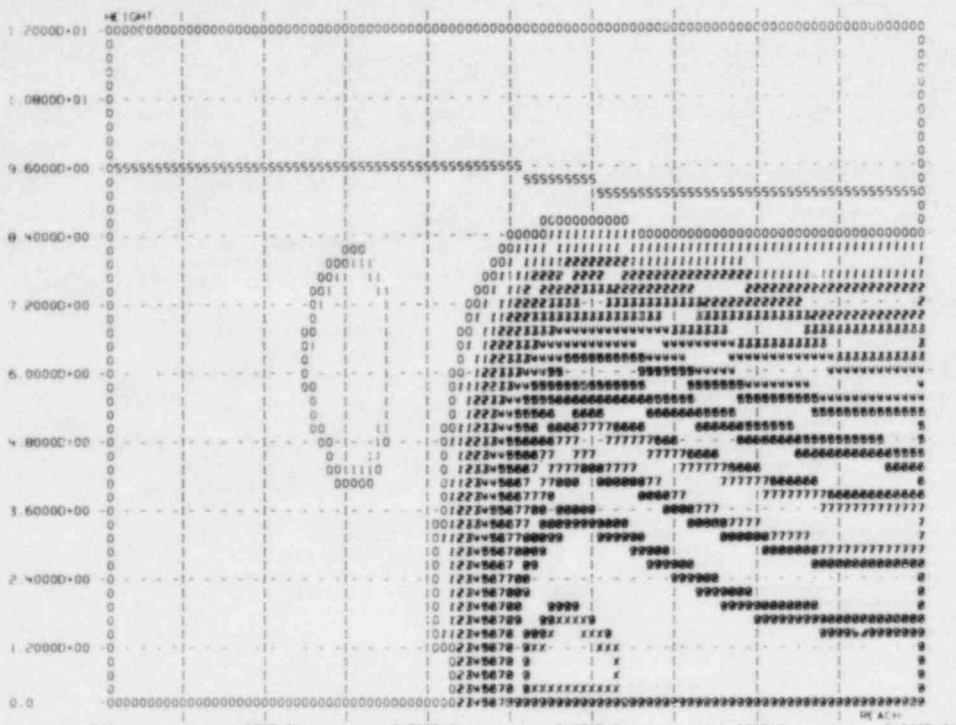


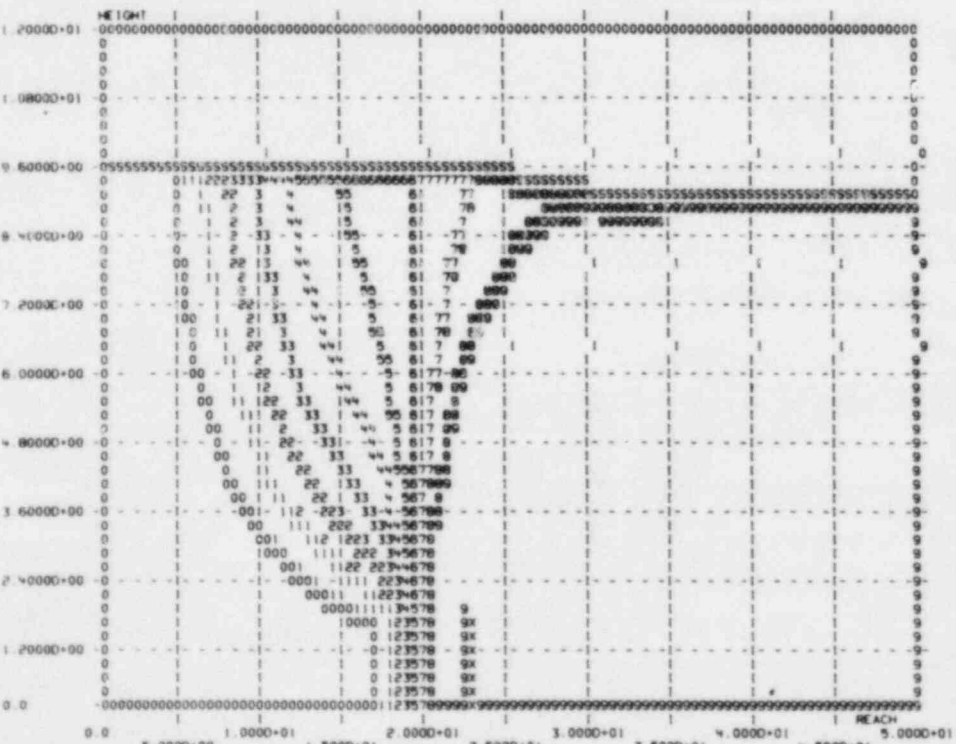
Fig. 5.11. ORSMAC results for a hot, turbulent, vertically-discharging bottom jet shows predicted (a) streamlines and (b) isotherms.

HOT TURBULENT JET WITH LOW CROSSFLOW - VERTICAL DISCHARGE



(a)

HOT TURBULENT JET WITH LOW CROSSFLOW - VERTICAL DISCHARGE



(b)

downstream of the jet. These features are consistent with similar predictions obtained from the uniformly valid singular perturbation theory under isothermal conditions [Fig. 5.9(b)]. Figure 5.11(a) also shows the discharge-induced free-surface displacement identified by the letter "s" on this figure. Figure 5.11(b) shows predicted isotherms. Note the stable stratification which appears downstream of the discharge as a thin layer of warm water. Slight stratification appears immediately upstream of the discharge as a result of densimetric spreading.

6. RESULTS

The purpose of this section is to demonstrate the power and flexibility of the Unified Transport Approach. Various UTA codes have been used for a variety of applications, and, consequently, an exhaustive presentation of UTA results is well beyond the scope of this document. This section does, however, present several case studies selected to demonstrate how the UTA system can realistically portray complex situations and how multiple UTA codes can be efficiently applied to a particular situation.

6.1 The Hudson River Study

This subsection presents selected results using the sequential application of ESTONE, CHMONE, SEDONE, RADONE, the horizontal jet zone-matching methodology and FLOWER for assessing the impact to the Hudson River as a result of the operation of actual and hypothetical power plants. Many of the results presented here are taken from an analysis of power plant operation on the Hudson River (Barntouse et al., 1977).

The ESTONE code was used to simulate one-dimensional flow, temperature, and salinity over the entire Hudson River for a period extending from April through September 1974. The river between the Troy Dam and the Battery was represented by 77 discrete elements. The three-dimensional geometric characteristics of the river were input in the form of channel cross sections such as those shown in Fig. 6.1. This figure illustrates both actual cross-sectional geometry as obtained from

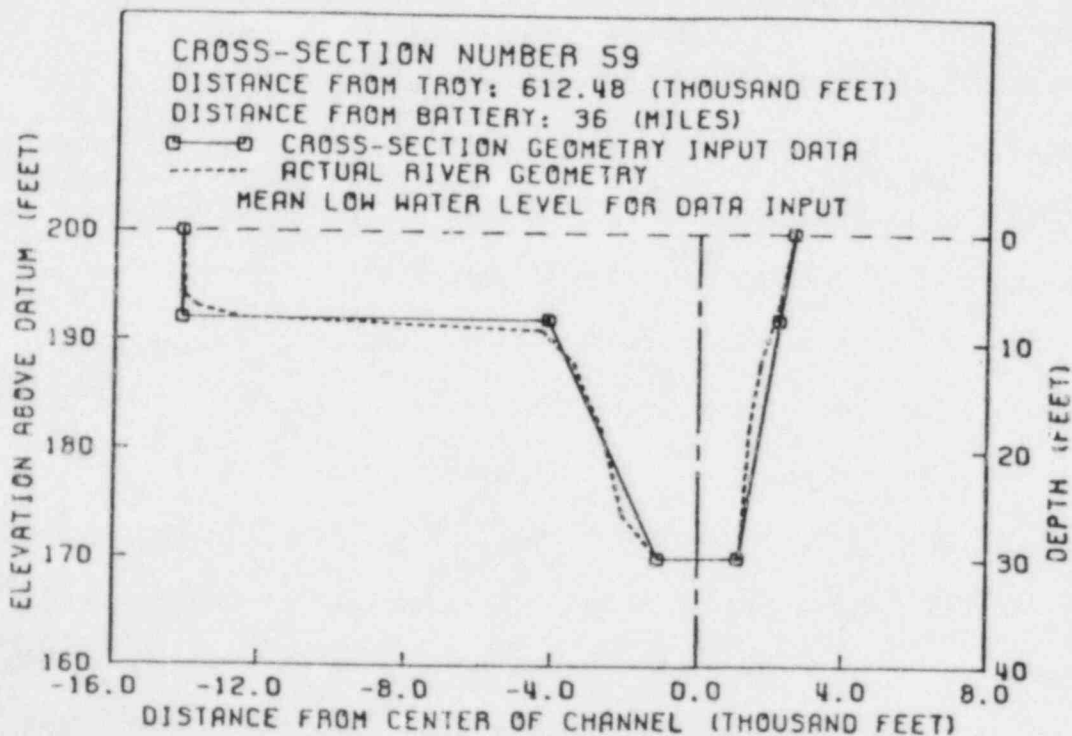
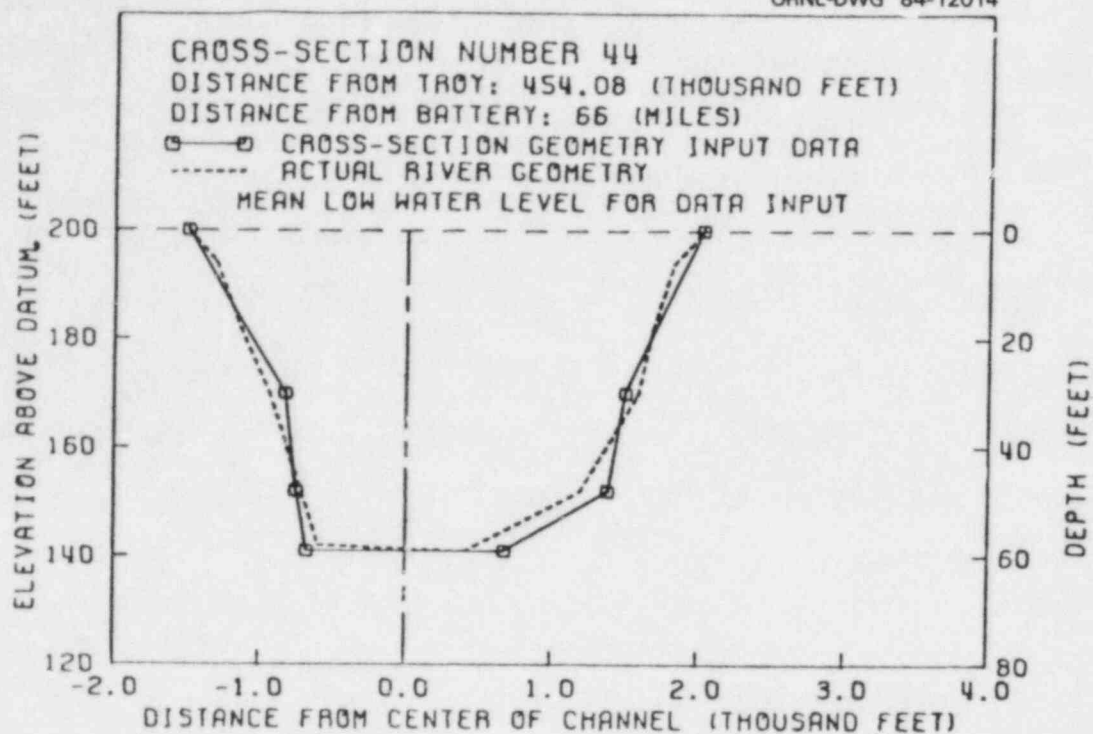


Fig. 6.1. Comparisons of detailed actual profiles and approximated input data to ESTONE model for two typical cross sections along the Hudson River. Actual profiles from U.S. Department of Commerce, National Oceanic and Atmospheric Administration, National Ocean Survey, CoGS Charts Nos. 282, 283, 284, 745, and 746.

navigational charts and as input to the ESTONE model. As boundary conditions, the model requires that time-varying flows, temperature, and salinity be externally specified at the upstream and downstream boundaries. The upstream boundary is the Troy Dam. The boundary conditions used here are the discharge flow and water temperature measured at the dam. Figure 6.2 is an example of the observed and input flow and temperature time series used for April 1974. The downstream boundary at the Battery is tide driven. Transient free-surface elevation data was specified at this boundary using a six-harmonic function, based upon National Oceanic and Atmospheric Administration (NOAA) tidal tables, as shown in Fig. 6.3. The specified downstream transient temperature and saline conditions are provided in Fig. 6.4. The ESTONE simulation also considered tributary inflows. Externally specified tributary flows were based upon gauging station data. Figure 6.5 is an example of the time-series tributary flow data as input to ESTONE. To represent properly surface heat transfer, the ESTONE code uses externally specified transient meteorological parameters. Figure 6.6 shows time-series of maximum solar radiation, cloud cover, air temperature, wind speeds, rainfall, and relative humidity as input to ESTONE based upon meteorological records. The final input data required by ESTONE are the cooling water discharge flow rates and temperatures for all power plants. The Hudson River study considered a total of nine power plants both collectively and individually. Figure 6.7 is an example of a time-series for cooling water flow and temperature for one power plant as used in ESTONE.

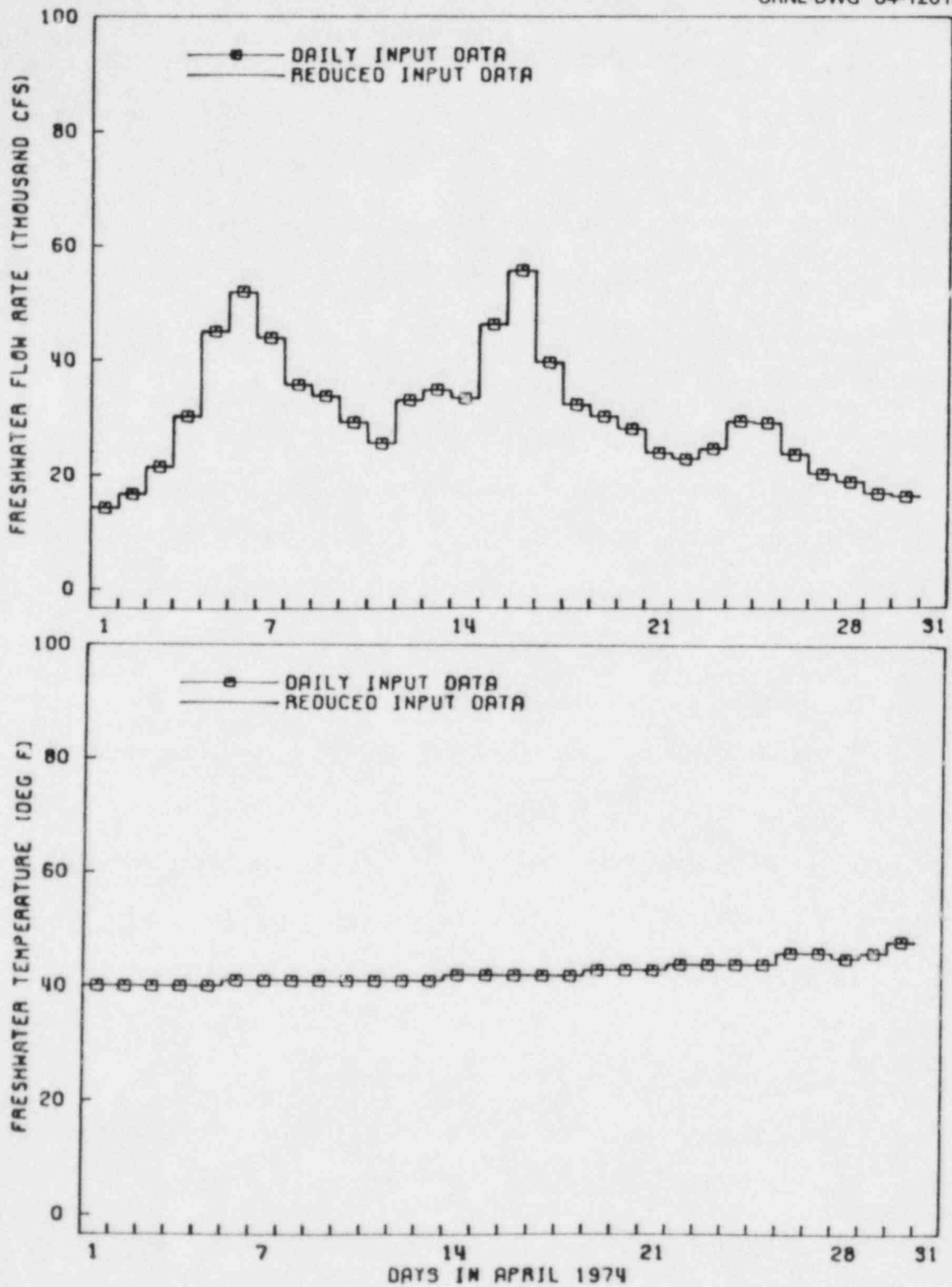


Fig. 6.2. Freshwater flow rate and temperature conditions at the Troy Dam as input data to the ESTONE code for April 1974.

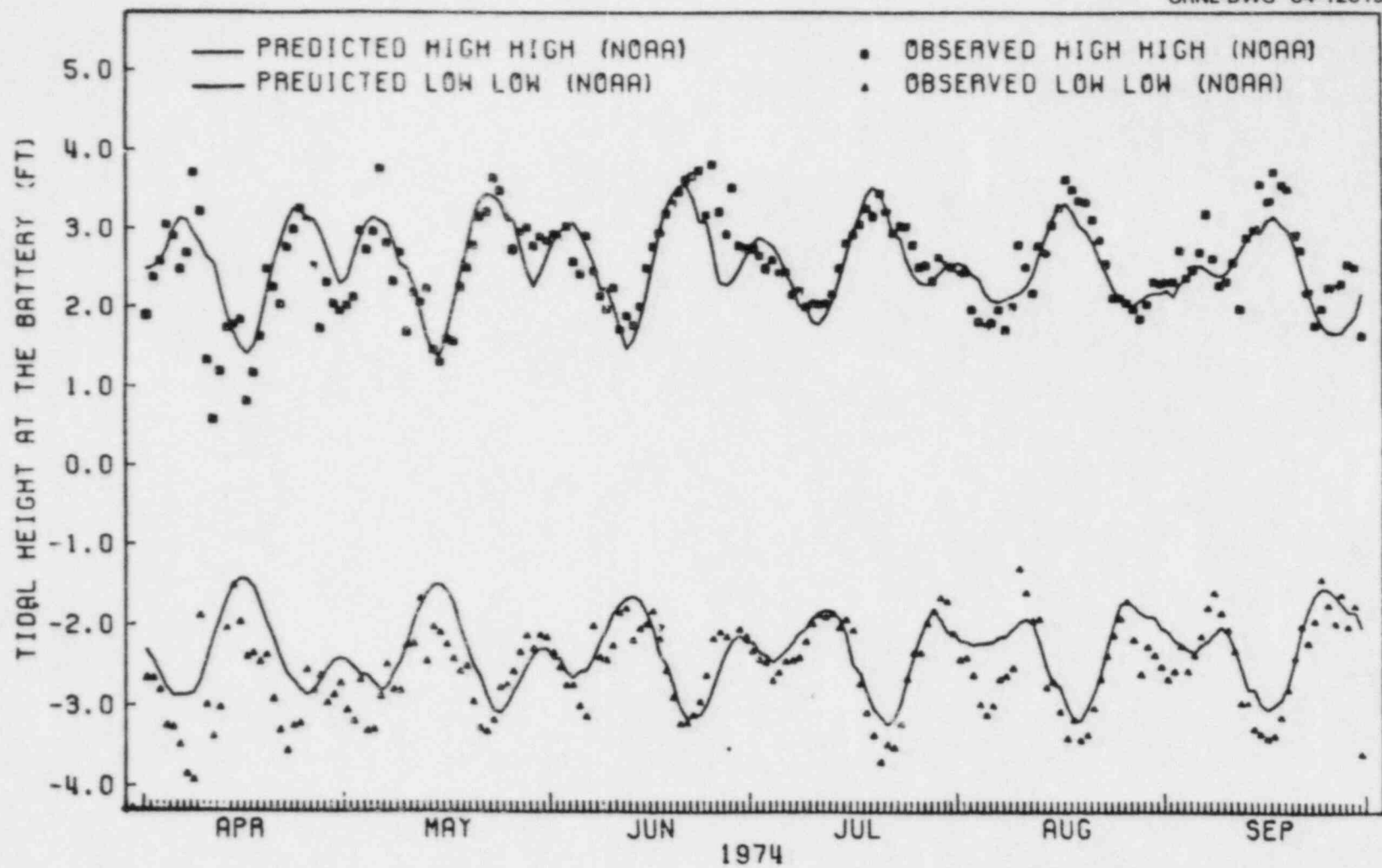


Fig. 6.3. Comparisons of six-harmonic functional predictions and field-measured tidal data at the Battery during April 1 - September 30, 1974, simulation period.

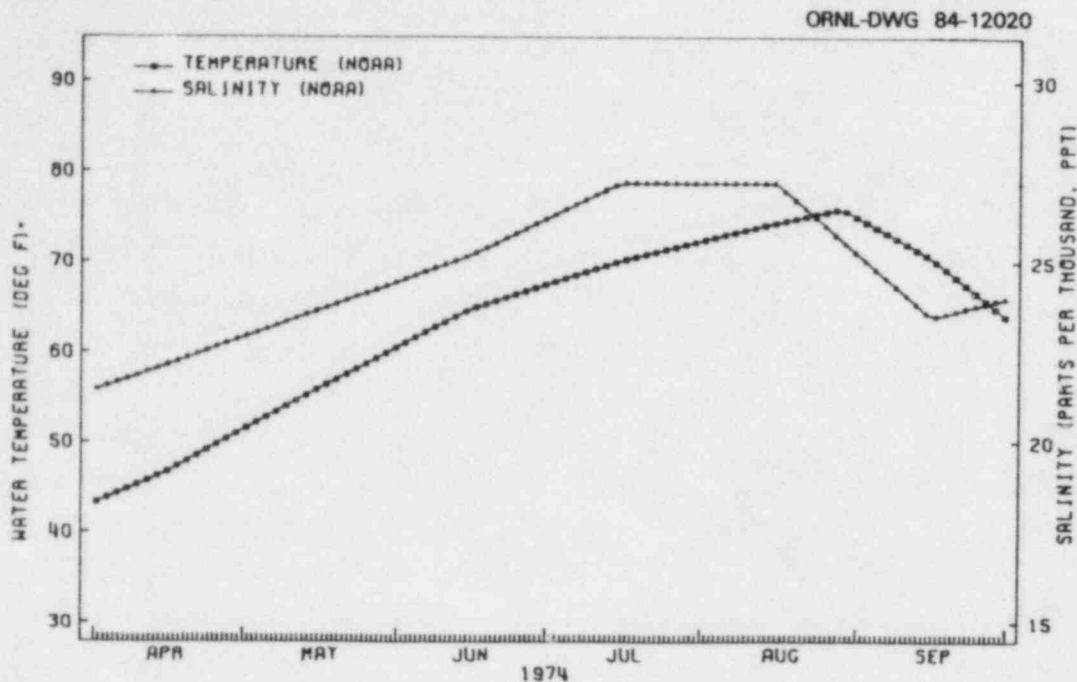


Fig. 6.4. Daily water temperatures and salinity conditions at the Battery during April 1 - September 30, 1973, simulation period.

Figure 6.8 shows ESTONE results as predicted at a discrete element in the vicinity of Indian Point for conditions as they existed during May 1974. For comparative purposes, this figure also indicates observed temperature and salinity. In comparing predicted and observed temperatures and salinities, the predicted values are cross-sectionally averaged at a given instant in time, while the observed values are either taken at fixed points in space and time and do not reflect cross-sectional variations, or are cross-sectional averages based upon boat transects which took hours to complete. In light of these differences, model predictions must be considered quite good. Figure 6.9 shows differences in predicted river temperatures for three different power plant scenarios at the same cross section as in Fig. 6.8 during June 1974. The "clean river" case represents model results in the absence of power plants; the "1974 conditions" case reflects power plant operations

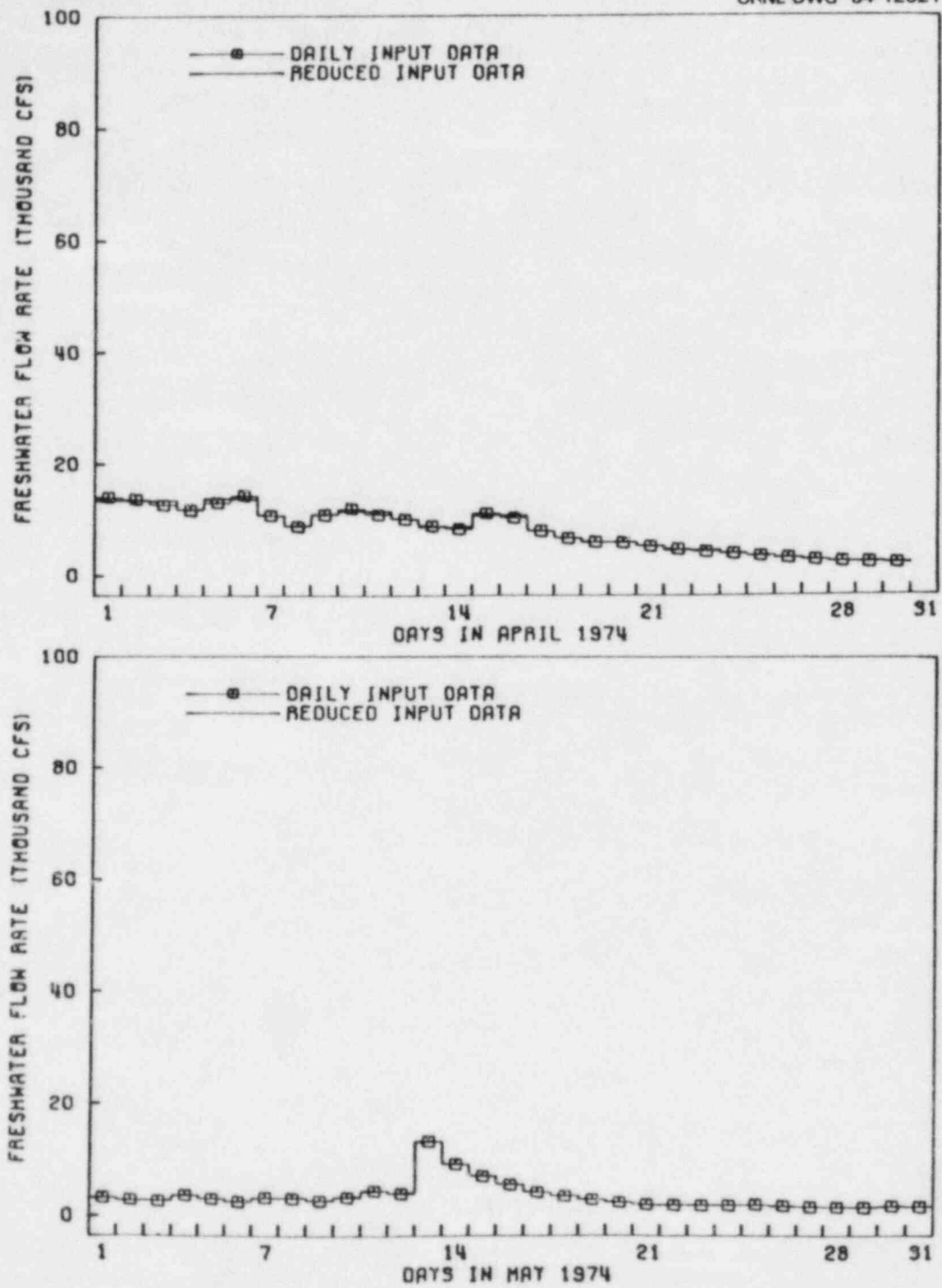
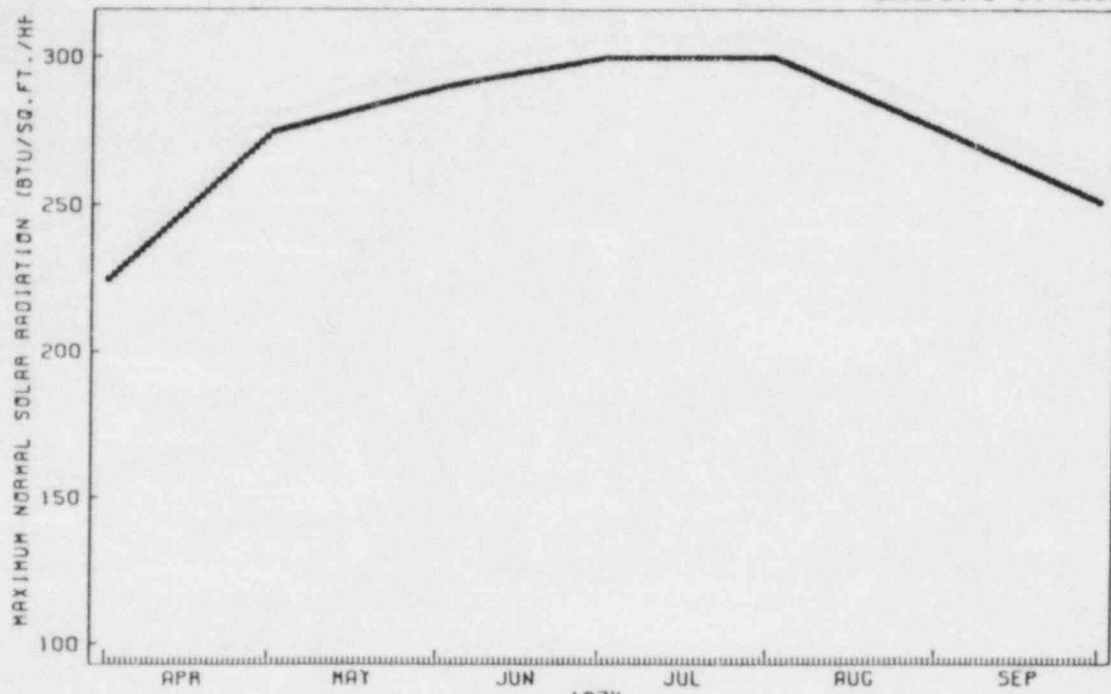
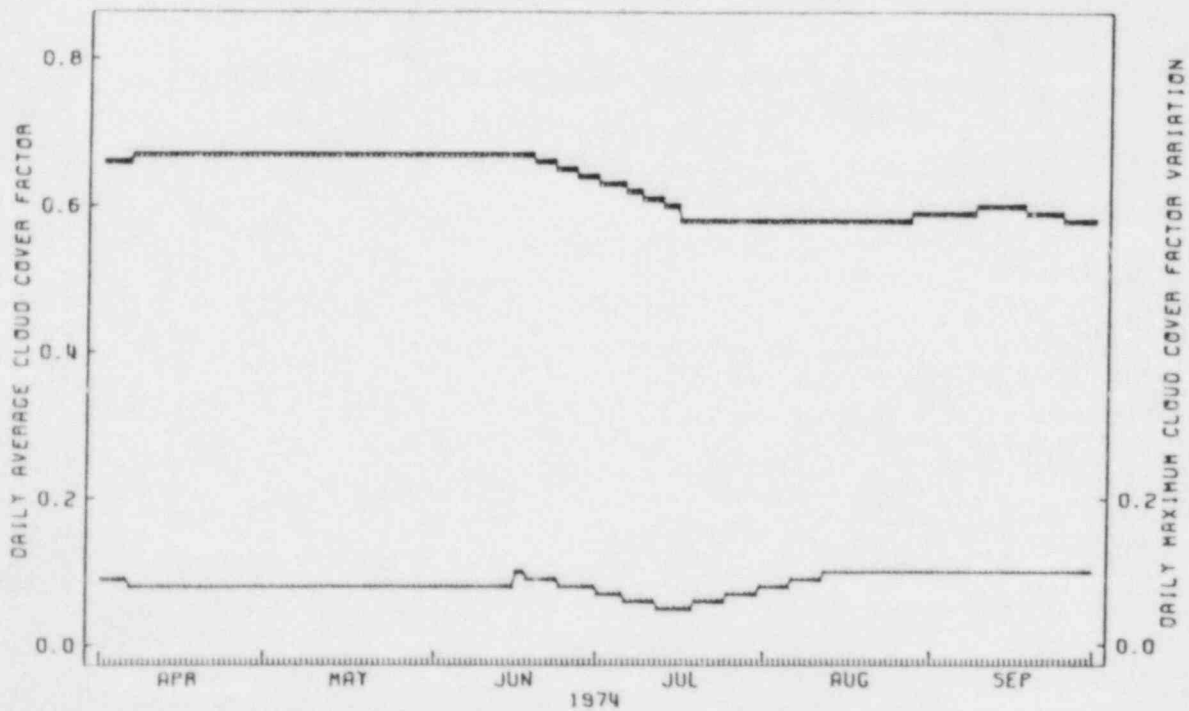


Fig. 6.5. Collective freshwater flow rate for two tributaries entering a discrete element as input data to the ESTONE code: April and May 1974.



(a)



(b)

Fig. 6.6. (a) Maximum normal solar radiation flux and (b) daily-averaged cloud cover factor and daily-maximum cloud cover factor variations, during the simulation period April 1 - September 30, 1974.

ORNL-DWG 84-12023

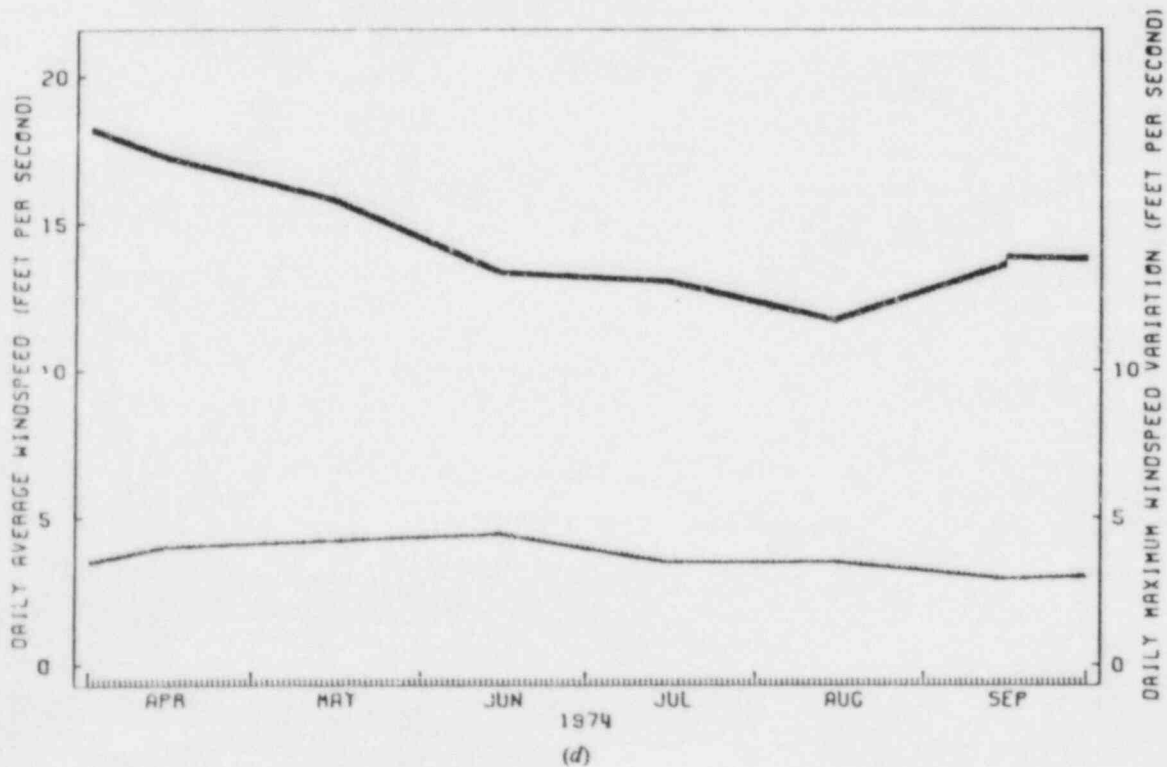
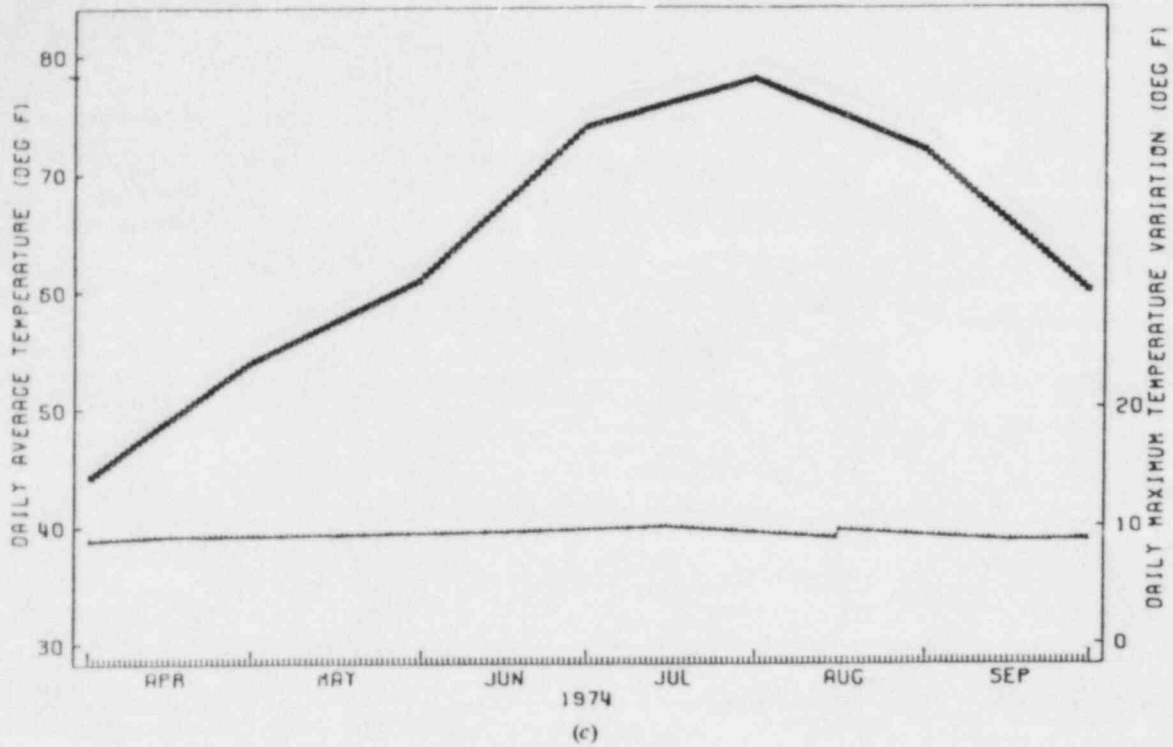


Fig. 6.6. (c) Daily-averaged air temperature and (d) daily-averaged wind speed and daily-maximum wind speed variations during the simulation period April 1 - September 30, 1974.

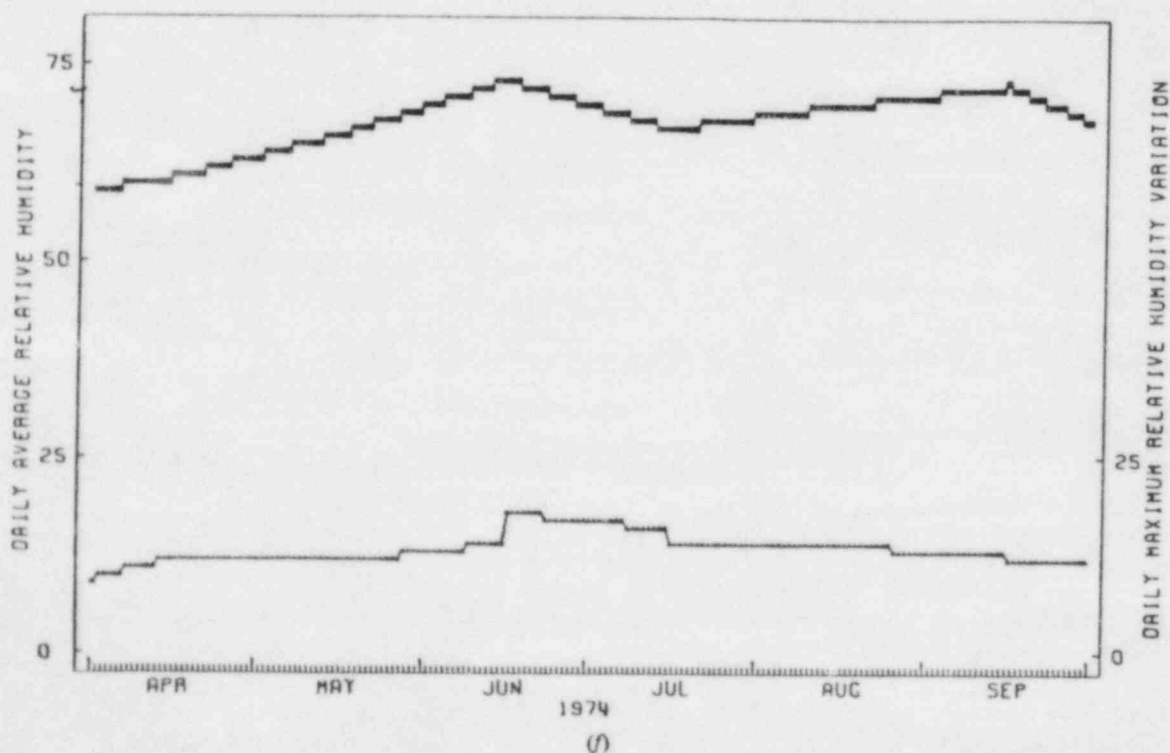
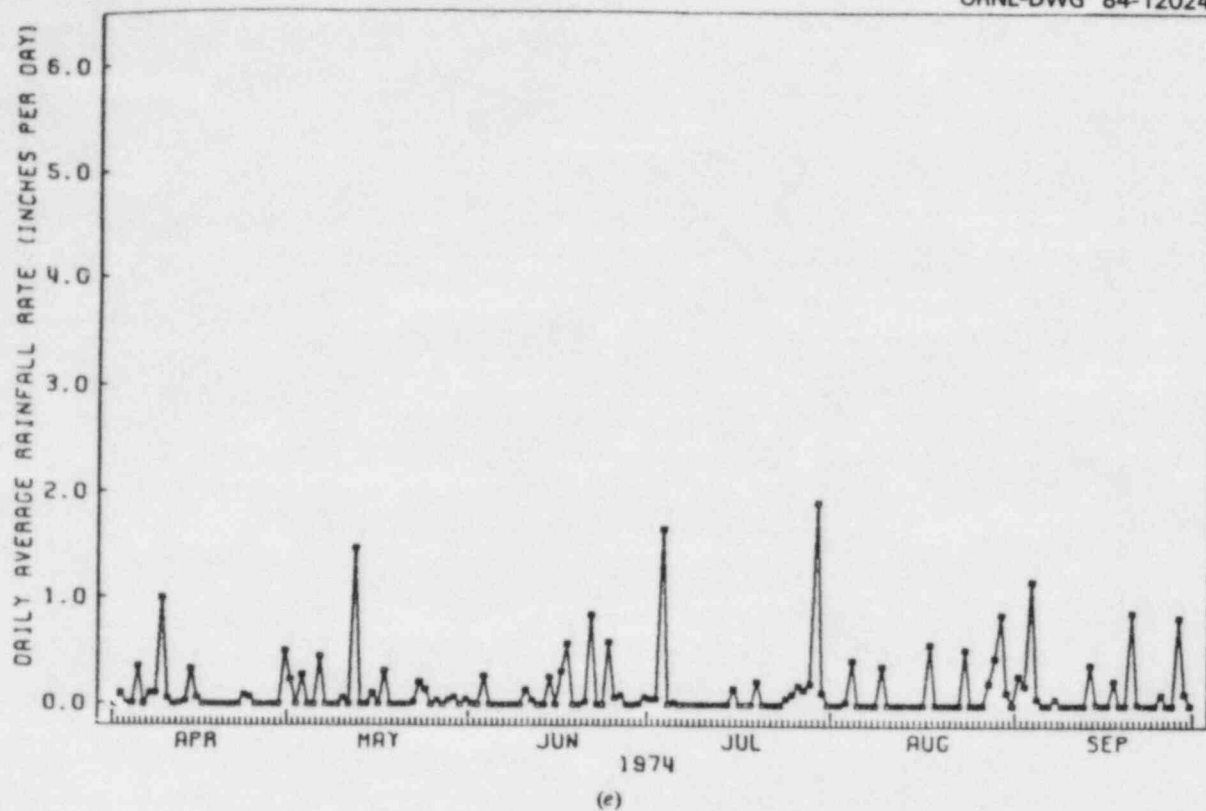


Fig. 6.6. (e) Daily-averaged rainfall rate and (f) daily-averaged relative humidity and daily-maximum relative humidity variations during the simulation period April 1 - September 30, 1974.

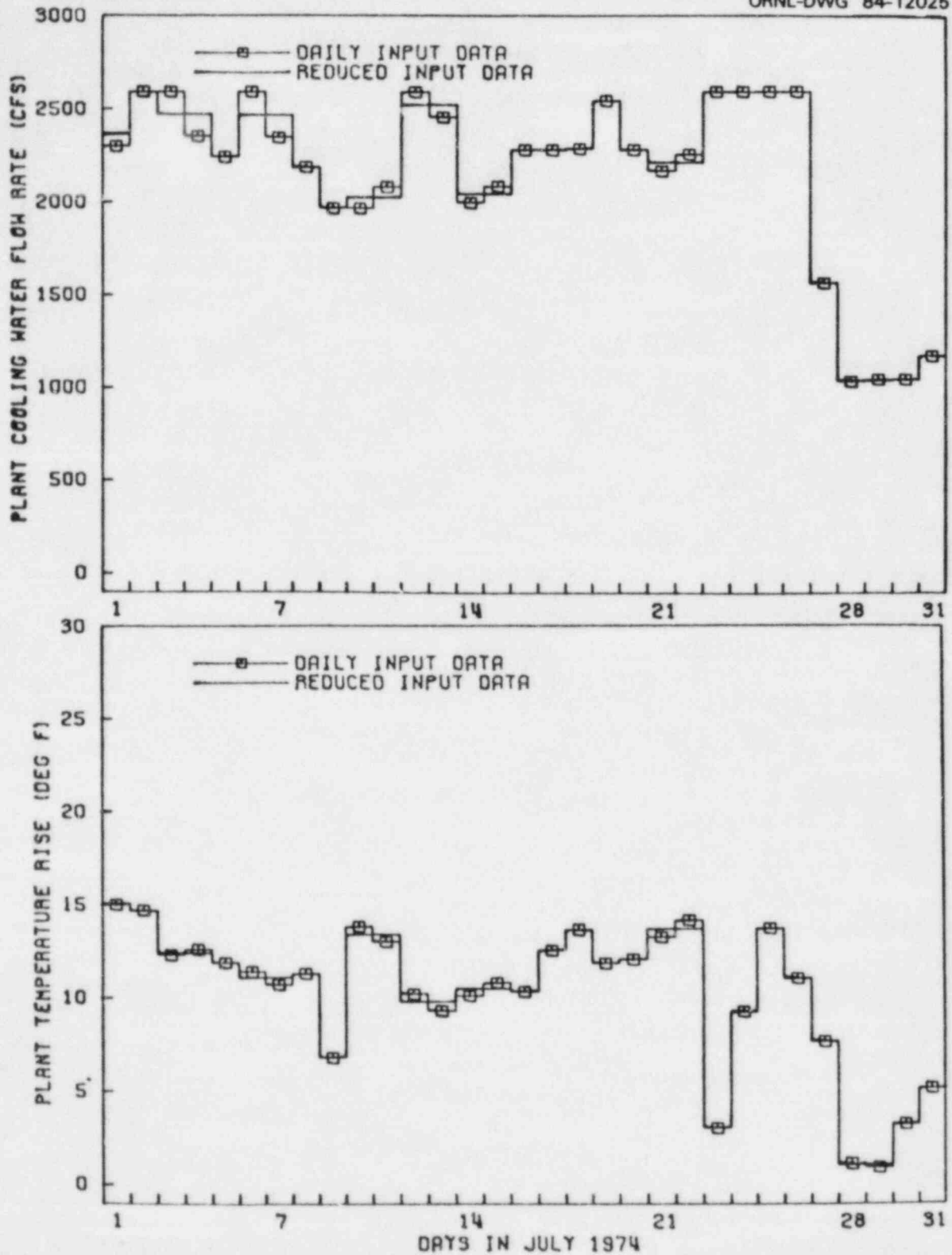


Fig. 6.7. Indian Point plant cooling water flow rate and plant cooling water temperature rise as input to ESTONE for July 1974.

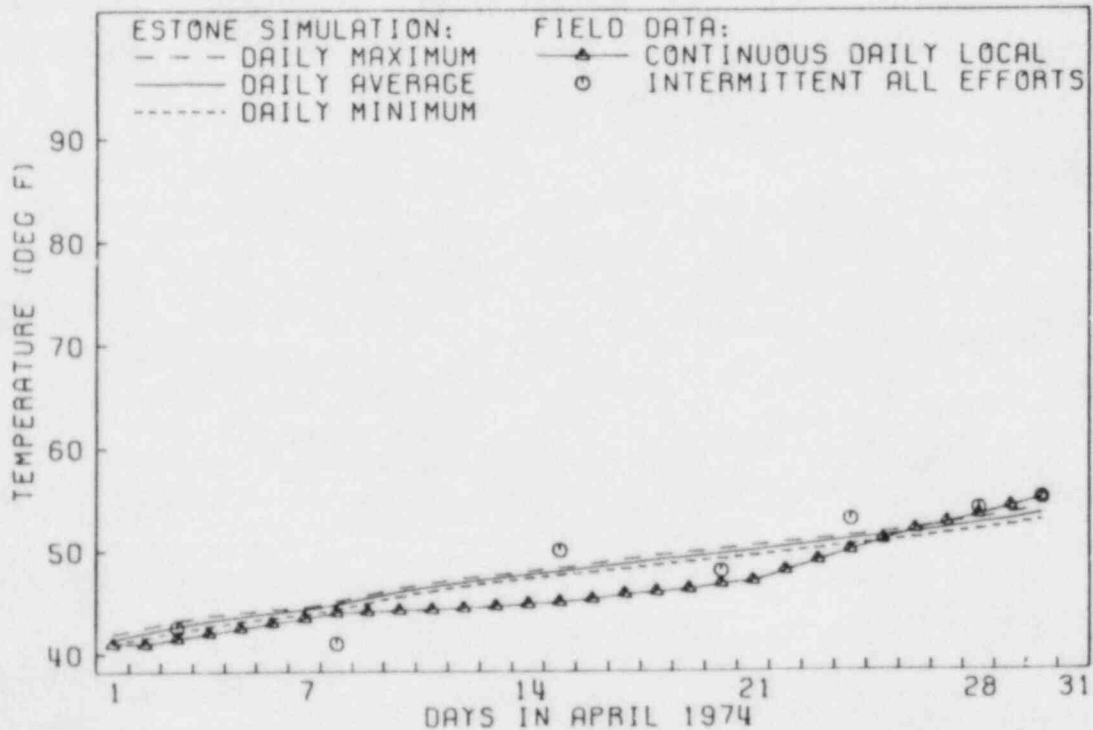
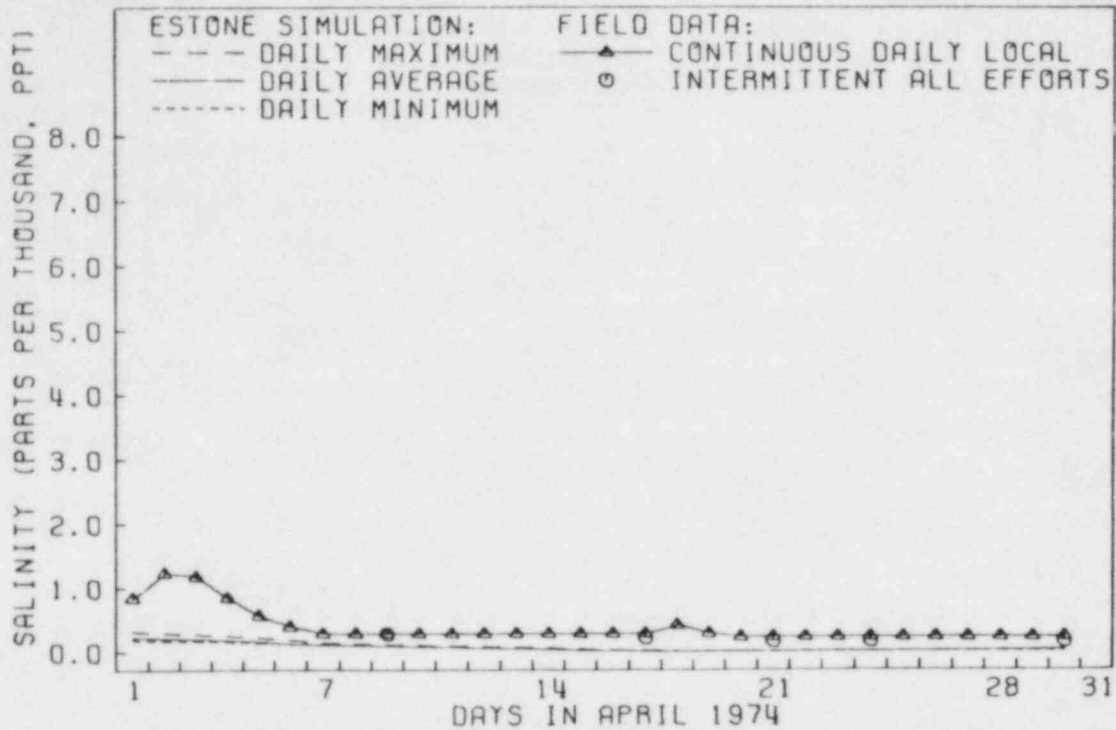


Fig. 6.8. Comparisons of computer simulation results by ESTONE for cross-section-averaged temperature and salinity variations and continuous daily measurements and field-measured data for temperature and salinity conditions in the vicinity of Indian Point area during May 1974. Measurements from Texas Instruments Incorporated Ecological Services, **Hudson River Ecological Study in the Area of Indian Point. Thermal Effects Report**, prepared for Consolidated Edison Company of New York, Inc., September 1976.

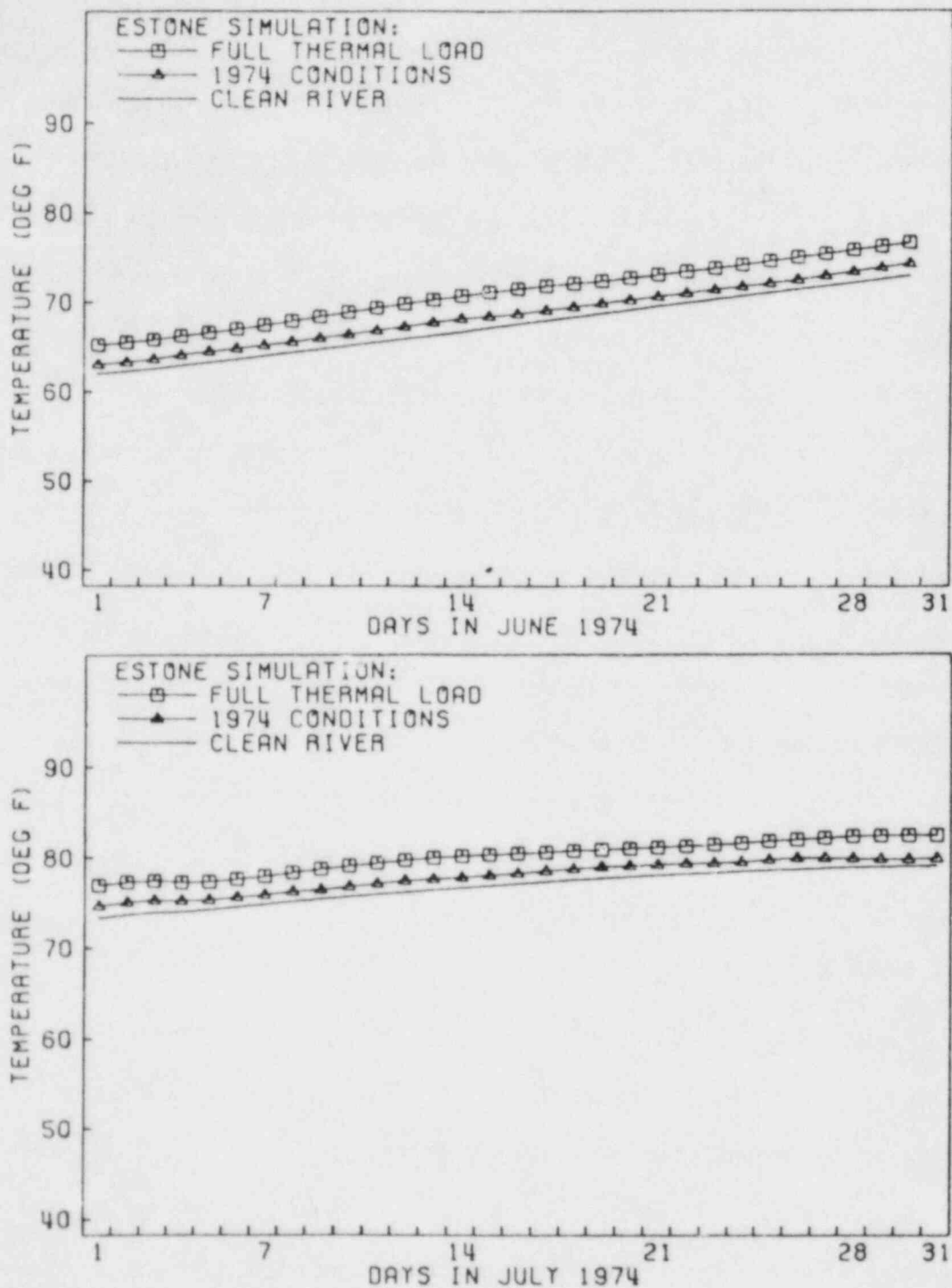


Fig. 6.9. ESTONE simulation results for the variations of daily-averaged and cross-sectional-averaged water temperature conditions in the vicinity of Indian Point Power Plant for three cases during June and July.

at that time; and the "full load" case assumes all nine power plants operating at 100% capacity with once-through cooling.

Although water chemistry, sediment transport, and radionuclide transport were not part of the Hudson River study, CHMONE, SEDONE, and RADONE can easily be applied with only minor modification to the ESTONE input data set previously assembled. Figure 6.10 is an example of CHMONE predictions showing downstream concentrations of monochloramine and hypochlorous acid as a result of cooling water chlorination of hypothetical power plants under 1974 conditions. SEDONE results for the Hudson River are shown in Fig. 6.11 as predicted downstream distribution of suspended and bed slurry sediments for four particle size classes under 1974 conditions. Figure 6.12 compares SEDONE predictions with sediment transport observations and illustrates good agreement between predicted and observed total sediment discharge in the Mississippi River. Figure 6.13 shows the predicted downstream radionuclide concentrations in the sediment layer of the Hudson River generated by the RADONE code for the case of a hypothetical short-term release from the Indian Point Power Plant.

As part of the Hudson River study, it was necessary to generate refined predictions in the vicinity of selected power plants. This was accomplished through the application of a two-dimensional depth-averaged version of FLOWER and, where appropriate, the horizontal jet zone-matching methodology. Apart from the additional geometric information required by the finer resolution and the supplemental open boundary conditions, all input data are identical to those used in ESTONE. Figure 6.14 shows the grid system, and Fig. 6.15 shows shoreline and

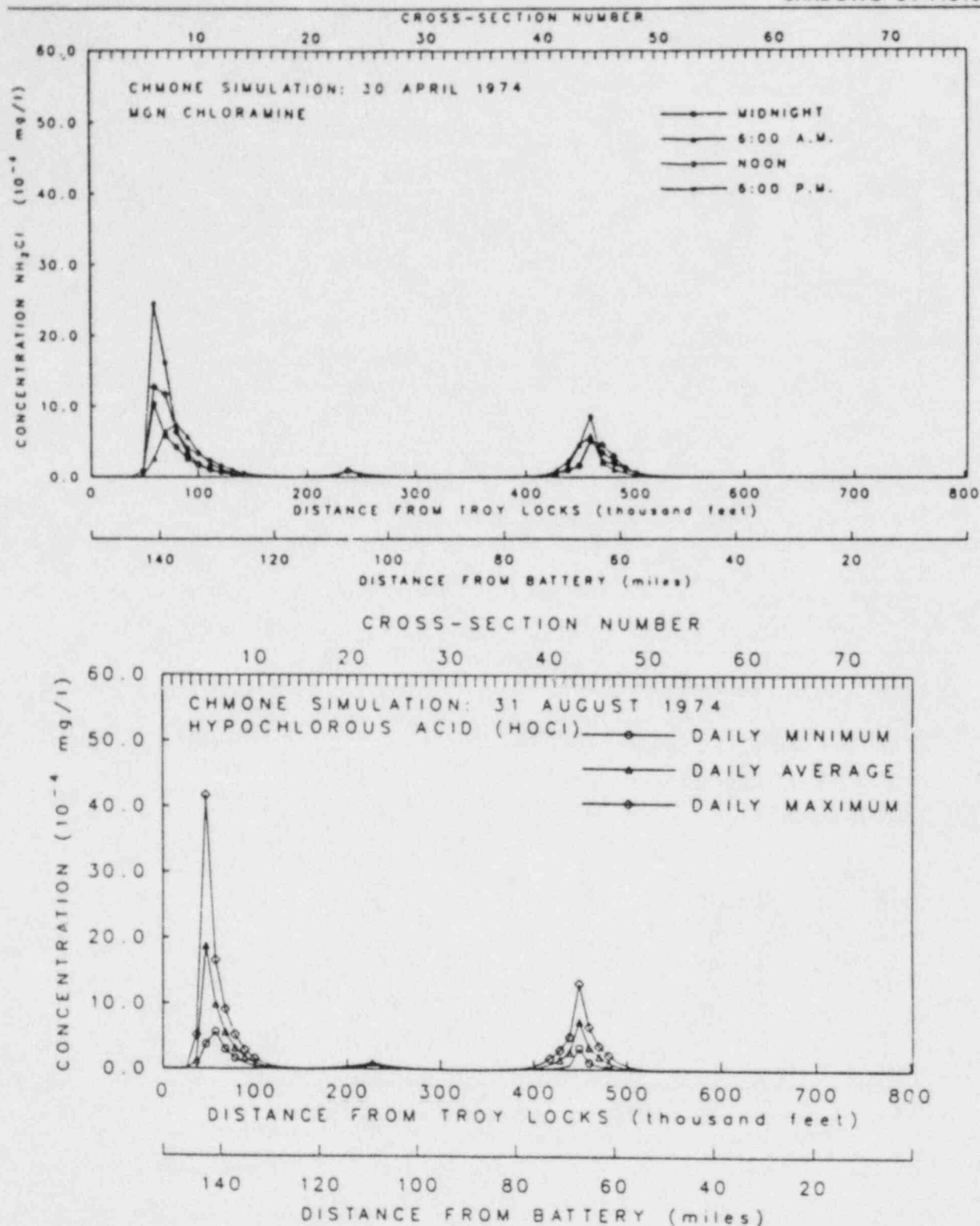
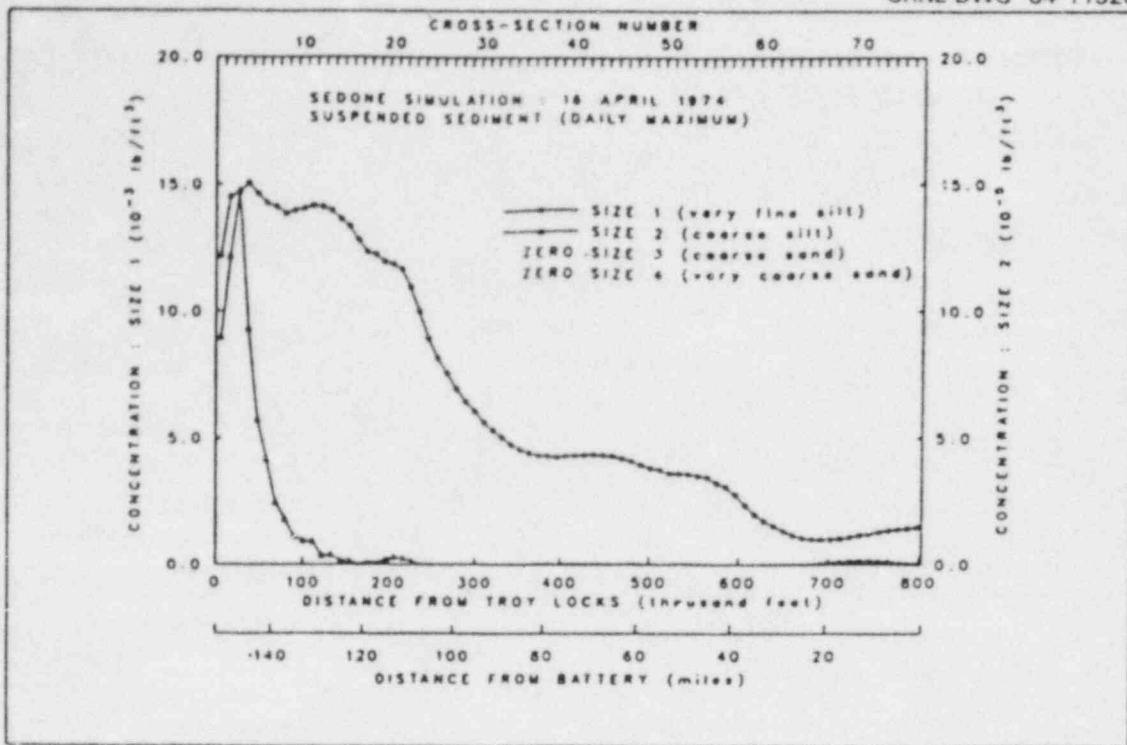
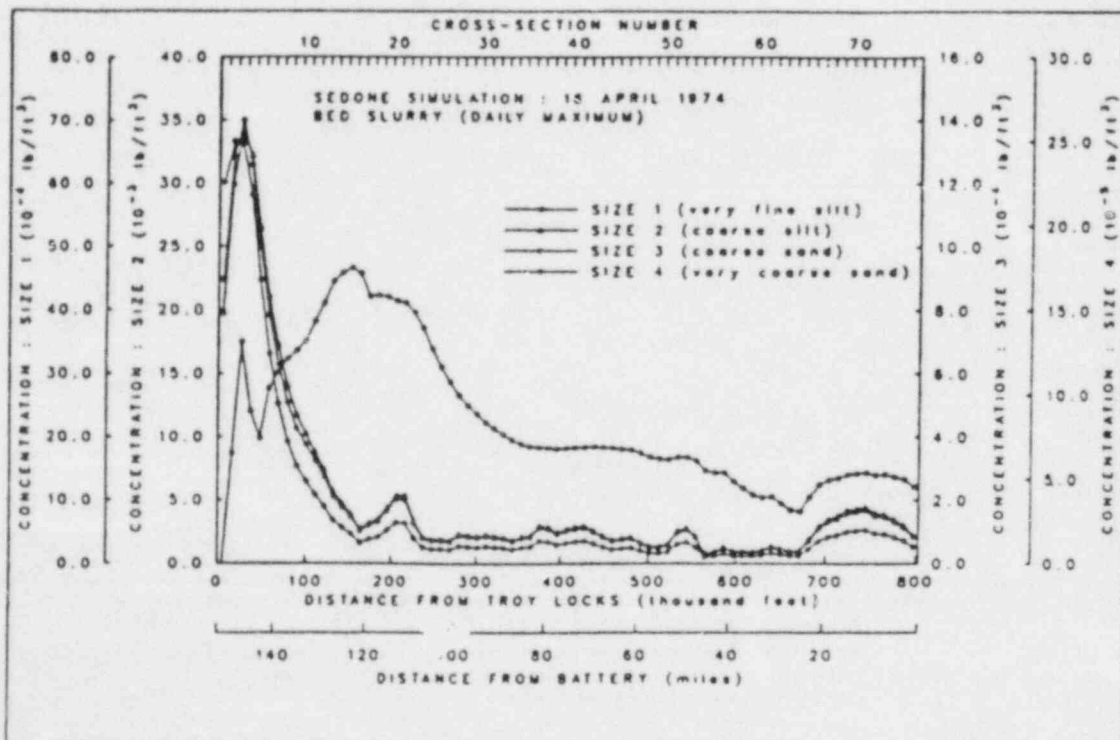


Fig. 6.10. Computer simulation results for the longitudinal distribution of Monochloramine (top figure) and hypochlorous acid (bottom figure) concentrations in the Hudson River for hypothetical power plant chlorination conditions.



(a)



(b)

Fig. 6.11. Computer simulation results for the longitudinal distributions of the sediment size classes in the Hudson River for (a) the suspended sediment layer and (b) the bed slurry sediment layer.

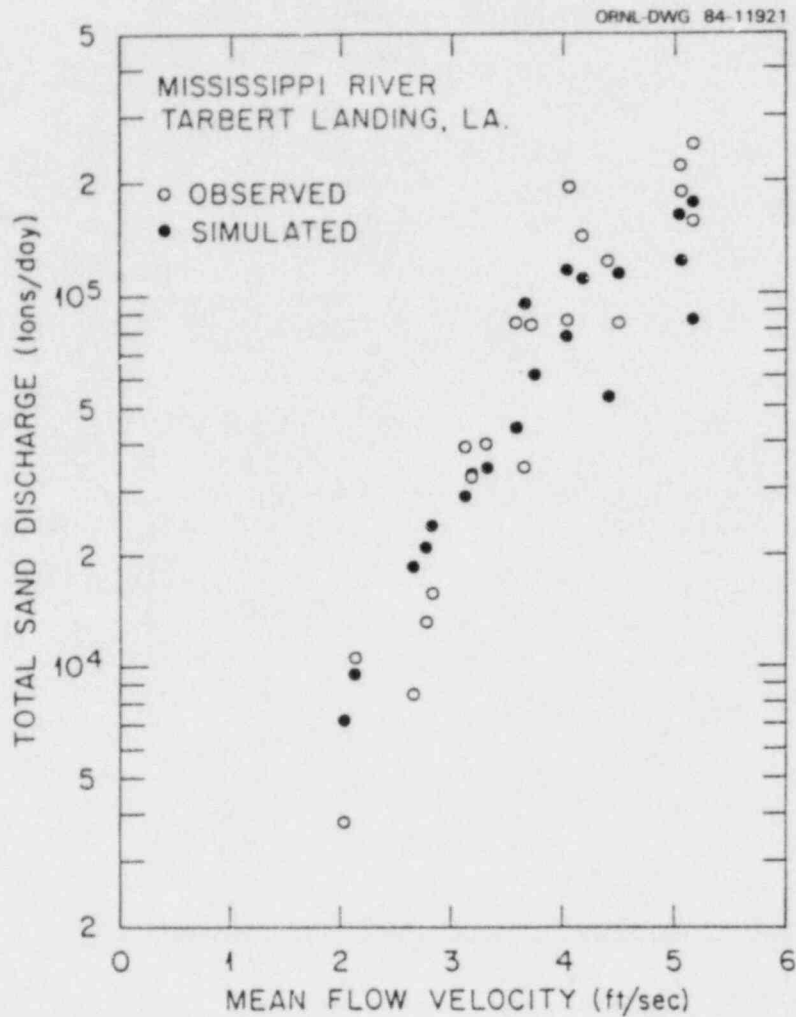


Fig. 6.12. Comparison computer simulation results and field-measured data for the total sediment discharge in the Mississippi River.

bathymetry as input to FLOWER for refined flow and temperature predictions in the vicinity of the Indian Point plant.

The specification of conditions at open boundaries such as those present here (see Fig. 6.15) is a problem common to many modeling studies. When modeling a limited reach of a river or estuary, the upstream and downstream ends of the reach of interest are frequently far removed from locations where flow rate or surface elevation observations are available. This presents a significant problem in establishing

ORNL-DWG 84-11922

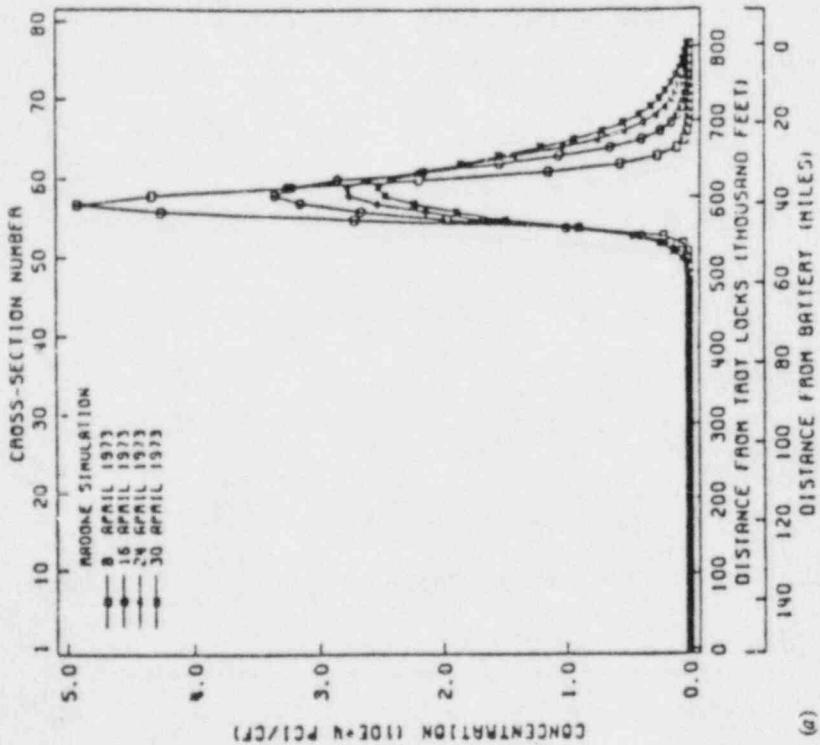
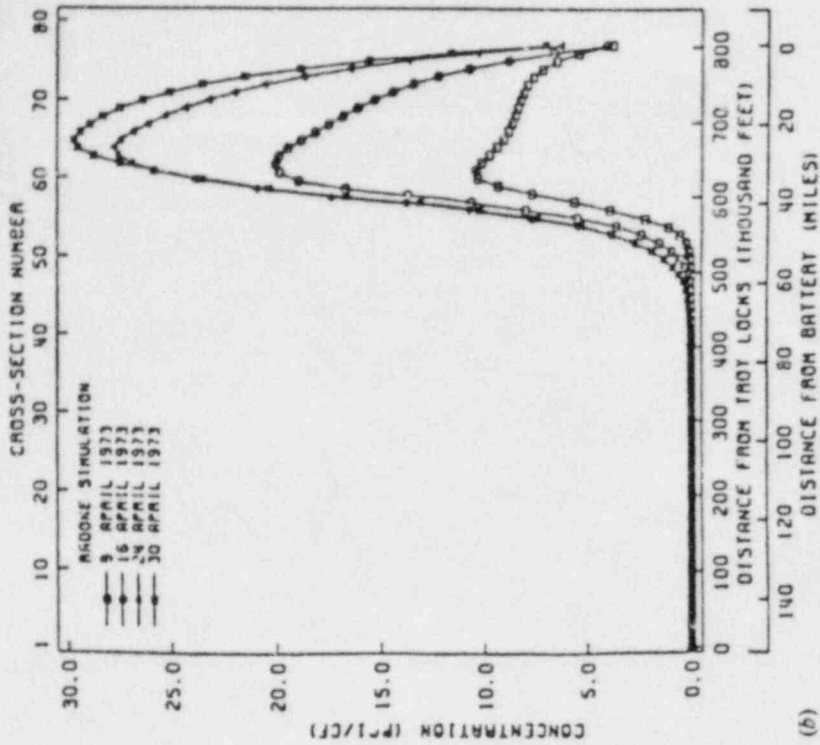


Fig. 6.13. Computer simulation results for the longitudinal distribution of radionuclide concentrations in the Hudson River for hypothetical prompt release conditions from Indian Point power plant as predicted in (a) the sediment layer and (b) the suspended sediment layer.

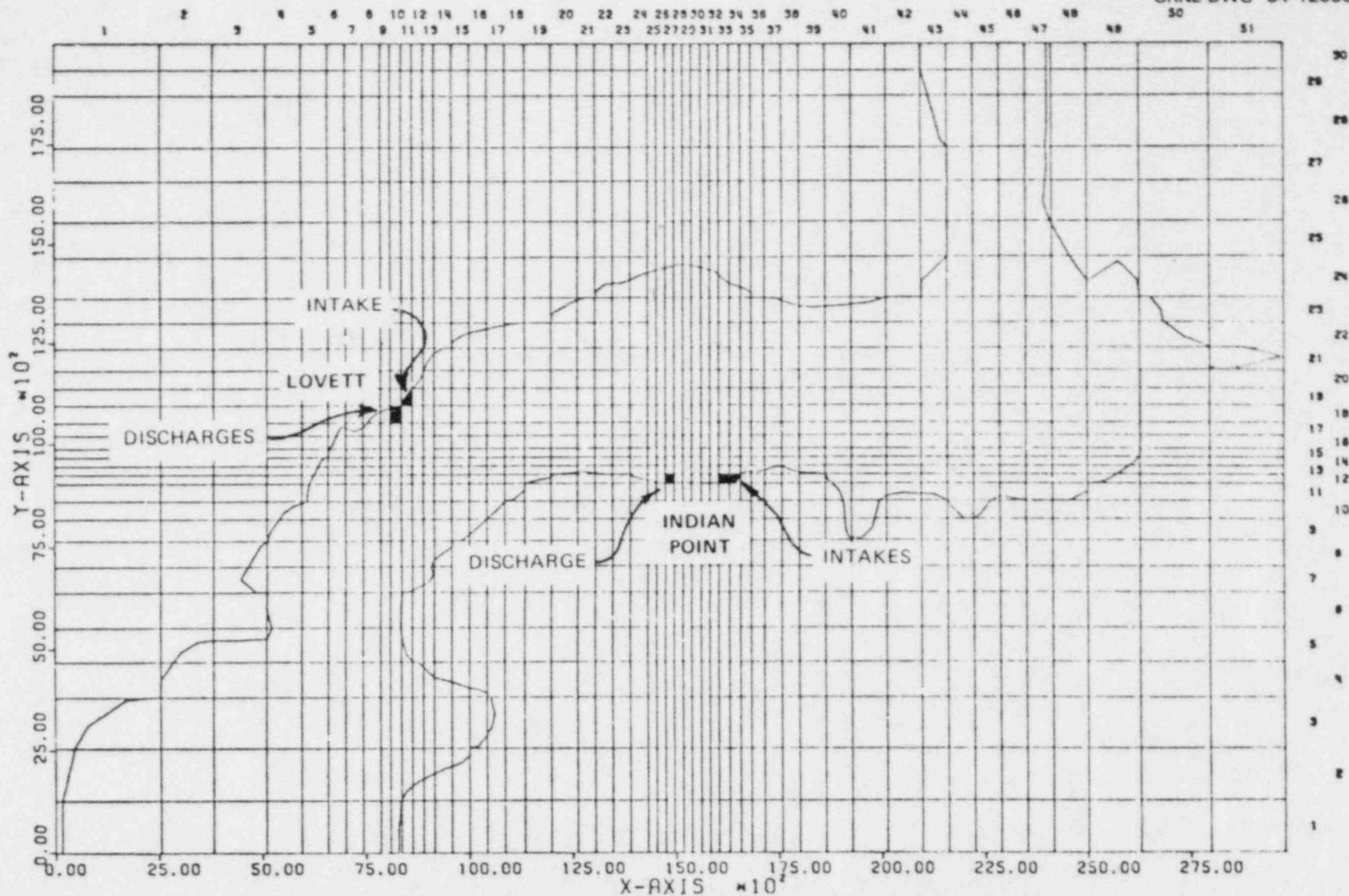


Fig. 6.14. Computer-generated discrete-element grid system for the section of the Hudson River in the vicinity of Indian Point and Lovett power plants.

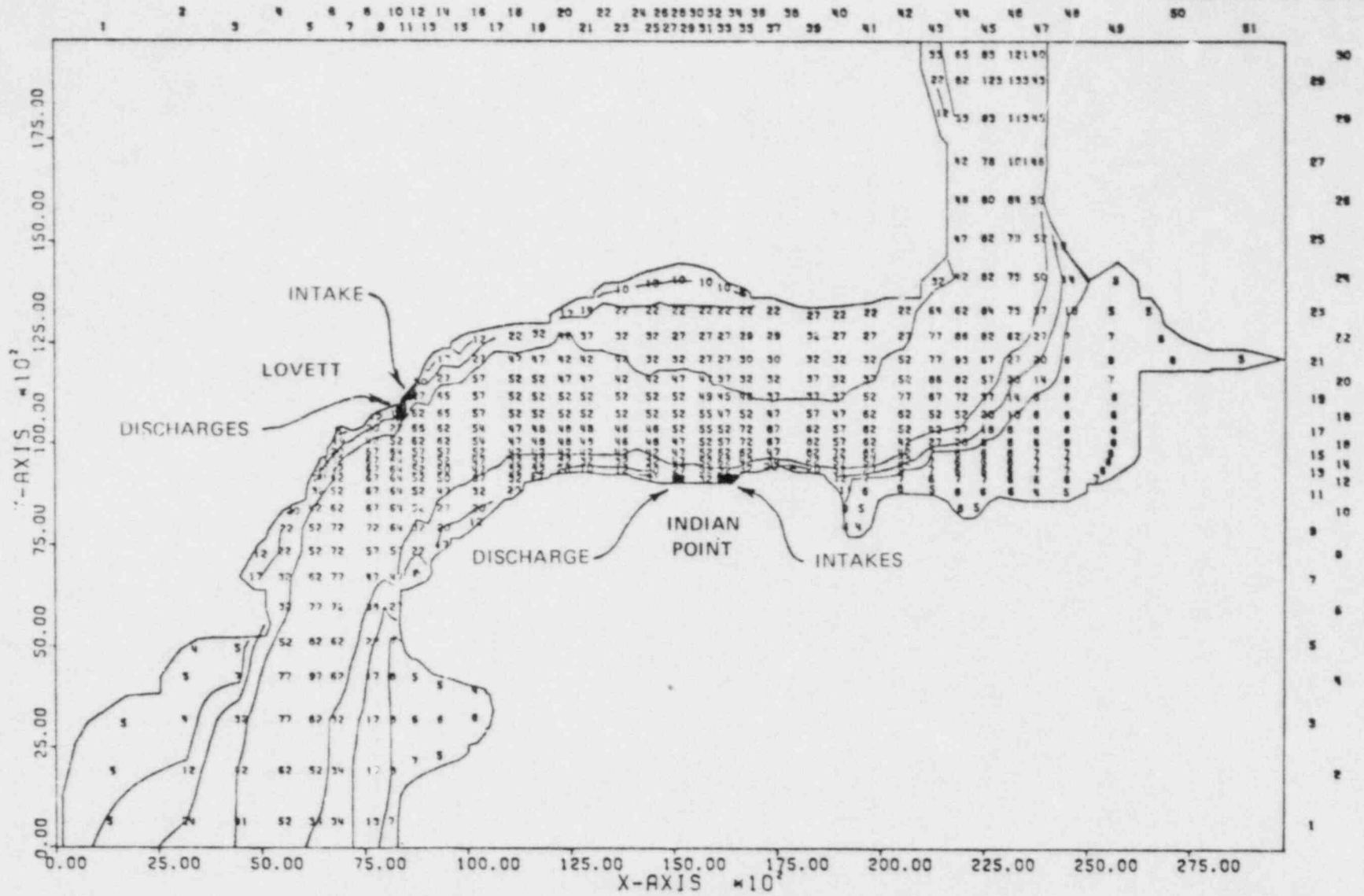


Fig. 6.15. Computer-generated constant-depth contours and depth values for the grid system shown in Fig. 6.14.

boundary conditions. The UTA approach presents a consistent means to overcome this problem. The one-dimensional, computationally efficient ESTONE code can be used to simulate conditions over a much greater extent of the river or estuary. The upstream and downstream ends of the modeled region are selected, for convenience, to coincide with locations where data is available. Volume flux and free-surface elevations conditions predicted at interior elements can be used as boundary conditions for a high resolution two- or three-dimensional simulation of a limit channel reach. Such a procedure has been applied here. The upstream and downstream boundaries of the modeled region shown in Fig. 6.14 were selected to coincide with computational points of the previously applied ESTONE code.

The fine structure of the flow field induced by the Indian Point shoreline discharge jet was simulated using the horizontal jet zone-matching methodology described in Sect. 5.1. Predicted jet flow-field results are given in Fig. 6.16. This flow field is input to FLOWER, where it is superimposed on the predicted natural flow field. Figure 6.17 shows the total predicted plant-induced and natural flow field in the vicinity of Indian Point at 9:00 a.m. on August 23, 1974. Figure 6.18 shows water temperature predictions at the same time. The figure clearly shows the power plant-induced thermal plume, as well natural horizontal variations in water temperature.

It should be noted that the UTA thermal codes are capable of accurately predicting natural thermal structures and total (natural plus plant-induced) thermal structures. Incremental temperatures can be accurately predicted by running the desired code both with and without the power plants operating and subtracting the two results. This

ORNL-DWG 84-12017

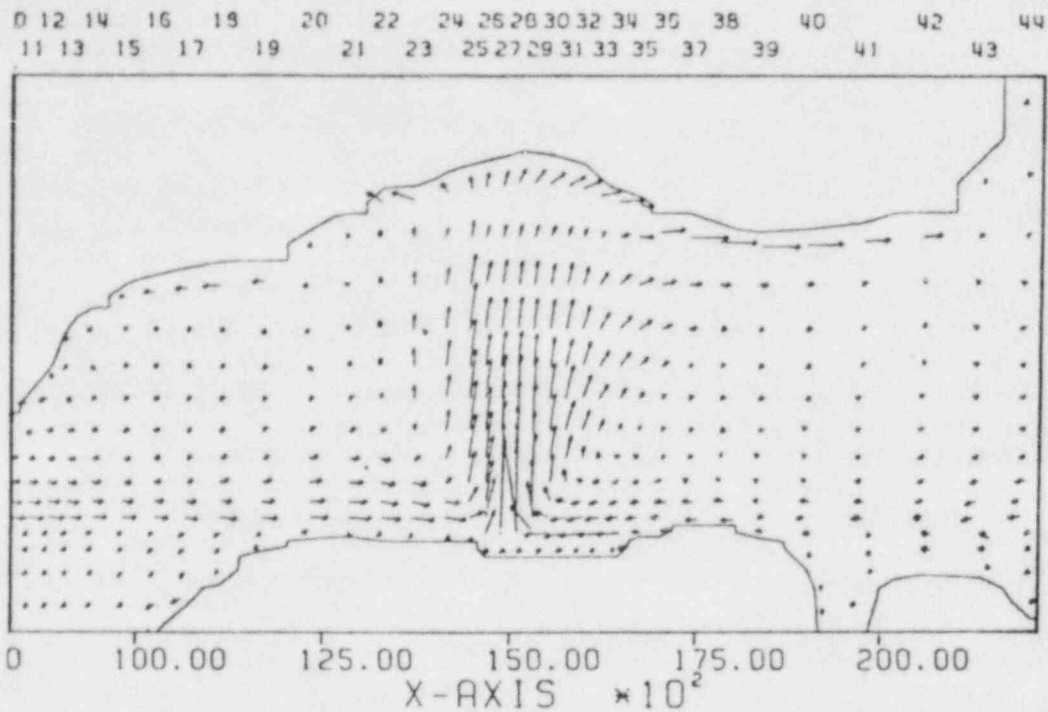


Fig. 6.16. Results of the horizontal jet zone-matching methodology applied to the Indian Point discharge using the grid system shown in Fig. 6.14.

approach is necessary in regions which exhibit large spatial variations in temperature, because it is difficult (if not impossible) to distinguish a thermal plume from natural variations.

6.2 San Onofre

San Onofre Nuclear Generating Station is a three unit nuclear power plant located on the coast of southern California. This case was selected for inclusion in this report because it demonstrates the systematic application of the horizontal jet zone-matching methodology, a simplified depth-averaged version of FLOWER, and RADTWO.

The San Onofre intake/discharge configuration is shown in Fig. 6.19. The Unit 2 and 3 discharges are submerged off-shore diffusers.

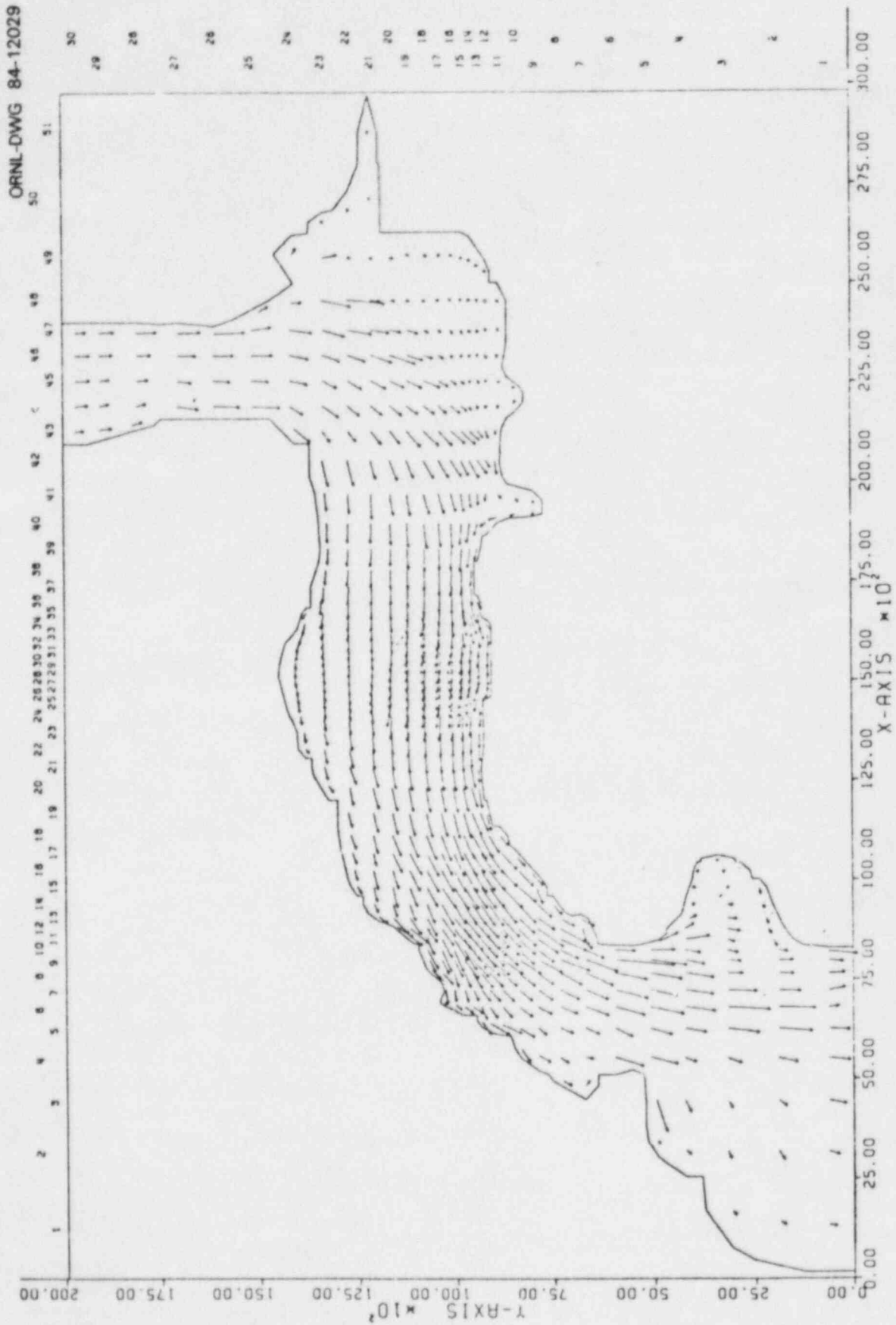
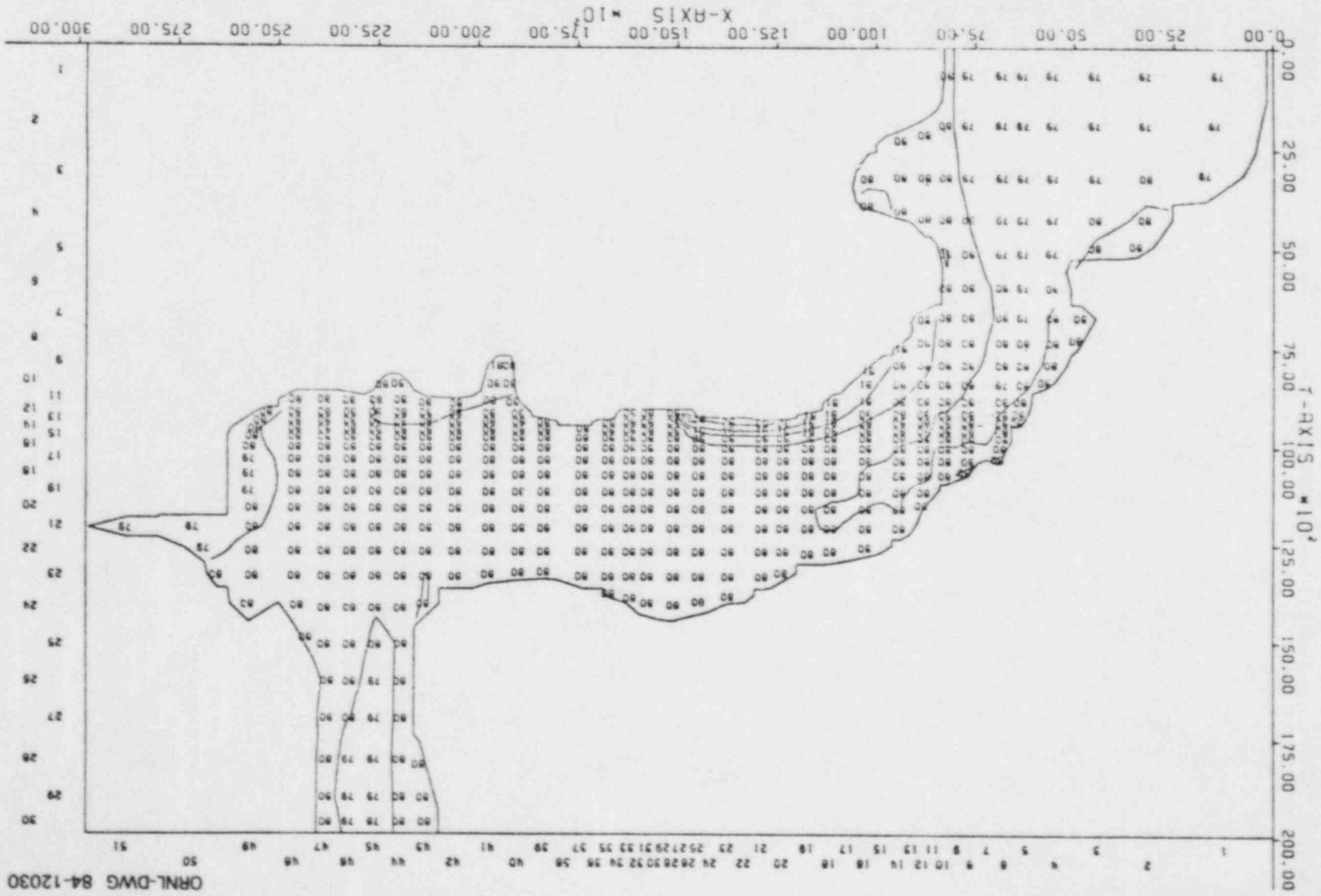


Fig. 6.17. Computer simulation results for the two-dimensional natural and plant-induced flow field in the region of Indian Point and Lovett power plants at 9:00 a.m. on August 23, 1974.

Fig. 6.18. Computer simulation results for the full two-dimensional (depth-averaged) temperature distribution in the region of Indian Point and Lovett power plants at 9:00 a.m. on August 23, 1974.



ORNL-DWG 84-12030

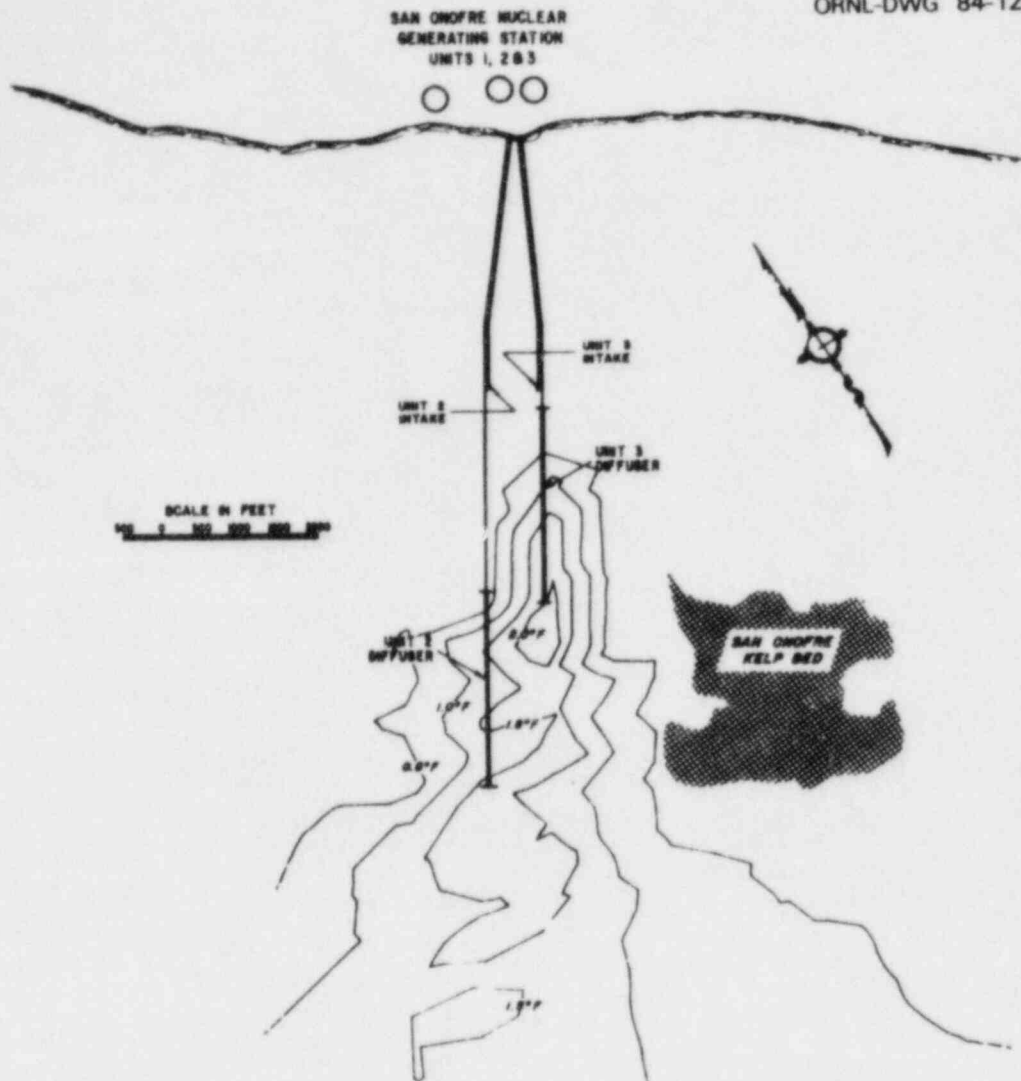


Fig. 6.19. Configuration of the San Onofre circulating water systems.

The Unit 1 discharge is a single submerged vertical pipe, and each unit has a submerged off-shore intake.

The computational grid and shoreline representation used in the San Onofre simulation is shown in Fig. 6.20. Bathymetric information was obtained from navigational charts. The diffuser-induced flow fields were simulated by representing each diffuser as five horizontal jets and superimposing individual jet solutions obtained from the horizontal jet

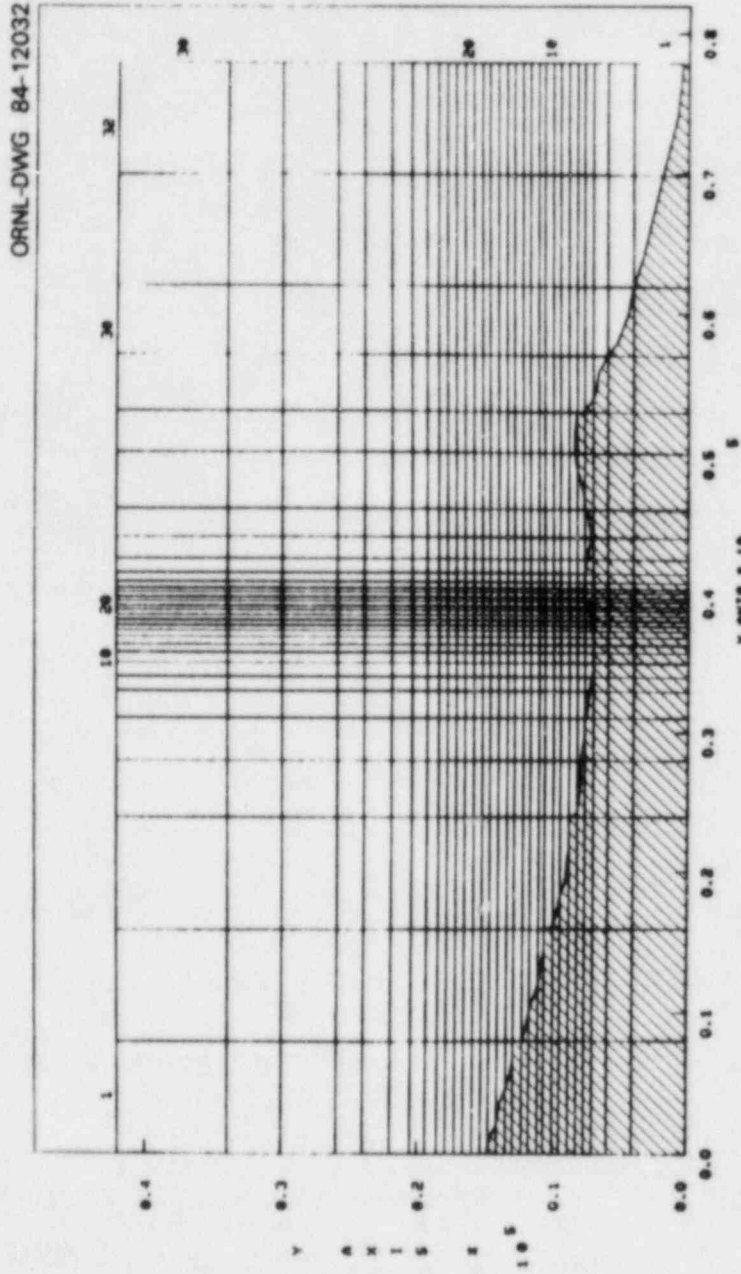


Fig. 6.20. Plot of actual shoreline and grid system used for the San Onofre application.

zone-matching methodology. The Unit 1 discharge was modeled as a point source, and all three intakes were modeled as point sinks. The total predicted power plant-induced flow field is shown in Fig. 6.21. Open-water boundary conditions used in FLOWER were developed based upon available current meter data.

Figures 6.22 and 6.23 present total predicted flow fields at maximum and minimum (6 hrs later) flow conditions, respectively. Figures 6.24 and 6.25 show predicted plant-induced excess temperatures at times corresponding to Figs. 6.22 and 6.23, respectively. Figure

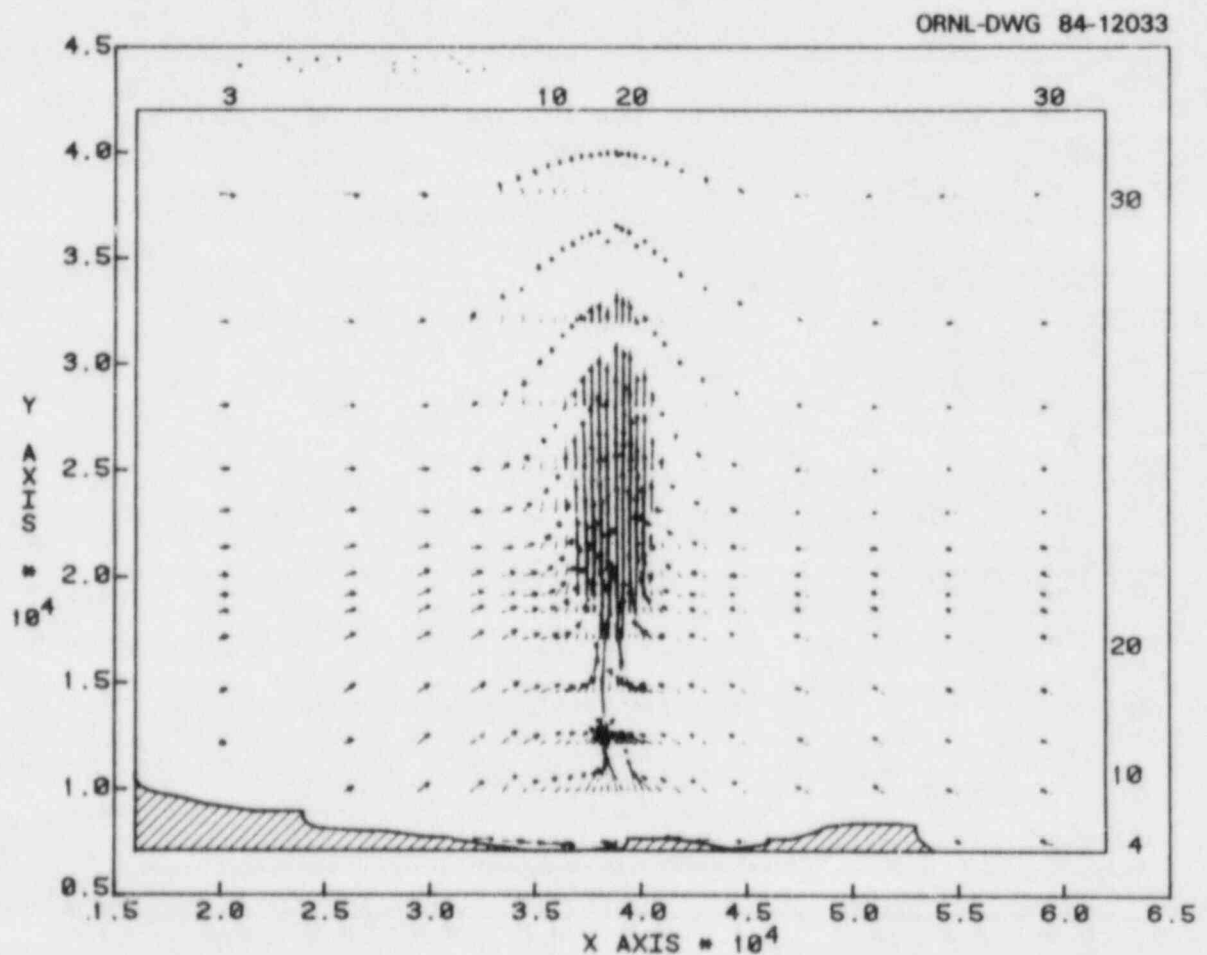


Fig. 6.21. Plant-induced flow field resulting from the operation of all three San Onofre units as predicted by the horizontal jet zone-matching methodology.

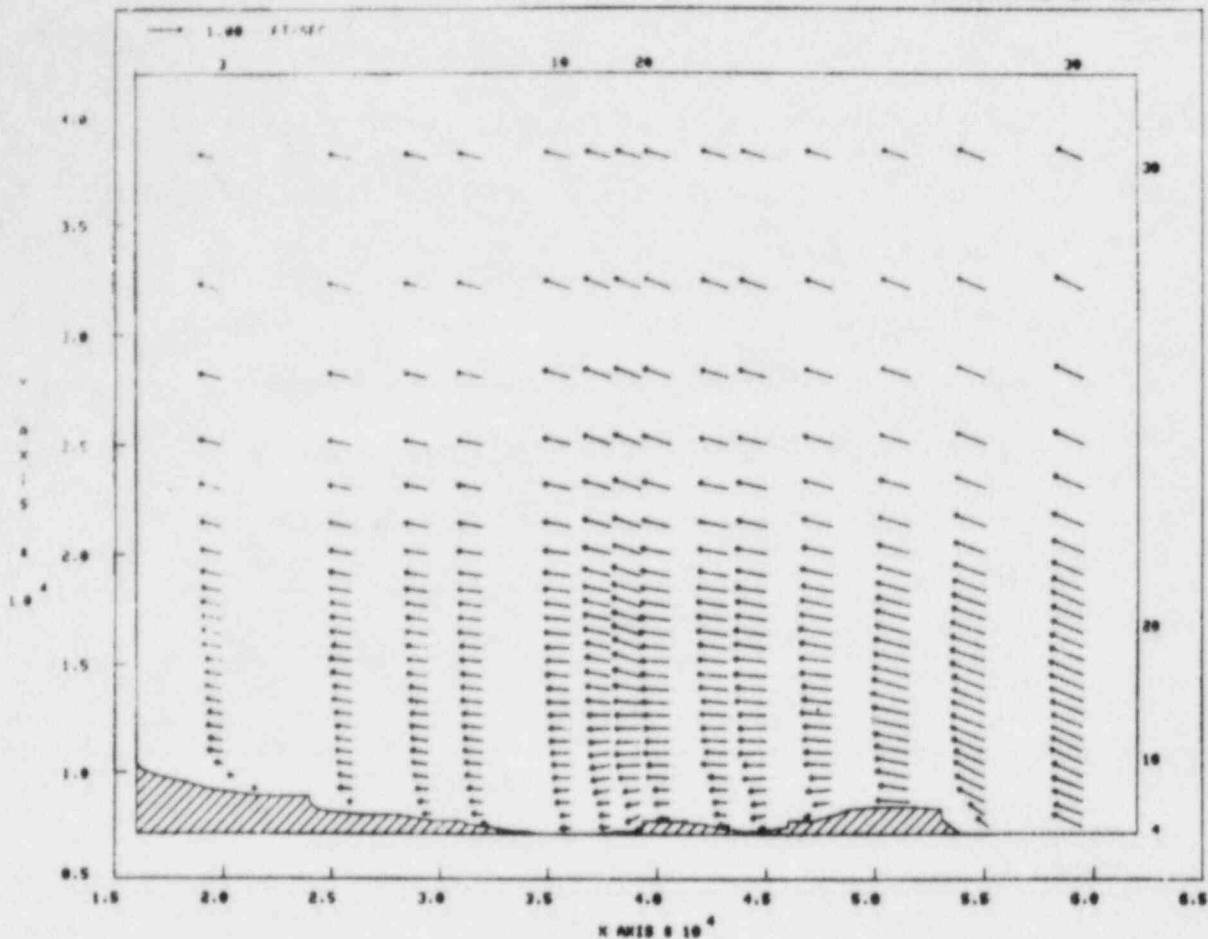


Fig. 6.22. Predicted, depth-averaged, full flow field in the San Onofre region at 2:00 a.m. on the fifth day of the simulation.

6.25 clearly shows the presence of each unit's discharge appearing as "hot spots" above each discharge structure. Excess temperatures were calculated by running the code with and without the plants operating and subtracting the two results. Unlike the Hudson River case, this procedure was necessary due to the large natural temperature gradient in the off-shore direction.

Using the input data set created for FLOWER and the FLOWER flow-field results, the RADTWO code was used to simulate the distribution of radionuclides resulting from a hypothetical accidental release from San

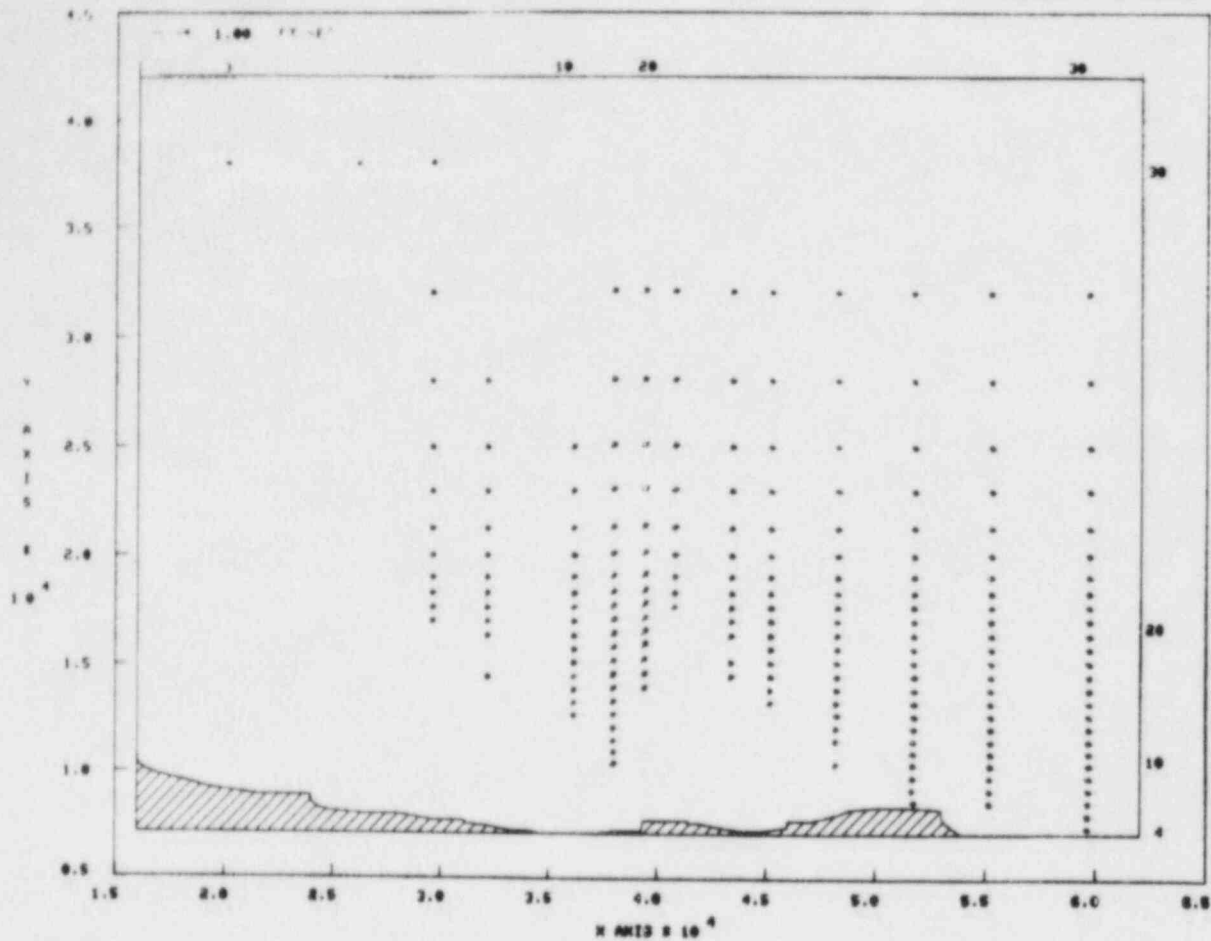


Fig. 6.23. Predicted, depth-averaged, full flow field in the San Onofre region at 8:00 a.m. on the fifth day of the simulation.

Onofre Unit 1. Figure 6.26 shows the predicted radionuclide distribution 24 hrs after the start of the accident and at the time in the tidal cycle comparable to that shown in Fig. 6.22.

6.3 The Green River Case

The Green River case was selected to illustrate a full three-dimensional application of FLOWER. The modeled region is a 1200 m reach of the Green River around the Paradise Steam Plant, and the FLOWER code is used to predict natural and plant-induced temperatures and flows.

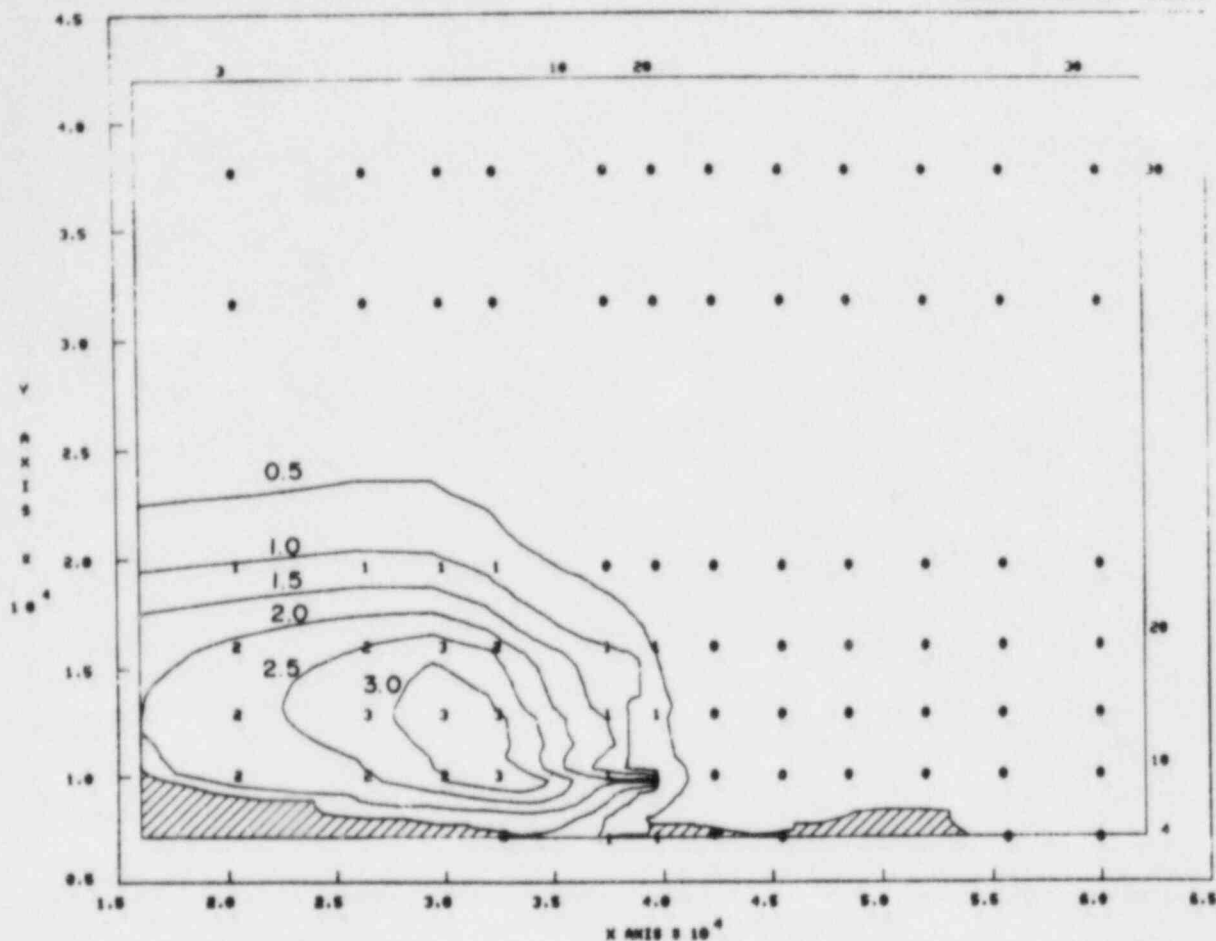


Fig. 6.24. Predicted, depth-averaged, excess temperatures in the San Onofre region at 2:00 a.m. on the fifth day of the simulation.

Figure 6.27 shows the horizontal grid system and shoreline representation used. Note that grid cells vary from 20 to 80 m in both the downstream and cross-channel directions. Four vertical elements or layers were used, with layer 1 being the bottom layer and layer 4 being the surface layer. Figure 6.28 shows the bathymetry used in model simulations.

Figure 6.29 shows predicted total (natural plus plant-induced) velocities for each layer at two times during the simulation period. The Paradise Steam Plant is located along the lower shoreline of these

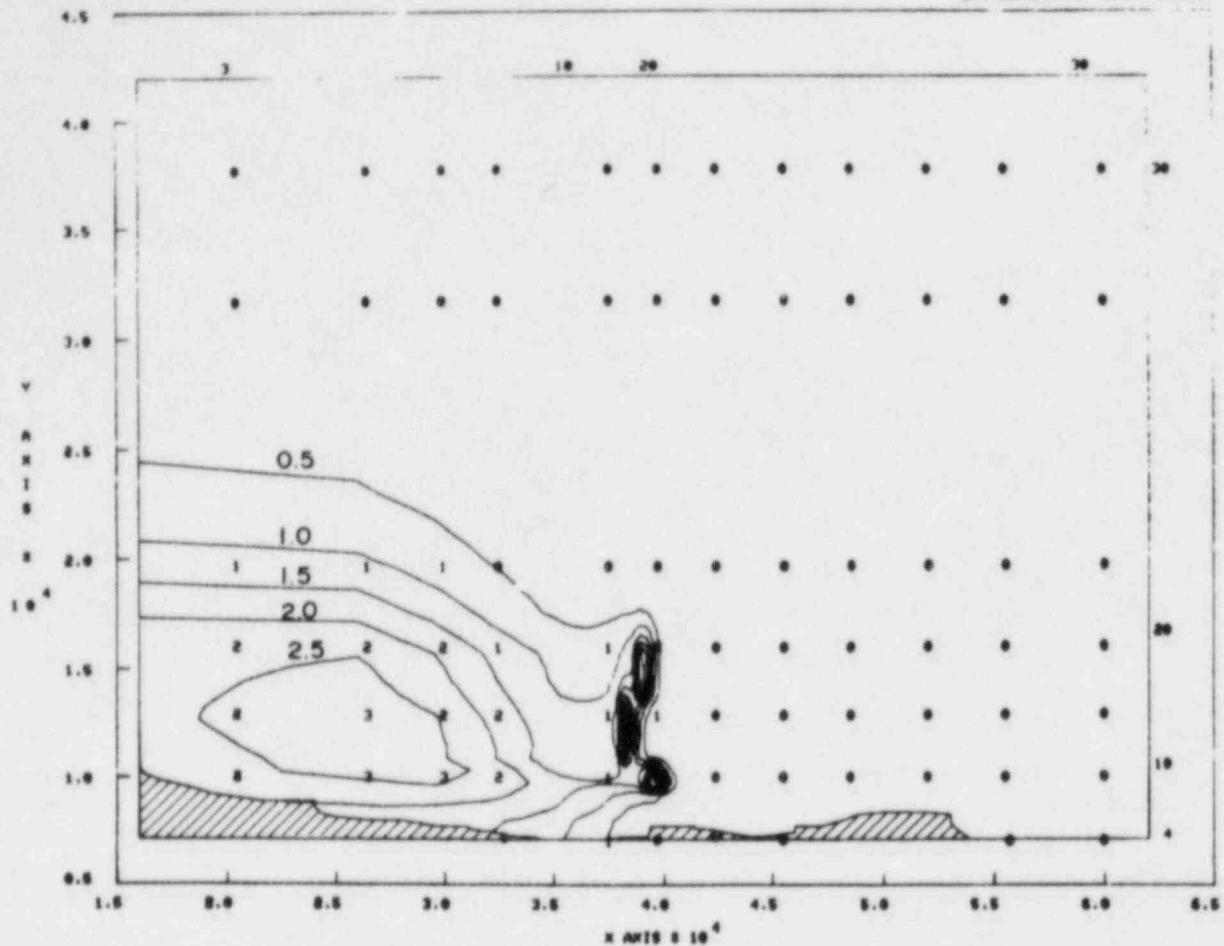
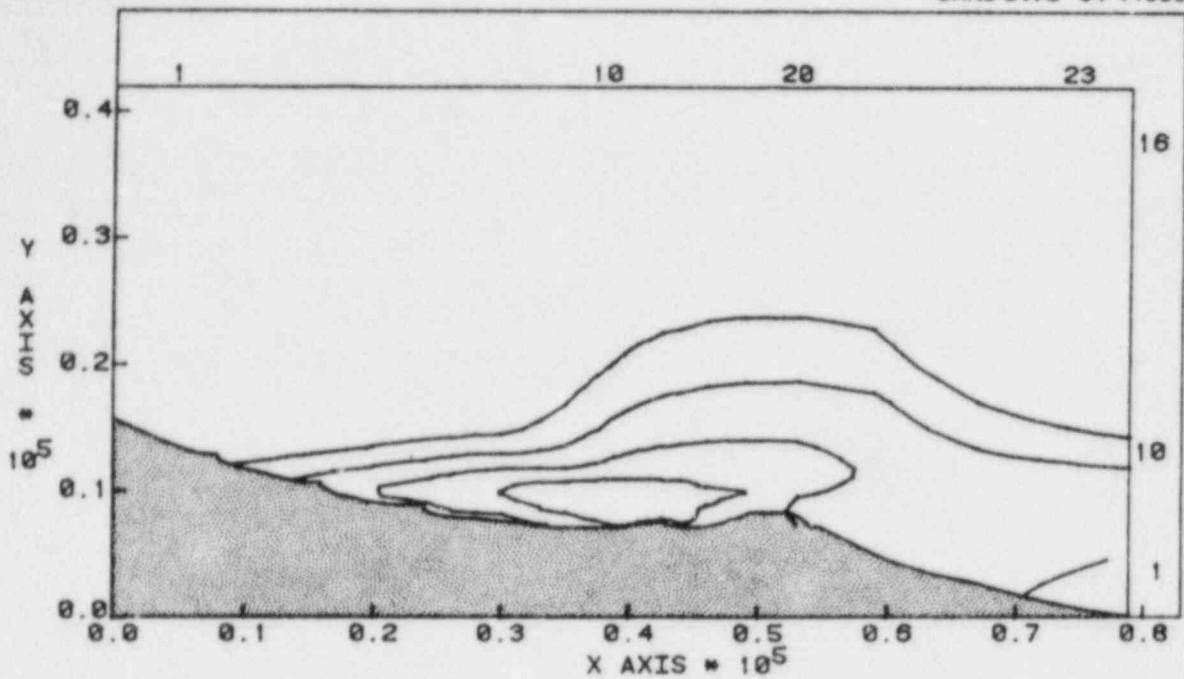


Fig. 6.25. Predicted, depth-averaged, excess temperatures in the San Onofre region at 8:00 a.m. on the fifth day of the simulation.

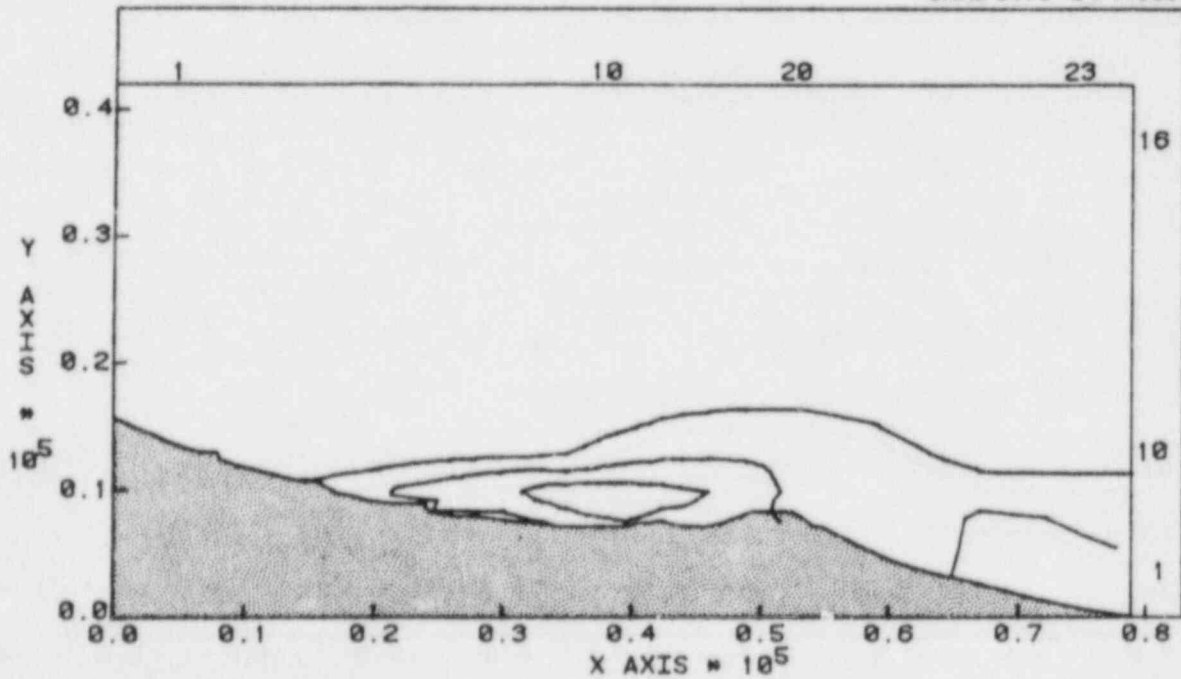
figures. Both the intake and discharge structures are located along the shore, with the discharge point occurring near the surface and the intake structure located near the bottom upstream of the discharge. Near the bottom, Fig. 6.29(a), the strong shoreward flow upstream is induced by the power plant intake, while the weaker shoreward flow downstream is entrainment induced by the surface discharge. In layer 2, Fig. 6.29(b), little intake flow is evident, however, entrained discharge flow is still apparent. In the upper two layers, Figs. 6.29(c) and (d), the dominant features are the natural flow, and the plant dis-

ORNL-DWG 84-11959



(a)

ORNL-DWG 84-11960



(b)

Fig. 6.26. Computer simulation results for the radionuclide concentration conditions for (a) the water layer and (b) the sediment layer in the San Onofre coastal region, 24 hrs after the start of the hypothetical accidental release scenario.

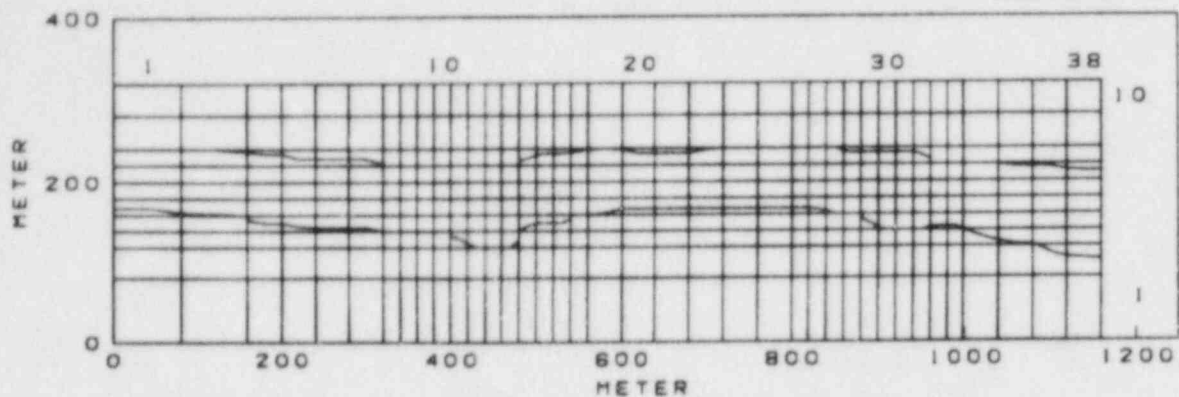


Fig. 6.27. Discrete-element, variable-size, rectangular grid system and shoreline representation used for the Green River power plant simulation.

charge, which extends over the entire channel width near the discharge point. Figure 6.30 shows predicted water temperatures for the four layers, which correspond to the flow-field predictions presented in Fig. 6.29. Viewing the results for the four layers collectively, it is apparent that this stretch of the Green River is well mixed and, under natural conditions, would be at or near isothermal conditions as are predicted to occur far upstream of the discharge. This figure also shows that the heated discharge has produced a significant vertical temperature gradient near the discharge and extending several hundred meters downstream.

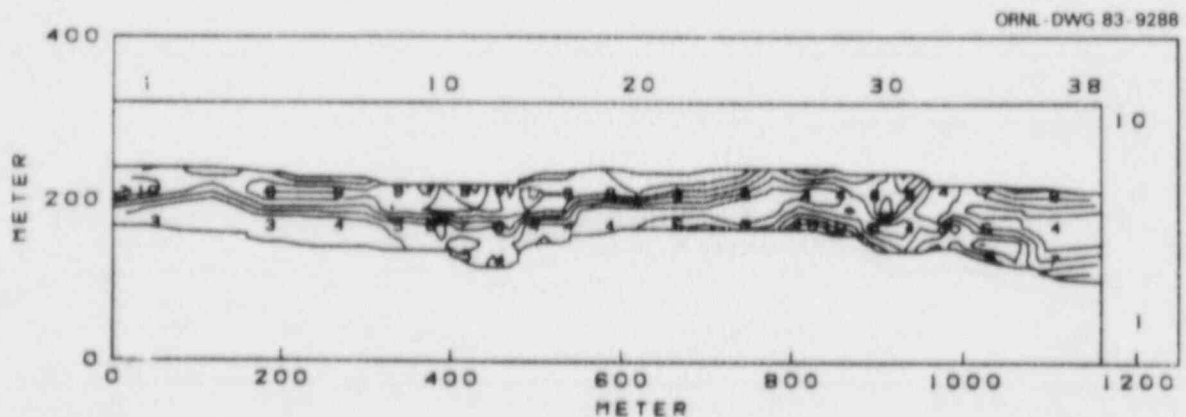


Fig. 6.28. Depth contours for the flow region of the Green River power plant simulation. Gradations of constant depth contours are from 3 to 10 m, respectively.

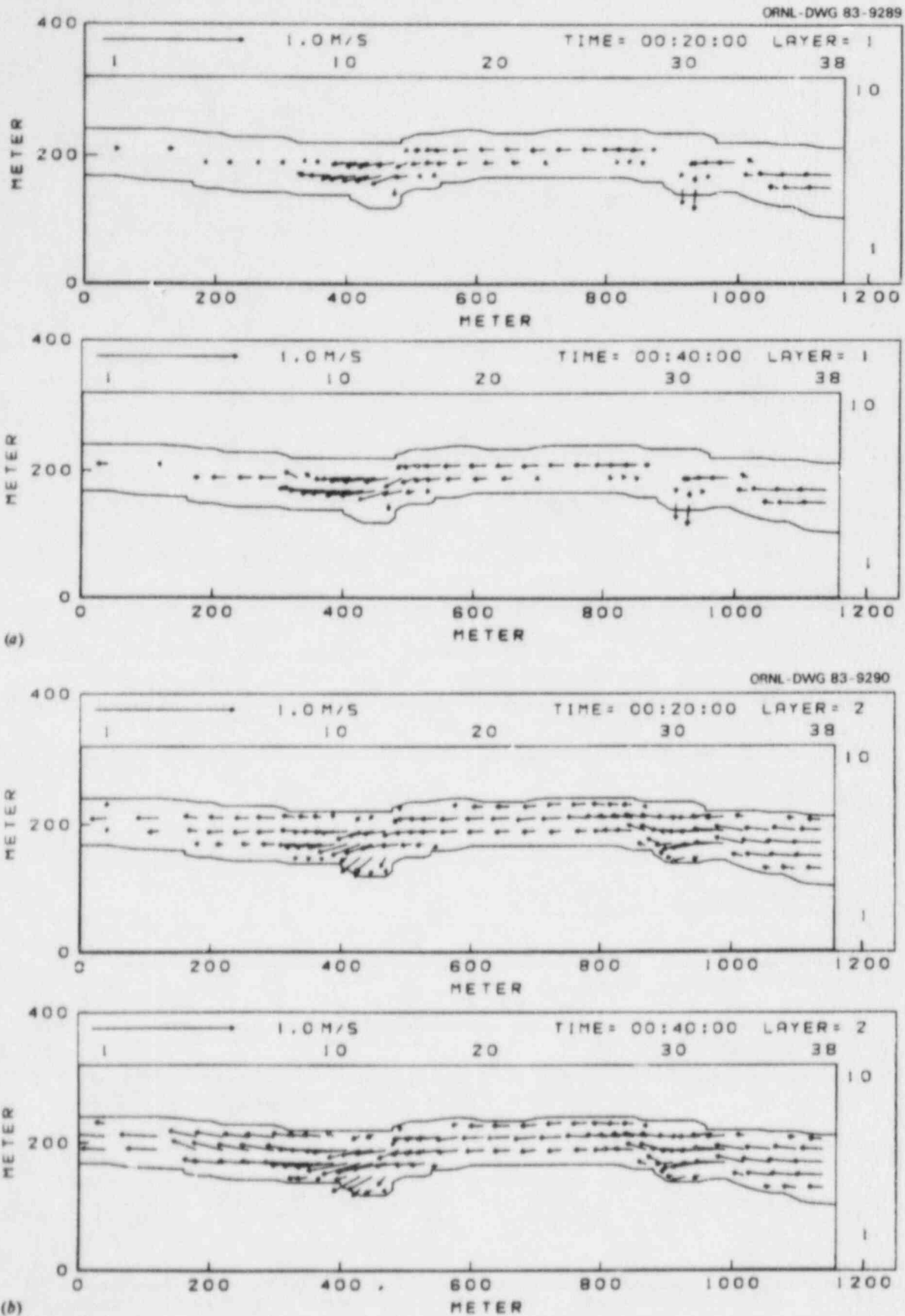
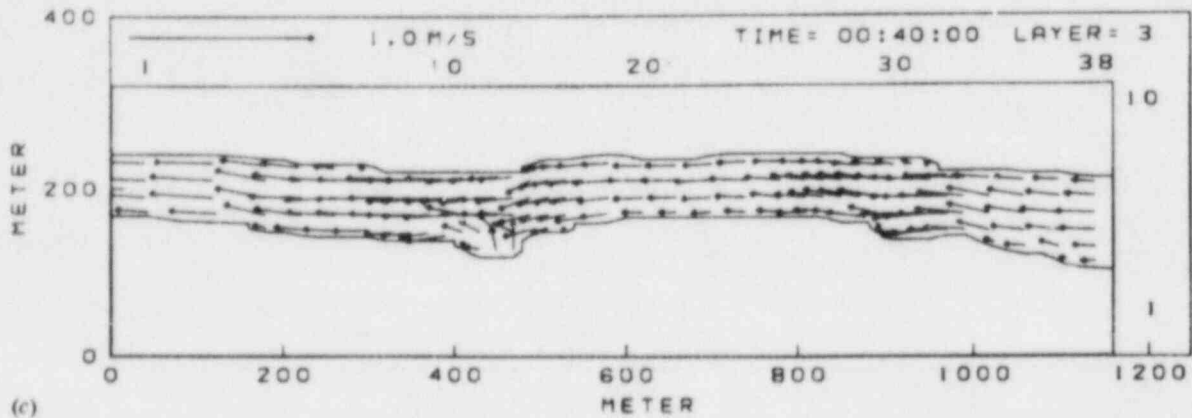
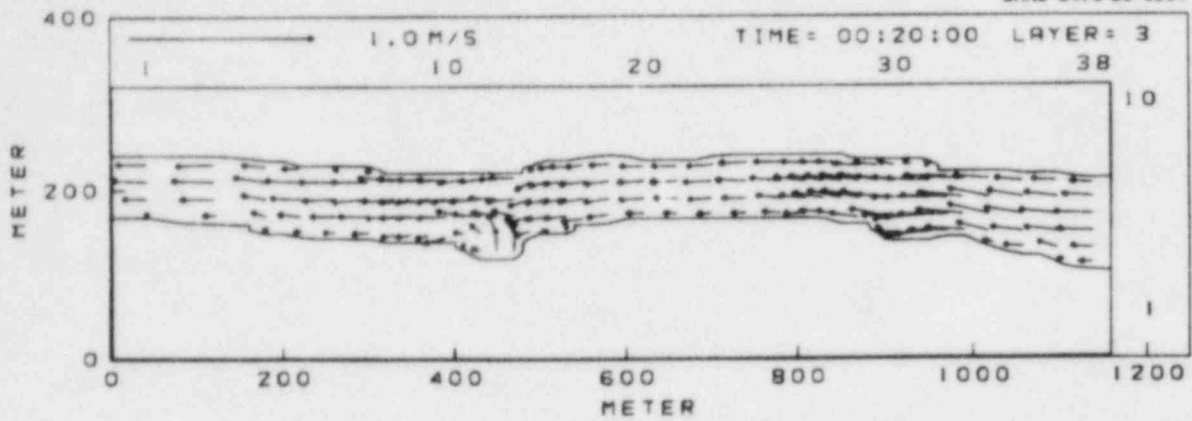


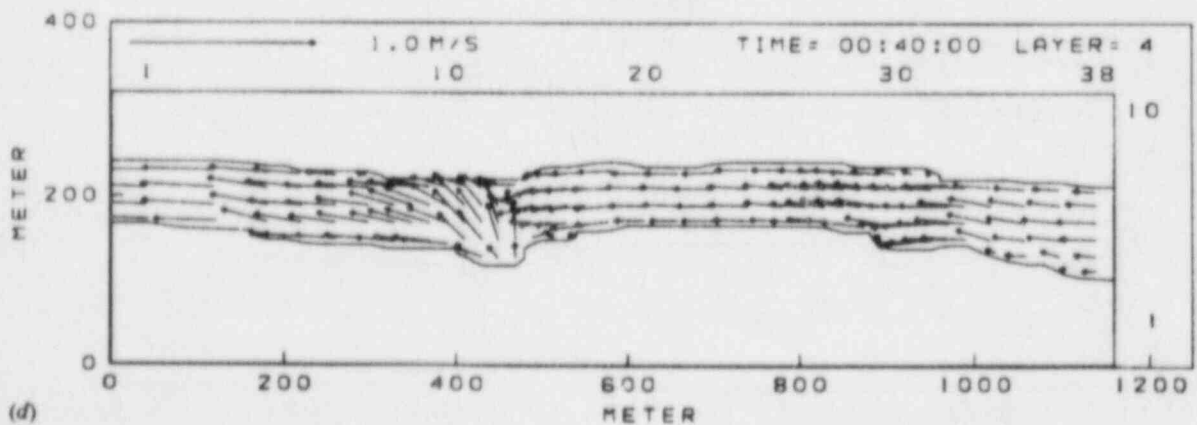
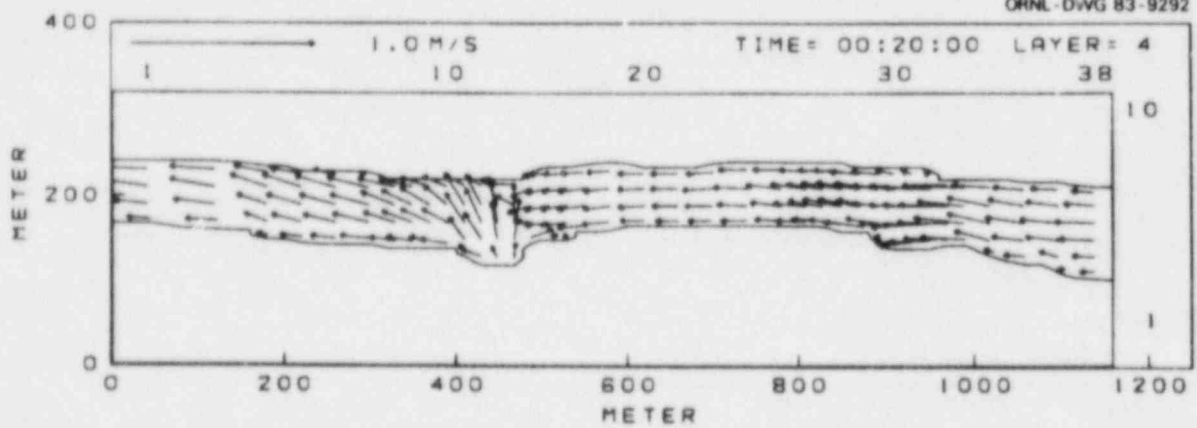
Fig. 6.29. Predicted horizontal velocity vectors in (a) the bottom layer and (b) layer 2 after 20 and 40 min of the simulation.

ORNL-DWG 83-9291



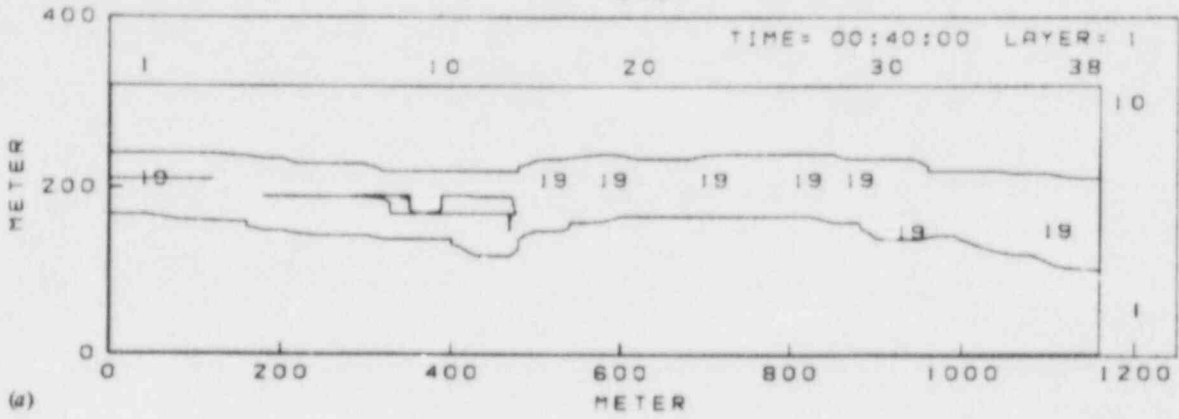
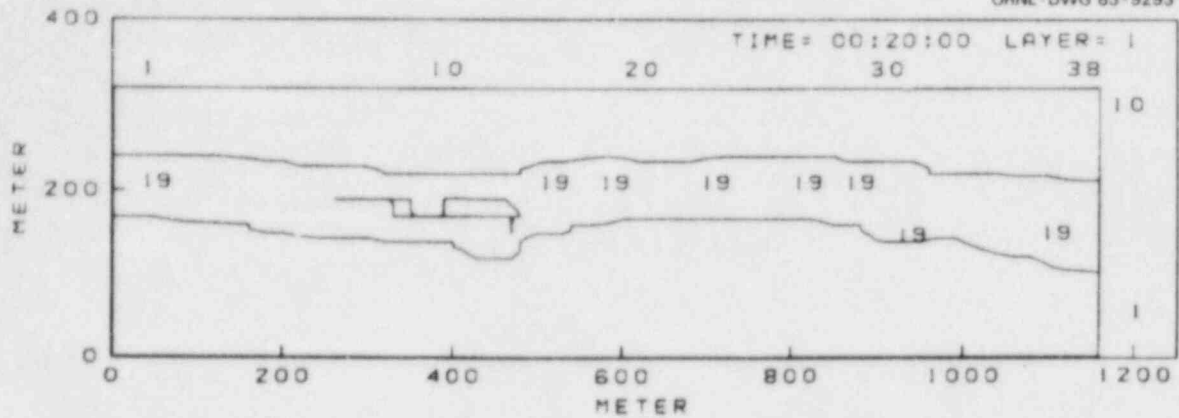
(c)

ORNL-DWG 83-9292

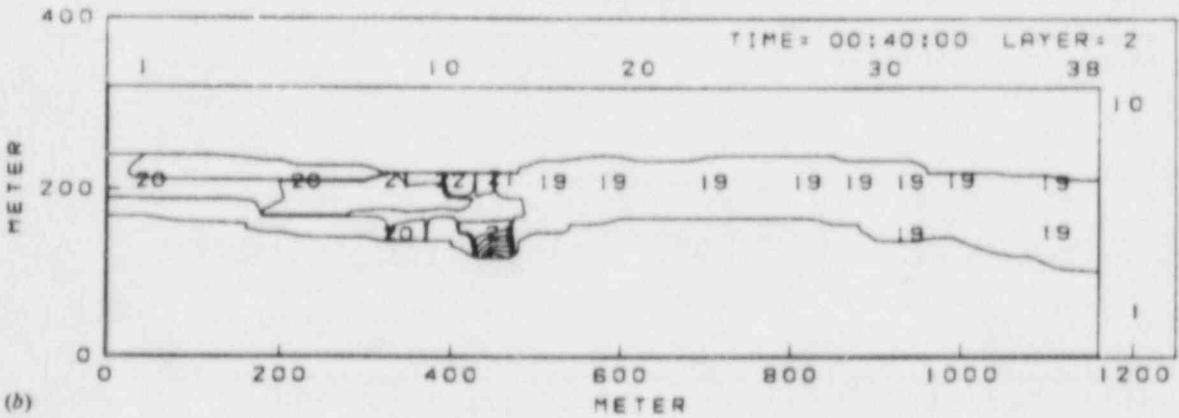
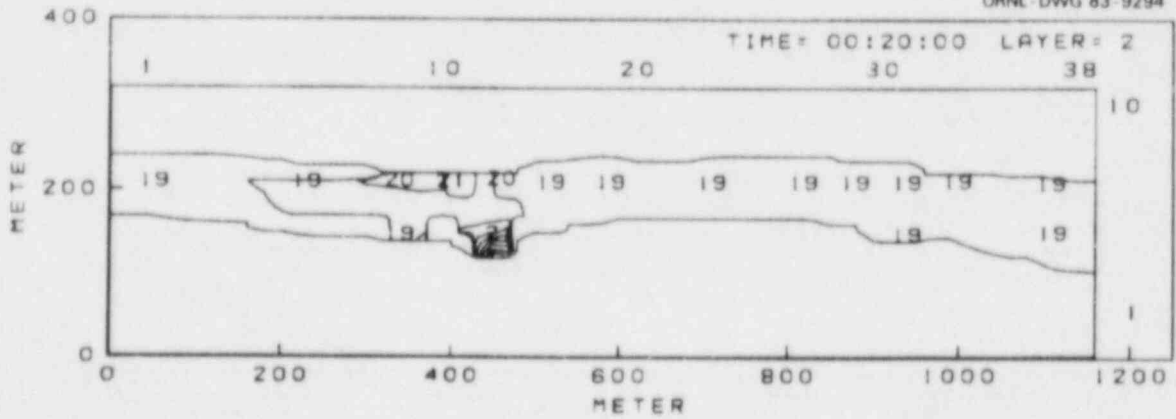


(d)

Fig. 6.29. Predicted horizontal velocity vectors in (c) layer 3 and (d) the surface layer after 20 and 40 min of the simulation.

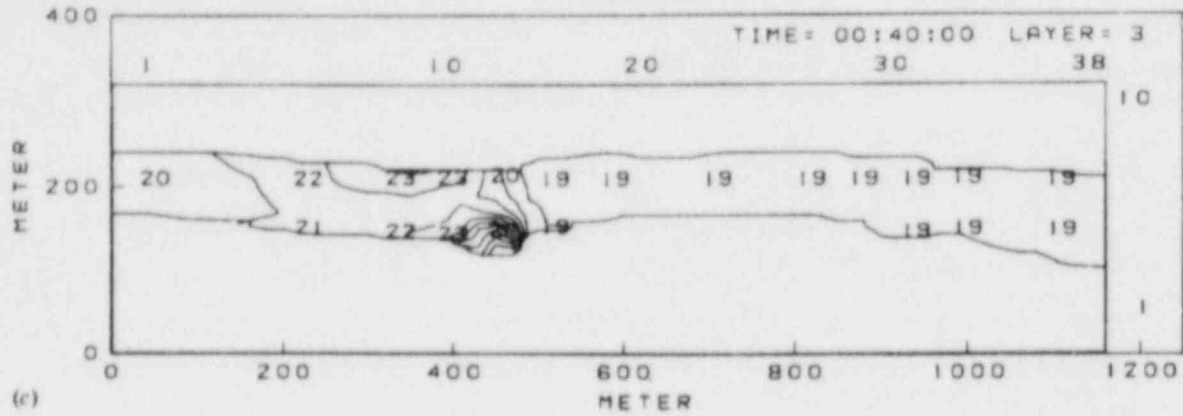
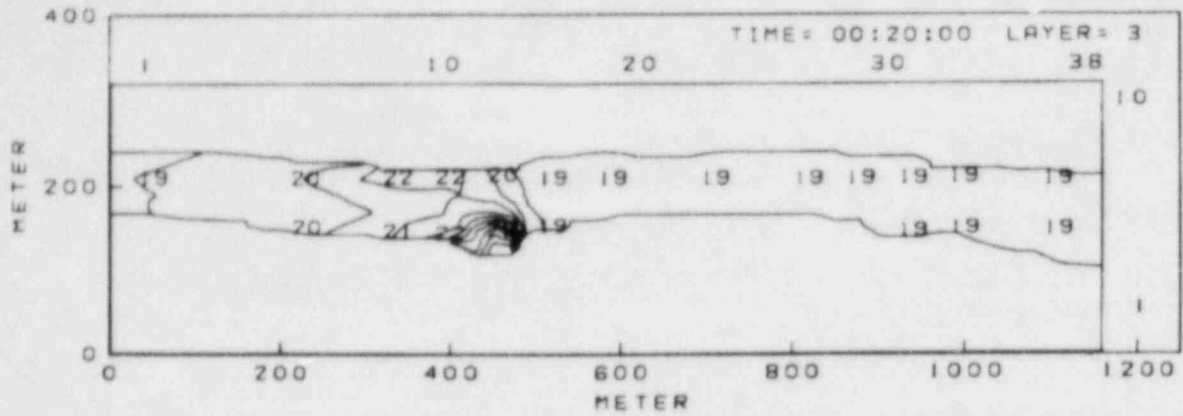


(a)

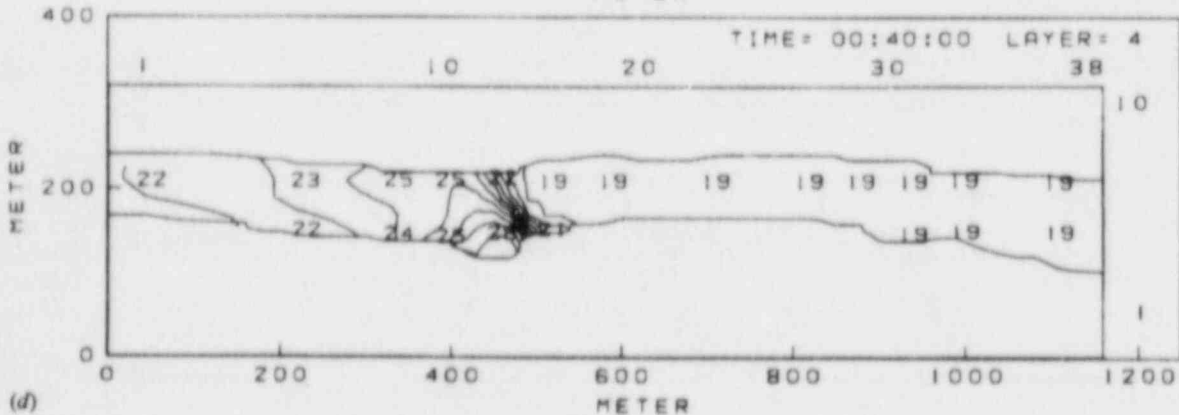
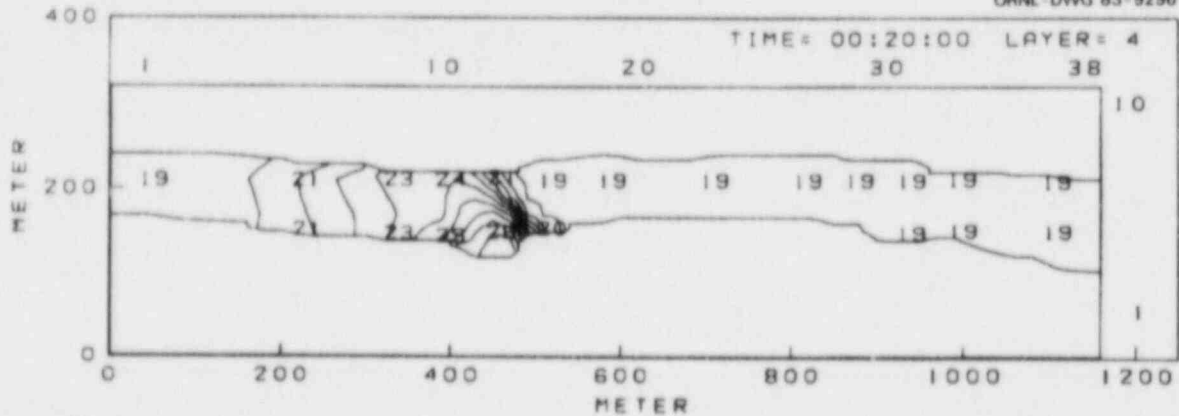


(b)

Fig. 6.30. Predicted total temperature shown as isotherms for (a) the bottom layer and (b) layer 2 after 20 and 40 of the simulation. Isotherms are drawn in 1°C increments between 19°C and 22°C.



(c)



(d)

Fig. 6.30. Predicted total temperature shown as isotherms for (c) layer 3 and (d) the surface layer after 20 and 40 min of the simulation. Isotherms are drawn in 1°C increments between 19°C and 22°C.

REFERENCES

- Barnthouse, L. W. et al. 1977. A Selective Analysis of Power Plant Operation on the Hudson River with Emphasis on the Bowline Point Generating Station, Report No. ORNL/TM-5877, Oak Ridge National Laboratory, Oak Ridge, Tenn.
- Batchelor, G. K. 1970. An Introduction to Fluid Mechanics, Cambridge University Press.
- Eraslan, A. H. Nov. 1983. ESTONE: A Computer Code for Simulating Fast-Transient, One-Dimensional Hydrodynamic, Thermal, and Salinity Conditions, in Controlled Rivers and Tidal Estuaries for the Assessment of the Aggregated Impact of Multiple Power Plant Operation. NUREG/CR-2621. U.S. Nuclear Regulatory Commission, Washington, D.C.
- Eraslan, A. H. et al. RADONE: A Computer Code for Simulating Fast-Transient, One-Dimensional Hydrodynamic Conditions and Radionuclide Concentrations Including the Effect of Bed-Deposition in Controlled Rivers and Tidal Estuaries. NUREG/CR-3441. In Press.
- Eraslan, A. H., and J. A. Benek. 1971. "A Note on Flow over a Flat Plate," Developments in Theoretical and Applied Mechanics, Ed. G. L. Rogers, Vol. 5, pp. 820-846.
- Eraslan, A. H., H. Diament, and R. D. Codell RADTWO: A Computer Code for Simulating Fast-Transient, Two-Dimensional, Two-Layer Radionuclide Concentration Conditions in Lakes, Reservoirs, Rivers, Estuaries, and Coastal Regions. NUREG/CR-3442. In press.
- Eraslan, A. H., and W. L. Lin. Oct. 1983. Zone Methodology for Slot Jets in Water Bodies. NUREG/CR-2596. U.S. Nuclear Regulatory Commission, Washington, D.C.
- Eraslan, A. H., W. L. Lin, and R. D. Sharp. Dec. 1983. FLOWER: A Computer Code for Simulating Three-Dimensional Flow, Temperature, and Salinity Conditions in Rivers, Estuaries, and Coastal Regions. NUREG/CR-3172. U.S. Nuclear Regulatory Commission, Washington, D.C.
- Eraslan, A. H., and A. J. Witten. June 1981. Application of Zone-Matching Methodology to Interacting Submerged Multiport Diffusers, ASME Publication No. 81-FE-12.
- Eraslan, A. H., and A. J. Witten. Oct. 1983. Application of Zone-Matching Methodology to Interacting Submerged Multiport Diffusers. NUREG/CR-3095. U.S. Nuclear Regulatory Commission, Washington, D.C.
- Fischer, S. K. et al. Apr. 1984. CHMONE: A One-Dimensional Computer Code for Simulating Temperature, Flow and Chemical Concentrations in Water Bodies. NUREG/CR-3410. U.S. Nuclear Regulatory Commission, Washington, D.C.

- Hetrick, D. M. et al. Feb. 1979. SEDONE: A Computer Code for Simulating Tidal-Transient, One-Dimensional Hydrodynamic Conditions and Three-Layer, Variable-Size, Sediment Concentrations in Controlled Rivers and Estuaries. NUREG/CR-0430. U.S. Nuclear Regulatory Commission, Washington, D.C.
- Park, J. E., and K. E. Cross. Dec. 1983. Calculation of Fluid Circulation Patterns in the Vicinity of Submerged Jets Using ORSMAC. NUREG/CR-3153. U.S. Nuclear Regulatory Commission, Washington, D.C.
- Schlichting, H. 1968. Boundary Layer Theory, McGraw-Hill, 6th ed.

NRC FORM 336 <small>(11-81)</small>		U.S. NUCLEAR REGULATORY COMMISSION BIBLIOGRAPHIC DATA SHEET		1. REPORT NUMBER (Assigned by DDC) NUREG/CR-3871 ORNL/TM-9249	
4. TITLE AND SUBTITLE (Add Volume No., if appropriate) An Overview of the Unified Transport Approach				2. (Leave blank)	
7. AUTHOR(S) A. H. Erastan, A. J. Witten				3. RECIPIENT'S ACCESSION NO.	
9. PERFORMING ORGANIZATION NAME AND MAILING ADDRESS (Include Zip Code) Oak Ridge National Laboratory P.O. Box X Oak Ridge, Tennessee 37831				5. DATE REPORT COMPLETED MONTH YEAR June 1984	
12. SPONSORING ORGANIZATION NAME AND MAILING ADDRESS (Include Zip Code) Division of Radiation Programs and Earth Sciences Office of Nuclear Regulatory Research U.S. Nuclear Regulatory Commission Washington, D.C. 20555				DATE REPORT ISSUED MONTH YEAR August 1984	
13. TYPE OF REPORT Topical				PERIOD COVERED (Inclusive dates)	
15. SUPPLEMENTARY NOTES				14. (Leave blank)	
16. ABSTRACT (200 words or less) <p>The Unified Transport Approach (UTA) consists of a set of nine complementary models developed for assessing the environmental impacts associated with nuclear power plant discharges to receiving water bodies. This set of models has the capability to simulate natural and plant-induced flow, temperature, salinity, sediment transport, radionuclide transport, and chemical species concentrations. While these UTA models were developed for predicting impacts associated with the operation of nuclear power plants, they are quite general and can be applied to a variety of situations. The UTA models have been used to simulate the impacts associated with the operation of many industrial and energy production technologies, as well as to simulate laboratory and naturally occurring conditions. In all cases where data have been available for validation, the UTA model results have compared favorably. The purpose of this report is to provide an overview of the UTA as whole, highlighting the important features and unique capabilities of this approach.</p>					
17. KEY WORDS AND DOCUMENT ANALYSIS Unified Transport Approach Zone-Matching Discrete Element Transport Models Nuclear Power Stations			17a. DESCRIPTORS		
17b. IDENTIFIERS-OPEN ENDED TERMS					
18. AVAILABILITY STATEMENT Unlimited			19. SECURITY CLASS (This report) Unclassified		21. NO. OF PAGES 5
			20. SECURITY CLASS (This page) Unclassified		22. PRICE 5

UNITED STATES
NUCLEAR REGULATORY COMMISSION
WASHINGTON, D. C. 20555

OFFICIAL BUSINESS
PENALTY FOR PRIVATE USE, \$300

FOURTH-CLASS MAIL
POSTAGE & FEES PAID
USNRC
WASH D C
PERMIT No. 667

120555078877 1 IANIRE
US NRC
ADM-DIV OF TIDC
POLICY & PUB MGT BR-PDR NUREG
W-501
WASHINGTON DC 20555